U.S. DEPARTMENT OF ENERGY

PNNL-21382

Prepared for the U.S. Department of Energy
under Contract DE-AC05-76RL01830

Electrical Generation for More-Electric Aircraft using Solid Oxide Fuel Cells

GA Whyatt
LA Chick

April 2012

Pacific Northwest
NATIONAL LABORATORY

Proudly Operated by Battelle *Since 1965*

DISCLAIMER

PACIFIC NORTHWEST NATIONAL LABORATORY
operated by
BATTELLE
for the
UNITED STATES DEPARTMENT OF ENERGY
under Contract DE-AC05-76RL01830

Printed in the United States of America

Available to DOE and DOE contractors from the
Office of Scientific and Technical Information,
P.O. Box 62, Oak Ridge, TN 37831-0062;
ph: (865) 576-8401
fax: (865) 576-5728
email: reports@adonis.osti.gov

Available to the public from the National Technical Information Service
5301 Shawnee Rd., Alexandria, VA 22312
ph: (800) 553-NTIS (6847)
email: orders@ntis.gov <http://www.ntis.gov/about/form.aspx>
Online ordering: http://www.ntis.gov


This document was printed on recycled paper.
(8/2010)

PNNL-21382

Electrical Generation for More-Electric Aircraft using Solid Oxide Fuel Cells

GA Whyatt
LA Chick

April 2012

Prepared for
the U.S. Department of Energy
under Contract DE-AC05-76RL01830

Pacific Northwest National Laboratory
Richland, Washington 99352

Summary

This report examines the potential for Solid-Oxide Fuel Cells (SOFC) to provide electrical generation on-board commercial aircraft. Unlike a turbine-based auxiliary power unit (APU) a solid oxide fuel cell power unit (SOFCPU) would be more efficient than using the main engine generators to generate electricity and would operate continuously during flight. The focus of this study is on more-electric aircraft which minimize bleed air extraction from the engines and instead use electrical power obtained from generators driven by the main engines to satisfy all major loads. The increased electrical generation increases the potential fuel savings obtainable through more efficient electrical generation using a SOFCPU. However, the weight added to the aircraft by the SOFCPU impacts the main engine fuel consumption which reduces the potential fuel savings. To investigate these relationships the Boeing 787-8 was used as a case study.

The potential performance of the SOFCPU was determined by coupling flowsheet modeling using ChemCAD software with a stack performance algorithm. For a given stack operating condition (cell voltage, anode utilization, stack pressure, target cell exit temperature), ChemCAD software was used to determine the cathode air rate to provide stack thermal balance, the heat exchanger duties, the gross power output for a given fuel rate, the parasitic power for the anode recycle blower and net power obtained from (or required by) the compressor/expander.

The SOFC is based on the Gen4 Delphi planar SOFC with assumed modifications to tailor it to this application. The size of the stack needed to satisfy the specified condition was assessed using an empirically-based algorithm. The algorithm predicts stack power density based on the pressure, inlet temperature, cell voltage and anode and cathode inlet flows and compositions. The algorithm was developed by enhancing a model for a well-established material set operating at atmospheric pressure to reflect the effect of elevated pressure and to represent the expected enhancement obtained using a promising cell material set which has been tested in button cells but not yet used to produce full-scale stacks. The predictions for the effect of pressure on stack performance were based on literature. As part of this study, additional data were obtained on button cells at elevated pressure to confirm the validity of the predictions.

An estimate of the electrical power required was developed based on an understanding of the Boeing 787 loads. The Boeing 787 engine generators produce 230 VAC power which is converted to ±270 VDC to drive the largest loads. In addition to generating a greater amount of electrical power than earlier aircraft, the 787 does so with dramatically improved efficiency. Compared to the 777, the 787 achieves twice the efficiency evaluated at the ±270 VDC loads. This is achieved using highly efficient direct drive variable frequency generators to replace less efficient generators with constant speed drives. In addition, advances in power electronics have enabled extraordinarily high efficiency in power conversions. The 787 Auto Transformer Rectifier Unit (ATRU) achieves 97% efficiency in converting 230 VAC to ±270 VDC and the transformer achieves 98% efficiency in conversion of 230 VAC to 115 VAC. Overall the 787 provides power to the ±270 VDC loads at 51% efficiency. This high efficiency reduces the amount of fuel that can be saved using highly efficient fuel cell systems compared to earlier aircraft. It is expected that similar measures could be taken on all future aircraft whether or not they are configured as more electric aircraft. This effectively raises the bar for the performance that must be achieved to provide a benefit using SOFC generated power. For SOFC generated power, a revised configuration for the 787 electrical distribution system was assumed to accommodate the fact that the SOFC produces DC rather

than AC power. The 230 VAC bus is eliminated, loads are moved to the DC bus and the DC power is inverted to provide 115 VAC loads. These changes reduce the weight of power conversion equipment but due to assumptions for power conversion efficiency not being as high as the values achieved in the 787, the overall power generation required of the fuel cell system is slightly higher (972kW vs. 944 kW).

ChemCAD modeling examined several potential reforming and flowsheet options and determined that steam reforming using anode recycle was preferred due to the higher efficiency. A parametric study was then performed to estimate the efficiency and weight impact to the aircraft as a function of cell voltage (0.70, 0.75, 0.80, 0.825, 0.85 V) and operating pressure (0.8, 3.0, 5.5, 8 atm). The systems included a compressor/expander to compress air drawn in from the atmosphere and to expand the exhaust gases to recover work. Operation was evaluated assuming a cruising speed of Mach 0.85 and altitude of 40,000 ft. Simplified weight estimates for non-stack components were estimated by a linear ratio to the known weight of an existing 6.9 kWe SOFC system, by comparison to a small jet engine for the compressor/expander and using stress calculations to estimate pressure vessel weight. Credit was taken for eliminating the turbine APU and reducing the electrical converter weights. The preliminary screening results are shown in Figure S.1

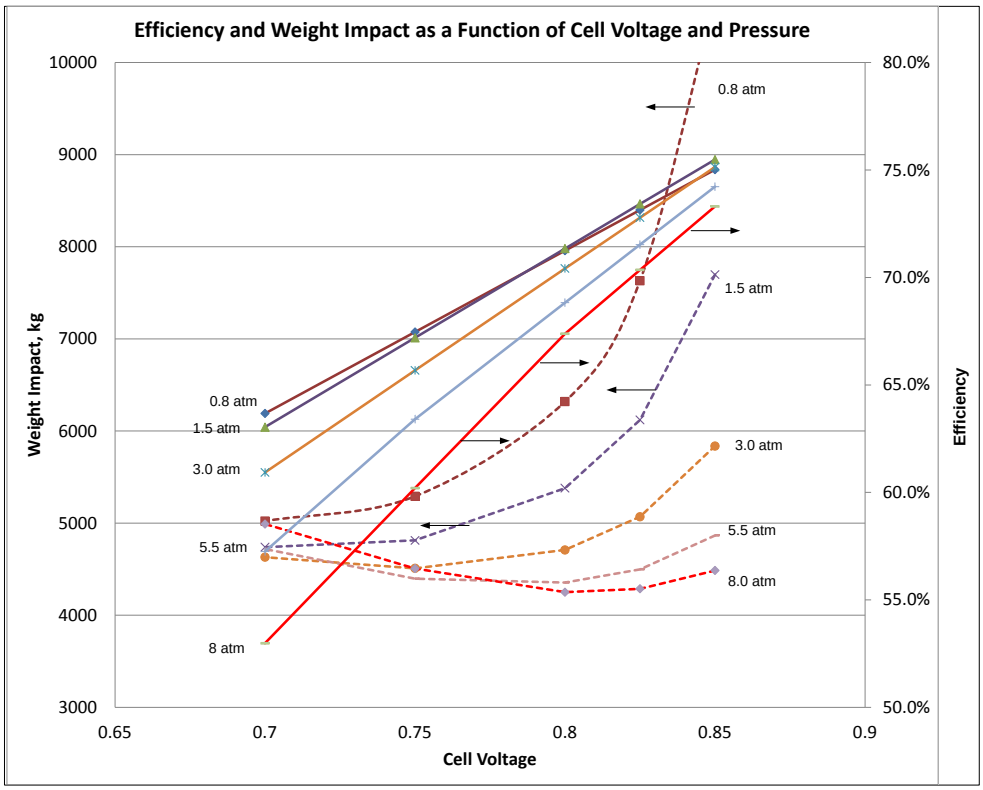

Figure S.1. Results of Preliminary Parametric Screening

Selecting the optimum condition from Figure S.1 requires a combination of the reduction in fuel due to electrical generation efficiency with the increase in main engine fuel consumption due to added weight. The effect of the SOFCPU weight impact on main engine fuel consumption was determined using a PianoX model of the 787-8. Flight profiles for trips of 1000, 3000, 5000 and 7000 nautical mile (nm) were calculated for a wide range of payloads to determine weight sensitivity for each trip length. A

breakeven weight for the SOFCPU was then calculated by determining the point at which the fuel saved due to the efficiency of the SOFC would be offset by the added fuel consumption due to SOFCPU weight. The optimum condition was then selected based on the difference between breakeven weight and the estimated weight. This relationship is shown in Figure S.2 for a trip length of 5000 nm where the optimum occurs at a cell voltage of 0.825 V and pressure of 8 atm.

The condition of 0.825 V/cell and 8 atm was then used to develop a conceptual design for the system. The pressure vessel is proposed to consist of an inner Inconel frame with outer titanium pressure shell with insulation between. The overall system is divided into three redundant systems to allow the turbine APU to be eliminated. The stack frame and header design was modified to obtain adequate flow distribution and to allow six stacks to produce ±270 VDC. Design calculations were performed to size the cathode recuperator. Ducting and frame components were added to improve the overall size and weight estimates. The Solidworks representation of the system is shown in Figure S.3.

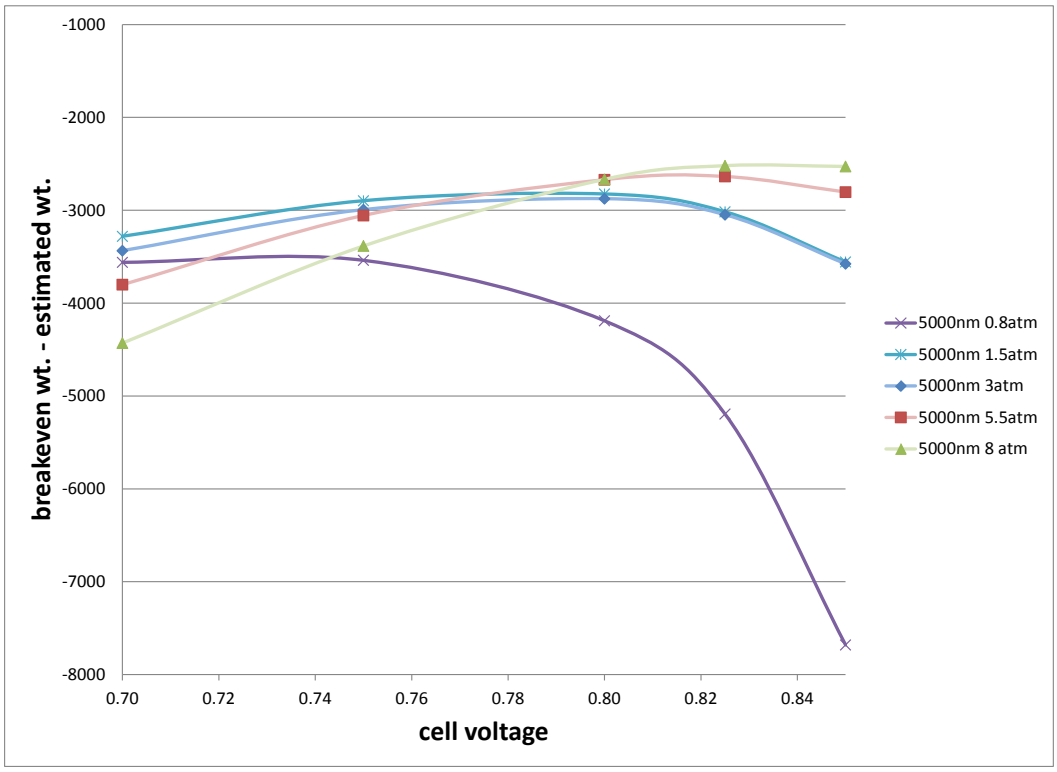

Figure S.2. Difference between Breakeven Weight and Preliminary Screening Weight Estimate Evaluated at 5000 nm Trip Length. Negative values suggest more fuel burned to carry the system weight than saved due to higher electrical generation efficiency.

Based on the conceptual design, the total weight impact of adding three SOFCPU systems to supply the 787-8 (after adjusting for elimination of the APU and reduction in converter weight) would be 2822 kg. This is significantly less than the scoping weight of 4287 kg. The reduction is primarily due to effects of pressure on balance of plant (BOP) components which were not incorporated into the original screening approach.

The spread between the current system weight estimate and the breakeven weight is shown as a function of flight distance in Figure S.4. The smallest spread between the estimated weight and the breakeven weight occurs for shorter flights where the estimated system weight is about double the breakeven weight. The trend in breakeven weight results from the fuel consumption per mile for electrical generation being greater during the combined climb and descent phases of the flight where the velocity is lower than during the cruise condition.

While there are a number of areas within the conceptual design that may increase in mass as the design increases in fidelity, the current mass is about three-quarters because of the stacks (62%) and the pressure vessel (15%). To begin saving fuel on the 787, the stacks will have to increase their specific power (power/weight) by more than a factor of two. However, the conceptual design may still be a viable system where a highly efficient SOFC system is needed but weight is not as critical.

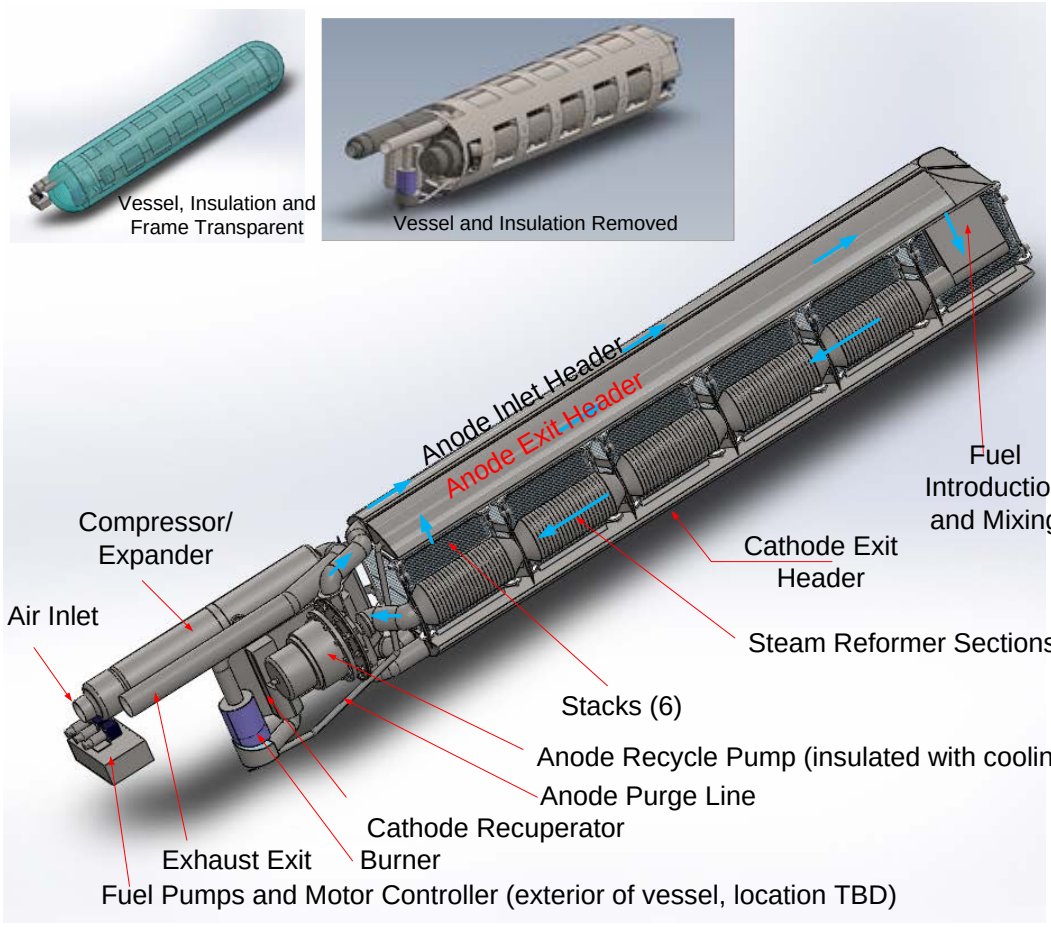

Figure S.3. Solidworks arrangement for one of three SOFCPU for Boeing 787. As shown, design is for 821kW from three systems. Linear scaling of weight was used to adjust mass to target power level of 972 kW.

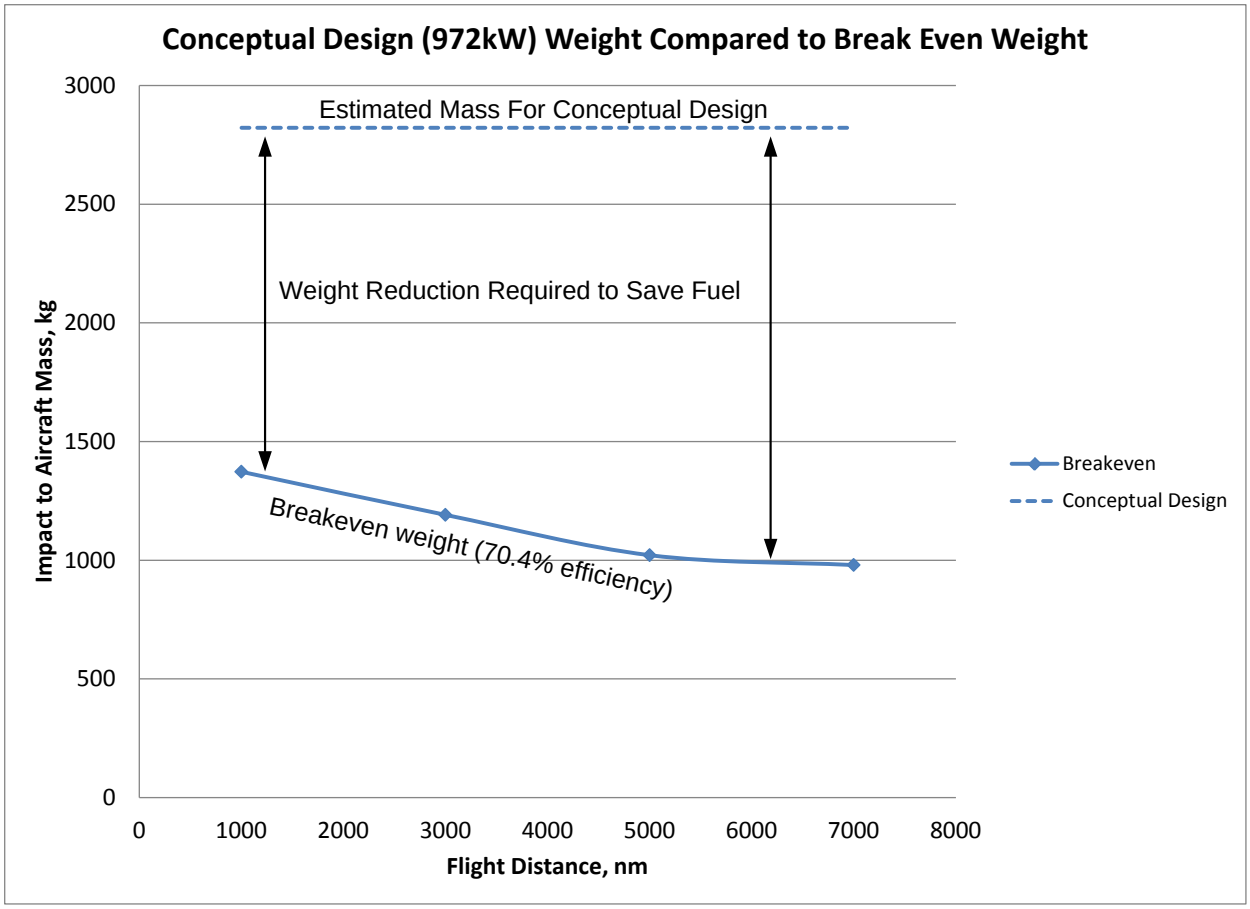

Figure S.4. Comparison of Weight Estimate for Conceptual Design to Breakeven Weight

Acknowledgments

The authors would like to acknowledge Pete Devlin, Market Transformation Program Manager of the U. S. Department of Energy, Energy and Efficiency Office, Hydrogen and Fuel Cells Program, for funding this project. We would also like to thank Joe Breit of Boeing Commercial Airplanes for much valuable information on the workings of the 787 aircraft. Thanks to Dylan Tribbey of Williams International for information and advice on small jet engines. Lastly we would like to acknowledge the contributions of the following PNNL staff who are not listed as authors: Chris Coyle for performing the button cell experiments at pressure, Jim Davis for Solidworks drafting, and Kerry Meinhardt for technical consulting on SOFCs.

Acronyms and Abbreviations

AC	Alternating Current
APU	Auxiliary Power Unit
ATR	Auto-Thermal Reformer
ATRU	Auto Transformer Rectifier Unit
BOP	Balance Of Plant, refers to components other than the fuel cell itself
DC	Direct Current
GT	Gas Turbine
MEA	More Electric Airplane
nm	Nautical Mile, equal to 1.15 land miles
PEM	Polymer Electrolyte Membrane (fuel cell)
POX	Partial OXidation reformer
RAT	Ram Air Turbine
SOFC	Solid Oxide Fuel Cell
SOFC-GT	Solid Oxide Fuel Cell – Gas Turbine
SOFCPU	Solid Oxide Fuel Cell Power Unit
TRU	Transformer Rectifier Unit
VAC	Volts Alternating Current
VAC-var	Volts Alternating Current – variable frequency
VDC	Volts Direct Current

Contents

Figures

Tables

1.0 Introduction

This study examines approaches to providing electrical power on board commercial aircraft using solid oxide fuel (SOFC) technology. The focus of this study is on application to "more-electric" airplanes with the Boeing 787 used as a case study. More-electric airplanes minimize extraction of bleed air from the engine compressor stages and instead run electrical generators off the main engine shaft to satisfy electrical loads. More-electric airplanes have higher electrical generation rates and thus stand to show greater benefit from an increase in the efficiency of electrical generation.

SOFC technology has the potential to generate electrical power at higher efficiency than is achieved by using power from the main engine shaft to run a generator. Hence, unlike the existing auxiliary power unit (APU) which is turned off once the main engines are started, a solid oxide fuel cell power unit (SOFCPU) would operate throughout the flight to maximize fuel savings. SOFCPU's are expected to be somewhat heavier than turbine APUs resulting in a heavier aircraft. A key hurdle to demonstrate the feasibility of a SOFCPU is to show that the increase in fuel consumption due to the increase in aircraft weight is less than the savings obtained by operation of the SOFCPU.

1.1 Review and Discussion of Literature on SOFC's for Aircraft Electrical Power

This section is a review and discussion of several reports and papers available in open literature that address the design and development of SOFC power systems for aircraft.

1.1.1 Daggett at al. (2003)

Daggett et al (2003) proposed development of an SOFC-turbine power system to replace the turbine APU, based on expected fuel savings, reduced noise and reduction of NO_x emissions. They proposed using the SOFC-turbine APU both on the ground and during flight. Only a high-level discussion of how the system would be designed was presented. This paper discussed pre-reforming of jet fuel followed by complete reforming on the SOFC stack. They anticipated a 75% reduction in fuel consumption compared to the turbine APU. Among the technological challenges to be overcome, they mentioned the need to increase specific power to near 1 kW/kg, the need to develop reformers for jet fuel, the problem of sulfur poisoning, the need to extend operating life and the necessity of cost reduction. The basis for the 1 kW/kg goal was not given.

1.1.2 Daggett (2004)

Daggett (2004) discussed a hybrid SOFC-turbine APU system, intended for the Boeing 777, with (we assume) an autothermal reformer in which water is supplied by condensation from the anode exhaust followed by steam generation. Outside air is used to cool the condenser. Heat for steam generation and reformation is supplied by a burner running on jet fuel. Cathode air is drawn from cabin air and compressed to an unspecified pressure. He predicted the SOFC APU would be 60% efficient at sea-level. He again stated that SOFC stack power density would need to exceed 1 kW/kg to make the SOFC APU feasible.

1.1.3 Daggett et al. (2005)

Daggett et al. (2005) again discussed replacement of the turbine APU with a hybrid SOFC-turbine system. It was suggested that either catalytic partial oxidation or autothermal reformation could be incorporated, with some anode recycle and the remainder of the anode gas fed to the combustor. The paper discussed condensing water from the turbine exhaust to be used both for grey water and autothermal reforming. They estimated that about 25% of the system's power would be generated by the turbine. Lastly, they estimated the potential market at 1570 common-sized units per year, although they did not specify what the power output of these common-sized units should be.

1.1.4 Eelman et al (2003)

Eelman et al (2003) studied use of 370 kW SOFC-GT to generate electrical power on MEAs. The concept was to develop a continuously operating, efficient APU. They stated that the total efficiencies of the combined generator and main engine would be around 40-45%. They chose to operate the SOFC at 3.5 bar. The turbine was driven by expanding the cathode exhaust. The kerosene was stated to be autothermally reformed, although air addition rate is described as being small and the reformer may be operating primarily via steam reforming. The fuel reforming reactions are assumed to proceed completely to CO_2 and H_2 without considering methane equilibrium. Not including methane formation increases the amount of heat that can be adsorbed by the reforming reaction and reduces the temperature at which heat may be delivered to the reformer providing an unrealistic benefit to the system. Single pass utilization on the anode was 80%. Normally, this high a utilization would have a negative impact on power density. However, in this study a future stack technology with 1 kW/kg power density was assumed so any reduction in stack power density at high fuel utilization is lumped into the development of the future stack technology. The H_2 exiting in the anode exhaust was proposed to be recovered and recycled with 90% efficiency using a hydrogen permeable membrane and returned to the anode. The pressure differential to drive the membrane permeation was provided by a jet pump with the driving fluid being the incoming fuel. The high level of recovery would require a high pressure ratio be generated by the fuel driven jet pump (~100:1) and would be extremely difficult to achieve in practice. Water was condensed, with 70% returned to the steam reformer and 30% stored for airplane use. Our own analysis of the flowsheet energy balance suggests that the temperature across the stack is approximately 300°C meaning the stack inlet is ~550°C. This would normally impact on power density but does not impact the future stack assumed. Also, it appears that the energy cost for vaporizing the water that is recycled is not reflected in the efficiency. This is a very significant factor for this flowsheet and our calculations assuming a S:C ratio of 3.5 in the reformer estimate it accounts for 23.6% of the fuel feed LHV. They compared running the system off cabin air versus ambient and estimated there would be a 5% efficiency improvement (from 70% up to 75%) by running on cabin air during cruise at 43000 feet. Maximum system efficiency occurred at cruise altitude because the efficiency of the turbine cycle was increased. They sized the SOFC to the power requirements on the ground, since that was where the system was least efficient. The option of reducing stack voltage and sacrificing efficiency could not be assessed since the 1 kW/kg power density input assumption was not tied to a particular operating condition. They estimated the SOFC-GT would be 174% the weight of a "super efficient" GT APU. No details were given on the assumed weights for the components. The methodology for assessing the breakeven weight for an APU was to compare the mass of fuel burned for electrical generation using the main engines to the sum of the mass of fuel burned in the APU plus the mass of the APU. This is a very simplistic comparison that fails to reflect the impact of the APU on main engine fuel consumption for flight. The result is that for a short flight the APU must save an amount of fuel equal to its own weight to appear favorable. Similarly, a very

heavy APU could look favorable for a very long flight since the fuel burn to keep the APU in the air is not included. As a result the conclusion from the approach is the savings are greater for longer flights and less for shorter flights.

1.1.5 Eelman et al. (2004)

Eelman et al. (2004) assessed using 400 kW SOFCs or PEMs on long range MEAs. They performed their analysis using MATLAB / Simulink simulations. They chose steam reforming as giving highest system efficiency. One point they made was the wing de-icing only operates for comparatively short times and since it consumes ~200 kW, the electric generating system would have to be sized accordingly. Therefore, they conclude it is best to continue de-icing using bleed air. Also, they conclude that several hydraulic functions (landing gear, brakes, and thrust reversal) should not be electrified "as these systems need a high power density and redundancy, which is not the strength of electric systems." They assumed steam reforming of jet fuel that had been de-sulfurized on the ground. They compared using cabin air versus ambient air, with the former yielding 75% efficiency for the SOFC versus 70%. It is not clear how they accounted for cabin air pressurization loss in calculating their system efficiencies. They included a turbine / compressor / generator, but the turbine was fueled directly (apparently with desulfurized kerosene) rather than by SOFC anode exhaust. This was necessary because they assumed 95% fuel utilization in the SOFC stack, followed by 90% recovery of the remaining H2 from the exhaust, apparently by using a palladium membrane and a jet pump. It appears the fuel was combusted with the heat being transferred to a pressurized air stream, which in turn drove the turbine. The system was pressurized to 3.5 bar. Stack temperature was between 800 and 1000°C. They condensed water, 70% of which was used for reforming and 30% for airplane usage. Liquid water was vaporized and supplied to the steam reformer rather than using anode recycle. It appears (Figure 2) that the pressurized air was expanded through the turbine before being exhausted. They concluded for the SOFC system that, "Even if system weight is about 2.75 times higher than that of a super efficient future conventional APU, mass balance reveals a benefit for missions longer than over two and a half hours with full net water recovery and four and a half without any net water recovery." They also concluded a PEM system would be 50% heavier and ~20% less efficient than the SOFC system.

1.1.6 Gummalla et al. (2006)

In a study done for NASA by United Technologies and Sunstrand, Gummalla et al. reported on an SOFC turbine hybrid system concept for a 162 passenger, more electric, short-range (1000 nm) aircraft. The aircraft had peak load of 360 kW. The design included an on-board desulfurizer, which added substantially to system weight. The system was estimated to save 6.7% of the fuel compared to the baseline system, which had generators on the main engines and a turbine APU. Virtually all of the system and component design was proprietary, so critical evaluation of the concept is not possible.

1.1.7 Srinivasan et al. (2006)

Srinivasan et al. (2006) performed a study for NASA similar to that by Gummalla et al., but for long range aircraft. The baseline for the study was the Boeing 777-200ER. The SOFC-turbine hybrid was sized for 450 kW and operated during all phases of the mission. Their most promising architecture ran at one atmosphere to reduce compressor power. This system produced overall fuel burn savings of 0.77%. Again, virtually all of the system and component design was proprietary, so critical evaluation of the concept is not possible.

1.1.8 Rajashekara et al. (2008)

Rajashekara et al.(2008) modeled a 440 kW SOFC-GT hybrid system, sized for the Boeing 777. System weight goal was <880 kg, although there was no discussion of the basis for that weight goal. Several different system configurations were considered including a range of reforming reactions, variation of stack operating temperature and pressure, cooling strategy and water recovery. Both cabin air exhaust and outside air were considered. They modeled up to 95% anode recycle. All modeling was performed for a stack with 250,000 cm^2. Thus, when pressure, temperature or anode gas composition was changed, the stack voltage had to change to meet the power demand. This affected system efficiency. They recommended operating the stack at 850-880°C in order to increase the stack voltage (and efficiency) for the same power level. They recommend using heat exchangers made of titanium to decrease weight. Their optimum design achieved 79% LHV efficiency at 42,000 feet. An apparent error in this article in contained in their Figure 4, in which the turbine exhaust, at 523°C is used to transfer heat to a 226°C incoming air stream, thereby somehow heating it to 650°C. Also, they specified an O/C ratio of 1.2 going into the reformer; it is suspected that coking could result.

1.1.9 Braun et al. (2009)

Braun et al. (2009) reported on the same study as Gummalla et al., three years later and in somewhat more detail. As before, the analysis was for a 162 passenger aircraft and a 1000 nm flight. The study examined replacement of the 300 kW turbine APU with a hybrid SOFC-turbine power system. Whereas the turbine APU is normally used only on the ground and for the in-flight de-icing or emergencies, the SOFC APU was assumed to continue operating in-flight, reducing the load on the main engine generators. Two system architectures were evaluated.

In Architecture A, on-board de-sulfurization was assumed. An autothermal reformer was used in which desulfurized fuel was mixed with some anode recycle gas and air. Cabin air was used for the cathode and the autothermal reformer. Stack fuel utilization was 88%; power density was 0.25 W/cm^2 at 0.745 volts/cell and 3.1 bar pressure. Partial anode gas recycle was assumed. Stack inlet temperature was chosen as 615°C, even though the analysis showed stack efficiency increasing and parasitic power decreasing substantially as the inlet temperature increased up to 690°C. Outlet temperature was set at 690°C. The assumed stack specific power required development of a conceptual and proprietary light-weight metal-supported cell design, which does not yet exist. During the in-flight phase exhaust gasses were used to pre-heat the fuel going to the main engines. During ground operations about 18% of the power was generated by the turbine, with the remainder generated by the SOFC stack. During flight the ratio changed to 63% SOFC, 37% gas turbine. The LHV efficiency of the system was 45% on the ground, increasing to 64% during flight. This overall efficiency increase must have been due to an increase in SOFC cell voltage during flight, resulting from the decreased load on the SOFC stack. A 3.3% fuel burn per day savings was realized for ground operations with an additional 1.3% fuel burn per day savings realized for in-flight operation.

Architecture B was similar to Architecture A, with three changes: The SOFC turbine and the cabin pressurization turbocharger were put on the same shaft, the SOFC system was downsized by assuming the main engines could handle the increased ground cooling loads on the hottest days, and a more efficient SOFC system was assumed. The first concept decreased the weight of the power electronics. The second concept “provides a lower weight SOFC system while not compromising the efficiency on a typical day”.

Little is explained about how the higher efficiency SOFC system was to be implemented, except than, "by increasing the fuel processing efficiency by operating the ATR at lower O_2/C and H_2O/C ratios than the current technology allows, increasing the cell-stack temperature" (by an unspecified amount), "and by cracking a portion of the fuel to enable some internal reforming to take place within the SOFC." However, minimum O:C ratios are driven by a need to avoid coke formation in the reformer. No explanation of how lower O:C ratios might be used without carbon formation was provided. Similarly, introducing thermally cracked jet fuel directly to the anode is likely to result in carbon deposition. On-stack reforming is beneficial in that it introduces stack cooling within the stack but significant levels of on-stack reforming would be difficult to control since there may be a tendency to overcool the inlet of the stack leading to a loss in power density. Assuming Architecture B could actually be developed, the paper estimates the APU daily fuel consumption would decrease by 6.7%.

2.0 Approach to Modeling the SOFC Aircraft Power System

A variety of potential system configurations and operating modes were analyzed to determine their efficiency and estimate their weight. Mass and energy balance was modeled using ChemCAD software coupled with a PNNL stack performance model of a planar anode supported SOFC.

Approaches evaluated using a ChemCAD flowsheet included auto-thermal reforming, steam reforming with a single pass across the anode and steam reforming using anode recycle. All systems include a compressor/expander to compress air drawn in from the atmosphere and then expand the exhaust gases to recover work. All systems modeled were assumed to operate using desulfurized jet fuel that is loaded into a dedicated tank. Systems were evaluated for a condition where inlet air is received at 0.279 atm and -29.6°C, corresponding to an adiabatic, isentropic stagnation of air at 40,000 ft with an aircraft velocity of Mach 0.85. The expander is assumed to exhaust to atmospheric pressure at 40,000 ft (0.185 atm). The drag associated with the air intake is not currently included in the model of aircraft fuel consumption.

The stack performance model is calibrated to actual data for a promising new electrode materials set. The methodology for estimating stack power density data collected to confirm predictions at high pressure are discussed in Appendix C while information on the new material set is provided in Appendix D. The stack model includes the effects of inlet temperatures, flows and compositions and the operating cell voltage on the power density achieved. SOFC operating pressures were examined at 0.8 atm approximately corresponding to cabin pressure at cruising altitude, 3 atm, 5.5 atm and 8 atm. Operating cell voltages of 0.70, 0.75, 0.80, 0.825 and 0.85V were analyzed.

The 787 generates 230 VAC power from engine generators and converts the power to ±270 VDC to drive the largest loads. Additional detail on the 787 electrical system is provided in Appendix E. For SOFC generated power, a revised configuration for the 787 electrical distribution system was considered in order to take advantage of the fact that the SOFC generates DC rather than AC power. An estimate of the electrical power required was developed based on an understanding of the Boeing 787 loads. The relationship between added aircraft weight and fuel consumption is complex and depends on a number of factors. The impact of the addition of the SOFCPU weight on main engine fuel consumption was determined using a PianoX model of the 787-8. Flight profiles for trips of 1000, 3000, 5000 and 7000 nm were calculated for a wide range of payloads. The PianoX model was allowed to select appropriate parameters for each flight such as rate of climb, initial cruise altitude, rate of descent, etc., and provided fuel consumption data as a function of payload. A breakeven weight for the SOFCPU was then calculated by determining the point at which the fuel saved during the flight due to the efficiency of the SOFC would be cancelled out by the added main engine fuel consumption required to carry the SOFCPU weight. Preliminary estimates of the weight of the most favorable SOFCPU configurations were then compared to the breakeven weight as a function stack cell voltage and aircraft trip length. Finally, a single SOFCPU configuration and operating point was selected for a more detailed design and evaluation.

This study was performed using input data provided for the Boeing 787 generators, ATRU and transformer efficiencies. Loads at the outlet of the generator were translated to loads at the point of use using the ATRU and transformer efficiencies. During review of the final report it was determined that the input data for generator, ATRU and transformer efficiencies corresponded to the Boeing 777 rather than the 787. Efficiencies for the 787 are much higher (51% vs. 25% efficiency overall evaluated at the ±270V DC bus) due to the use of a variable frequency generator and improvements in electronics for the

voltage conversion. The report has been corrected to reflect the 787 efficiencies. However, as a result of this error, the power rate used for the SOFC system design was lower (821 kW) than the revised target (972kW) for the reconfigured SOFC powered electrical system. Rather than repeat the design effort at a slightly higher power level the discrepancy was resolved by assuming the same specific power would be achieved and linearly scaling the weight to the higher power level.

2.1 Integration of the SOFCPU into the Boeing 787

The ability of a SOFCPU to save fuel once installed in an aircraft is a balance between more efficient electrical power generation which saves fuel and an increase in aircraft weight which requires more fuel be burned for a given flight. As the SOFCPU is integrated into the aircraft, a number of factors contribute to this comparison including:

- The SOFC system efficiency which results in a reduction in fuel consumption
- Weight added to the aircraft by the SOFCPU which results in more fuel being burned by the main engines for a given flight.
- Changes associated with direct generation of ±270 VDC and in conversion to obtain 120 VAC
  - Reduction in power conversion losses for direct generation of ±270 VDC
  - Increase in losses for 120 VAC (transformer more efficient than inverter)
  - Reduction in power converter weight
- Elimination of the turbine APU weight.

A breakeven weight is defined to be the weight impact at which the additional fuel consumed as a result of the weight addition is equal to the fuel saved due to the higher efficiency of the generating system. The breakeven weight is primarily a function of the SOFCPU efficiency but as will be discussed, also varies with the assumed length of the flight used to determine it.

2.1.1 Electrical Power Requirements during Boeing 787 Flight

For operation during weather conditions requiring maximum deicing power, the amount of power drawn from the engine generators is relatively constant over the major portions of the flight. At lower altitudes, greater power is used for ice protection and hydraulics while at higher altitude more power is used for the environmental control system and cabin pressurization. The two effects offset resulting in a relatively constant power output from the engine generators. There are brief periods when the power drops noticeably. For example, when landing gear is retracted the ice protection is turned off briefly resulting in a dip in the load on the engine generator. However, these periods are brief and unlikely to have a noticeable impact on fuel consumption for electrical generation. The variation in engine generator loads for major portions of the flight are shown in Figure 2.1. As a result of the relatively flat power profile it was decided to simplify the analysis by evaluating the electrical generating systems on the electrical loads existing during the cruise condition and then apply that power generation requirement as a constant over the entire period of a flight.

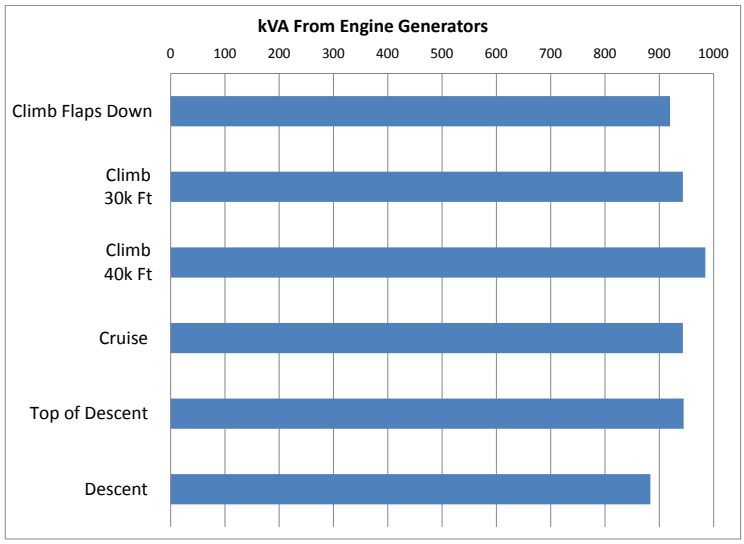

Figure 2.1. Total Electrical Load on 787 Engine Generators during Major Segments of Flight. Loads are for maximum ice conditions.

2.1.2 Boeing 787 Electrical Generation and Loads During Cruise Condition

The Boeing 787 electrical generation and conversion efficiencies are significantly higher than earlier non-MEA aircraft. The improvements in efficiency are primarily due to the use of a variable frequency generator and advances in electronics that allow much higher power conversion efficiencies. For example, comparing the 787 to the 777, the efficiency measured at the AC output of the generator is 53% compared to 34% and at the ±270 VDC bus the efficiency is 51% compared to 25%. This improvement in efficiency effectively raises the bar for the performance of fuel cell systems to show benefit on the aircraft.

The Boeing 787 has engine mounted generators that produce a variable frequency 230 VAC output. About 30% of the generated power is used directly, but to satisfy the largest loads the AC power is converted to ±270 VDC in an autotransformer rectifier unit (ATRU) with 97% efficiency. Power is also converted to 115 VAC 400 Hz in a 98% efficient transformer and to 28 VDC in an 80% efficient transformer rectifier unit (TRU). The electrical system as currently configured for engine generators with loads specified at cruise condition is shown in Figure 2.2.

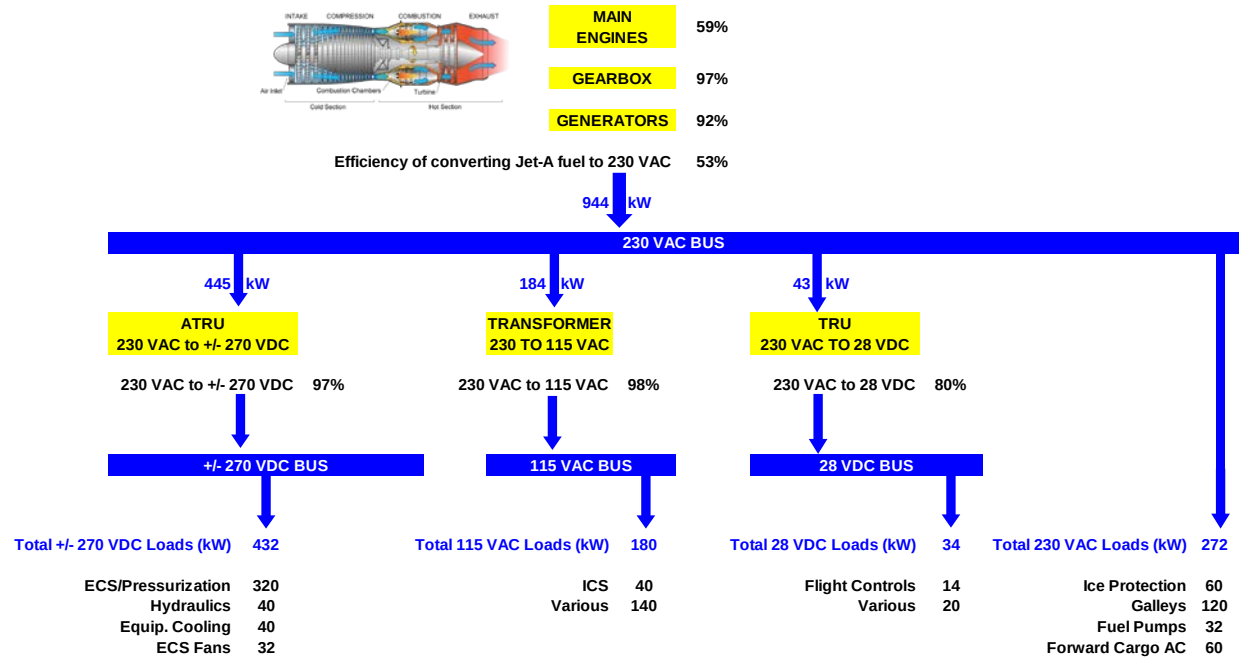

Figure 2.2. Existing Electrical System Loads at Cruise Condition in Boeing 787

2.1.3 Modification of Power Distribution

For the SOFC electrical system, the distribution system was modified so that the SOFC directly produces ±270 VDC. The present design does not include regulation of the ±270 VDC power and some additional losses may occur if tight regulation on the voltage is necessary. The 230 VAC loads are moved to ±270 VDC bus and DC/AC and DC/DC power converters with an efficiency of 80% are used to provide power to 115 VAC and 28 VDC loads. The selection of 80% efficiency for DC/AC and DC/DC conversions was in line with the initially provided Boeing 777 converter efficiencies. In light of the 97% efficiency being achieved in the 787 ATRU, future analyses should examine whether higher efficiency is possible for the DC/AC and DC/DC converters used when implementing the fuel cell power system.

Due to the SOFC system assuming 80% for DC/AC conversion while the generator based system achieves 97% efficiency for the transformer AC/AC conversion, the SOFC system must generate slightly more power (972 kW) than the generator system (944 kW). Prior to correcting the Boeing 787 input data the estimated power for the SOFC system was 821 kW. As a result, this is the power level selected for the more detailed SOFC design exercise. In addition, the change to direct generation of DC eliminates the ATRU and eliminates the 235 VAC power distribution bus. The revised SOFC based electrical system is shown in Figure 2.3.

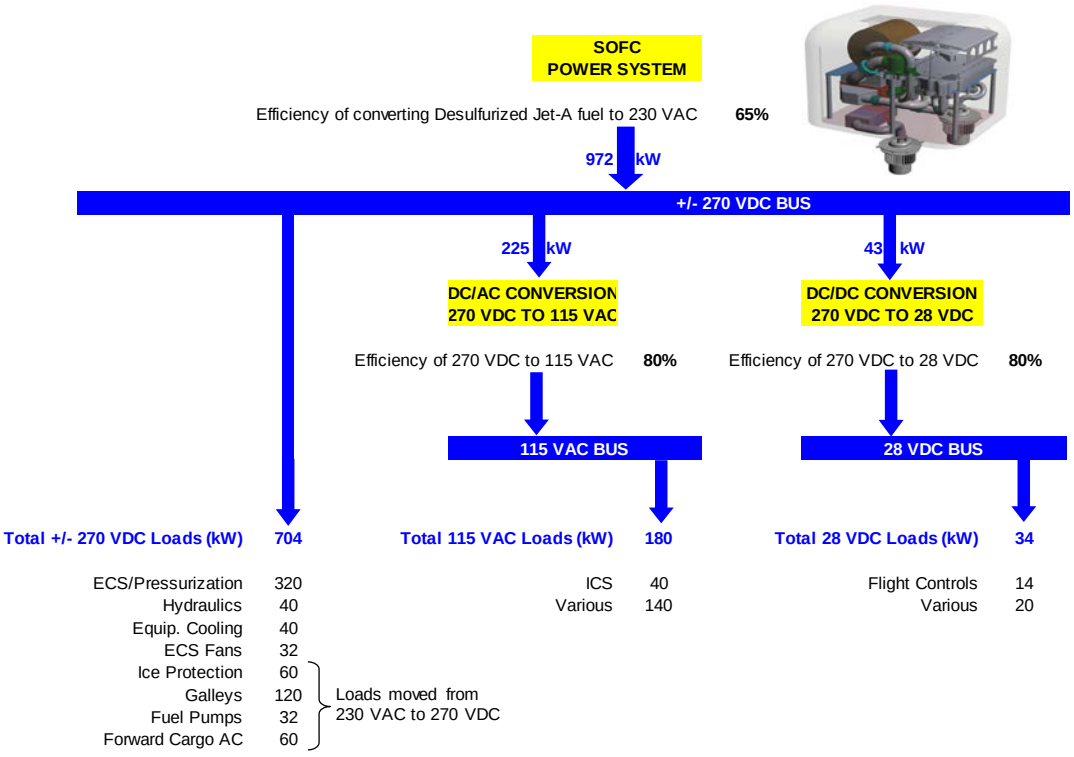

Figure 2.3. Boeing 787 Electrical System and Loads at Cruise Reconfigured for SOFC DC Generation

2.1.4 Power Conversion Weight

The weight saved in power conversion equipment is estimated to be 266 kg. This savings is based on weight per unit power output values summarized in Table 2.1. Most specific weight factors were based on a fairly close match to equipment designed for aircraft. However, a close match for the ±270 VDC→135 VAC 400 Hz inverter could not be found and a value of 1.0 kg/kw was assumed. Inverter units at <10 kW were heavier than 1.0 kg/kw but converter equipment specific weight typically falls with power output. The weight savings does not include any adjustment for changes in cooling demand (the 787 uses a liquid cooling loop to cool the power conversion equipment).

Table 2.1. Estimated Power Conversion Equipment Specific Weight

Voltage/Power Conversion	kg/kW output
235 VAC var. → ±270 VDC (ATRU)	0.65
235 VAC var. → 135 VAC 400 Hz	0.90
235 VAC var. → 28 VDC	1.0
±270 VDC→135 VAC 400 Hz	1.0
±270 VDC→28 VDC	1.0

2.1.5 Elimination of Turbine APU

Although the initial weight estimates used to compare system configurations are based on a single SOFC system, it is assumed that the SOFC power system would be divided into three independent units

in order to provide redundancy. In this configuration, it is expected that the turbine APU would no longer be needed for redundancy and could be eliminated, saving 245 kg. The Ram Air Turbine (RAT) was assumed to still be present. Engine generators cannot be eliminated since they double as starters for the main engines. No attempt was made to assess the weight savings (if any) which might be achievable via replacement of the four starter/generators (total mass ~363 kg) with dedicated starters.

2.2 SOFC System Configuration

The extent of fuel savings depends on the flowsheet for the SOFC system. Key system features include the air compression/expansion, the fuel cell itself and the approach to reforming the fuel.

2.2.1 Air Compression

In all cases, the SOFC system compresses ram air to operating pressure in a compressor (80% efficient) and then expands the exhaust gases through a turbine (85% efficient) to ambient in order to recover mechanical energy. For flowsheets in which more energy was required for compression than was available from expansion it is assumed an electric motor provides the additional power, which subtracts from the power generated. For flowsheets in which excess power was available the shaft power is assumed to be converted to ±270V DC at 57.6% efficiency based on: (96% gear box) x (80% mechanical to AC electric) x (75% to ±270V DC) =57.6%. This assumption places the efficiency for the mechanical to ±270V DC conversion at a lower value than achieved by the 787 generator and ATRU which is 86.6% (i.e. 97% gearbox X 92% generator X 97% ATRU).

Under normal flight conditions the aircraft compresses ambient air to cabin pressure and then releases the air back to ambient without attempting to recover energy. Although it might seem natural to use this compressed air to avoid compressing air in the SOFCPU it was decided not to take this approach. First, it was determined that the SOFCPU must operate in the event of a cabin decompression. Hence, a compressor capable of using ambient air is still required. Second, the amount of air required exceeds the rate of air compression for the cabin. In addition, not all the air compressed for the cabin leaves in the exit valve. Some quantity leaks through door seals or other locations and these leaks tend to increase with aircraft age, making it difficult to rely on a specific quantity of cabin air available at a leak valve. Finally, and most important, Boeing expressed significant concern over modification of the air outflow configuration. Anything that could potentially upset the controlled outflow of air from the cabin could lead to damage to the aircraft. Hence, although higher efficiency might be obtained by utilizing the exhausting cabin air as an input to the SOFCPU compressor/expander, this was not done for this study.

Weight and performance of the compressor/expander was initially based on a Williams WR2 jet engine. This engine compresses 1 kg/s of air at a compression ratio of 4.1 and weighs 13 kg. In effect, the SOFC power system takes the place of the combustor in the jet engine with compressed air being delivered to the SOFC from the compression stage and hot exhaust gases from the SOFC power system expanding through the turbine. The compressor and turbine combined on the shaft are shown in Figure 2.4 below. The engine is approximately the right size in terms of air flow for the power system operating at about 1.1 atm. To arrive at a weight estimate for various system configurations, the weight was scaled linearly based on the air flow and increased in linear proportion to the number of compression stages required. For example, for the 8 atm case the ratio of compression to existing engine is: (0.279 atm inlet P) $(4.1 \text{ base CR})^n = 8$ atm, where n is the number of repeats of the existing compressor stages in

series required. Solving yields n = 2.38 so the compressor weight estimate is increased by a factor of 2.38 to account for the higher pressure ratio. While it is not clear how accurate the extrapolation based on flow and compression ratio is, the weight impact of the compressor expander is relatively minor as long as construction similar to the jet engine can be used.

Figure 2.4. Compressor (left) and Turbine (right) from a Williams WR2-6 Engine. Outside diameter at compressor is 15cm.

2.2.2 Fuel Cell

The fuel cell is based on a Delphi Gen 4 stack with a new material set which is capable of 1.75 times higher power density than the more established materials currently used. The weight of the stack was taken to be 62kg for a 100 cell stack. This weight represents the current weight of a 100 cell Gen 4 stack design minus a relatively heavy base plate and frame (33.5 kg). When performing the subsequent detailed design a lighter weight header and frame was designed to provide for distribution of the gases into and out of the stacks.

The power density in the stack is a function of anode gas composition, fuel utilization, excess air (which determines average cathode oxygen concentration), the average inlet and outlet temperature of the stack and the operating pressure and voltage. Stack electrical conversion efficiency is purely a function of stack voltage. Appendix C discusses the development of the algorithm used to predict the SOFC power density.

In all cases the stack was assumed to operate with an outlet temperature of 800°C and this temperature was achieved by adjustment of the rate of cathode air supplied to allow a steady state heat balance with 800°C outlet on the stack. The fuel cell anode and cathode are operated at the same pressure and the fuel cell is operated inside a vessel maintained at the same pressure as the fuel cell.

2.2.3 Reforming Approach

Autothermal reforming (ATR), single anode pass steam reforming and anode recycle steam reforming flowsheets were modeled. In general, the anode recycle steam reforming provided significantly higher system efficiency compared to the other approaches. In this approach all steam required for reforming is generated on the SOFC anode such that it is not necessary to generate steam from liquid. In addition, waste heat from the fuel cell drives the reaction allowing heat from the fuel cell to be converted back to fuel in the endothermic reforming reaction. This allows some waste heat to be converted back to fuel and have another chance at being converted to electricity.

Different flowsheets obtained different amounts of power from the compressor/expander. For example for 3 atm and 0.8V the ATR flowsheet obtained 18% of power from the compressor/expander shaft. For the anode recycle steam reformer at the same pressure and stack voltage, only 4.3% of the power was obtained from the turbine. Since the SOFC offers higher efficiency than a turbine, efficiency is maximized by a flowsheet which has more power from the SOFC and less from the turbine as long as electrical power is not required as input to drive the compressor. Also, the decision to configure the system to generate DC power directly penalizes the turbine for losses in converting generated AC power to DC since there is no longer a 235 VAC bus. Figure 2.5 shows the logical layout of the anode recycle flowsheet and Figure 2.6 shows the higher efficiency compared to other flowsheets as a function of stack voltage. Only the anode recycle flowsheet will be discussed further.

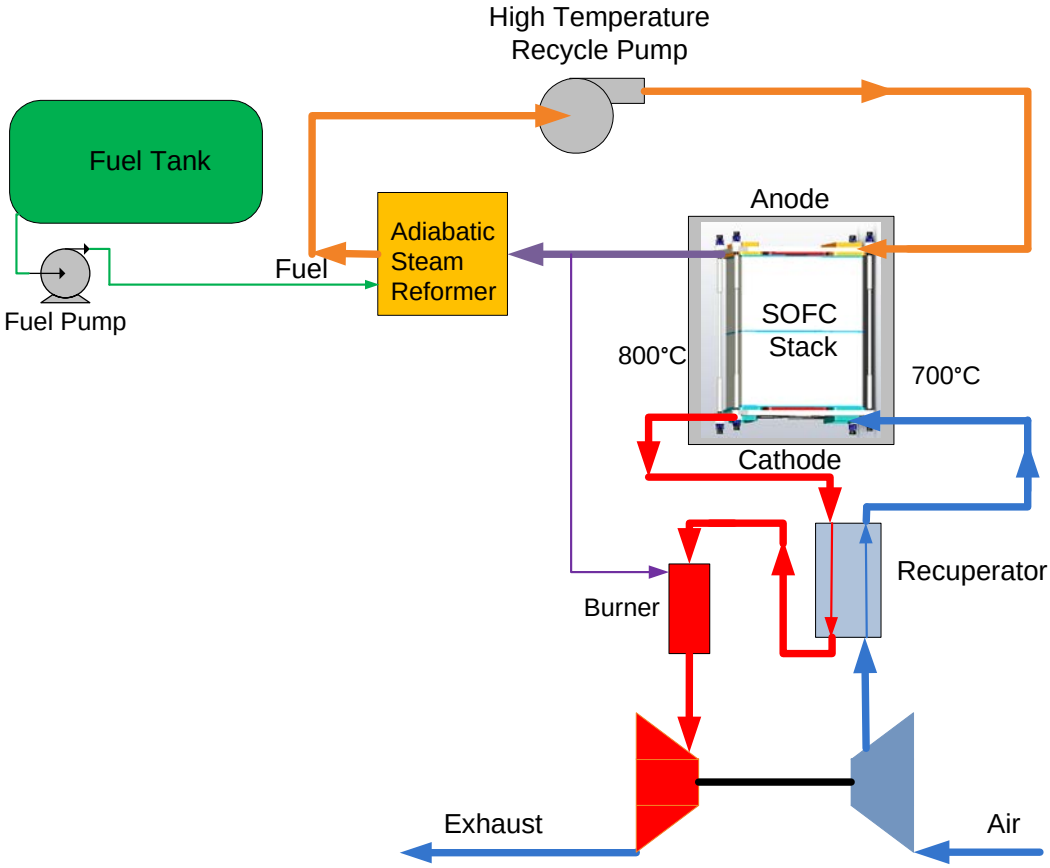

Figure 2.5. Configuration for Anode Recycle Steam Reforming

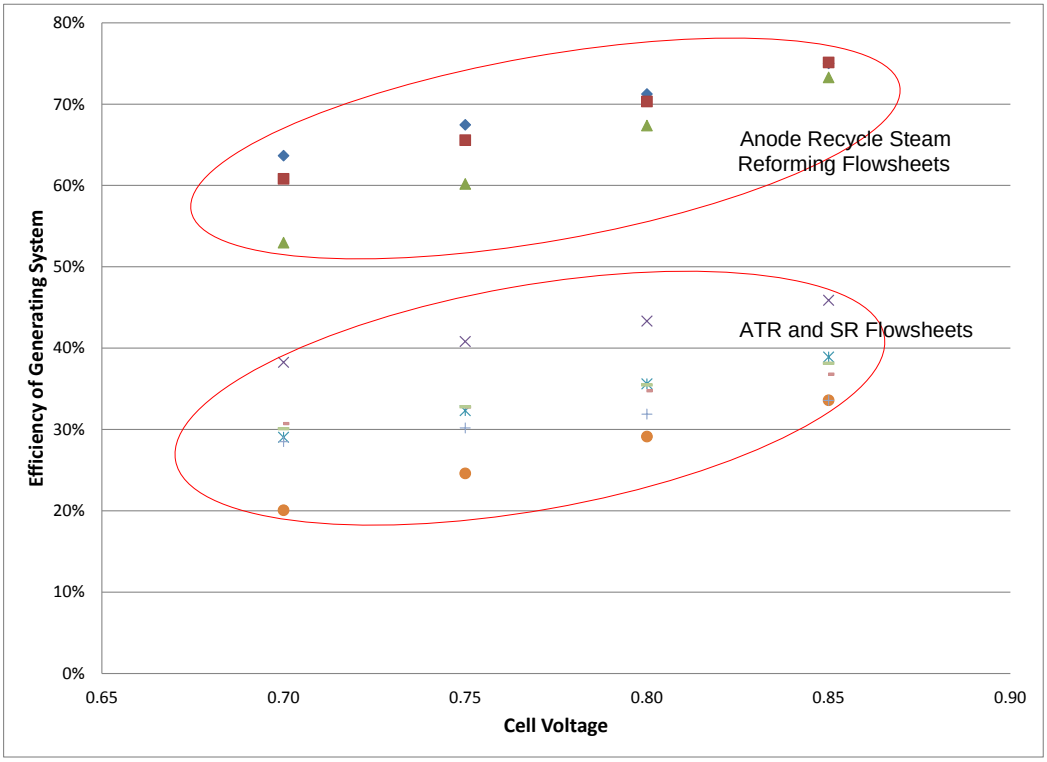

Figure 2.6. Efficiency of Anode Recycle Flowsheet as a Function of Cell Voltage. Points correspond to system pressures of cabin pressure, 3 atm and 8 atm.

2.3 Preliminary Weight Estimates

The system was assumed to be placed in a grade 5 titanium pressure shell designed for a safety factor of 1.5 on yield stress. Other heat exchangers, the anode blower and the reformer were scaled based on an existing SOFC power system operating at 6.29kW at 0.75V. The weight for the 0.75V case was proportioned based on power level. Adjustments for other voltages were then made by proportioning to the change in air flow or fuel flow as appropriate. Base values are shown in Table 2.2.

Table 2.2. Base Values for BOP Weights

Component	Base, kg	Scaling
Cathode recuperator	7.912	ratio to air flow
Anode recuperator	3.33	ratio to fuel rate
Reformer	4.336	ratio to fuel rate
Anode blower	6.46	ratio to fuel rate

Stacks were estimated at 62 kg/100 cells as discussed above. The preliminary weight estimates do not account for the insulation, connecting pipes, support structure, instrumentation and controls. Table 2.3 shows a summary of the anode recycle flowsheet cases efficiencies and system masses for major components.

Table 2.3. Estimated Net Efficiency and Weight Added to Aircraft by SOFCPU Scaled to 972kW (kg)

	SOFC Cell Voltage				
Pressure	0.850	0.825	0.800	0.750	0.700
0.8 atm	75% / 10690	73%/ 7631	71% / 6320	68% / 5291	64% / 5022
1.5 atm	76% / 7698	73% / 6120	71%/ 5379	67%/ 4813	63%/ 4739
3.0 atm	75% / 5837	73% / 5069	70% / 4709	66% / 4509	61% / 4630
5.5 atm	74% / 4867	72% / 4498	69% / 4355	63% / 4397	57% / 4719
8.0 atm	73% / 4485	70% / 4287	67% / 4250	60% / 4507	53% / 4990

The trends in the efficiency and weight impact data are illustrated in Figure 2.7. Solid lines represent the efficiency of the system while dashed lines represent the weight impact to the aircraft of implementing the SOFCPU. As the operating pressure is increased the efficiency declines due to a reduction in the amount of power obtained from the compressor/expander, partially offset by a reduction in parasitic power for anode recycle. On the other hand, the weight impact decreases with higher pressure due to a reduction in the stack weight. At pressures of 1.5 atm or less the weight impact monotonically increases as the voltage is increased due to the increase in stack size. However, at higher pressures the weight decreases as voltage is increased, reaching a minimum at a cell voltage which increases with increasing pressure. This occurs because at high pressure and low voltage the compressor must be driven electrically rather than yielding power. This in turn requires a higher gross power be produced requiring a larger stack. The minimum in the weight impact curve occurs close to the point where the compressor expander power has a small positive balance such that only a small amount of power is produced but no electrical power input is required.

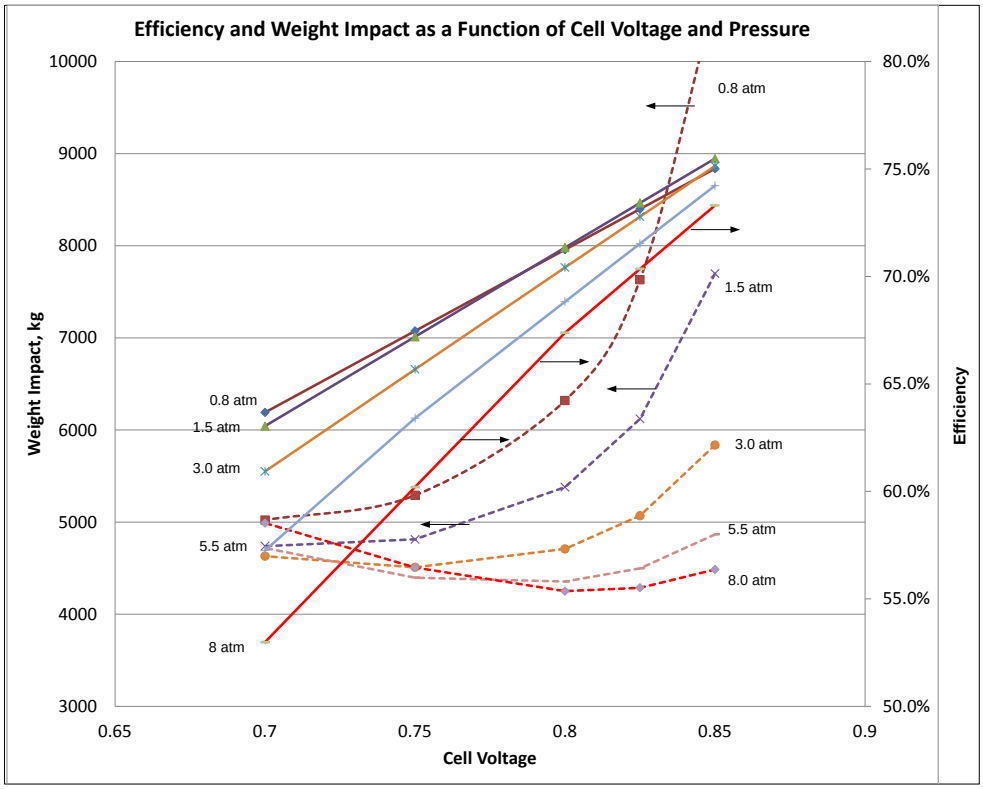

Figure 2.7. Efficiency and Weight Impact as a Function of Cell Voltage and Pressure

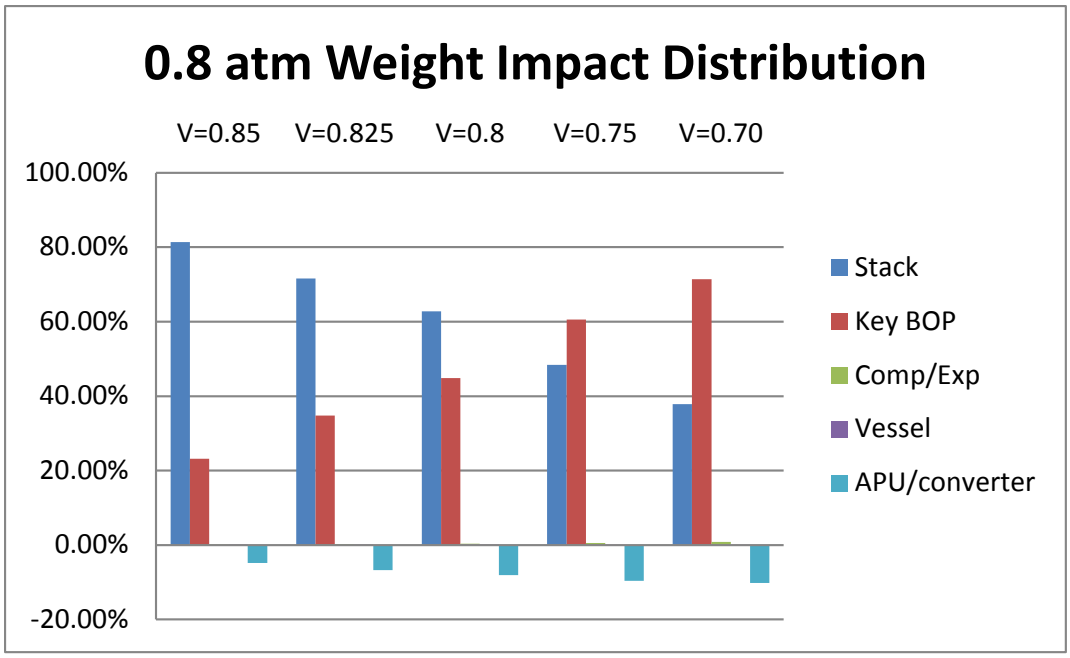

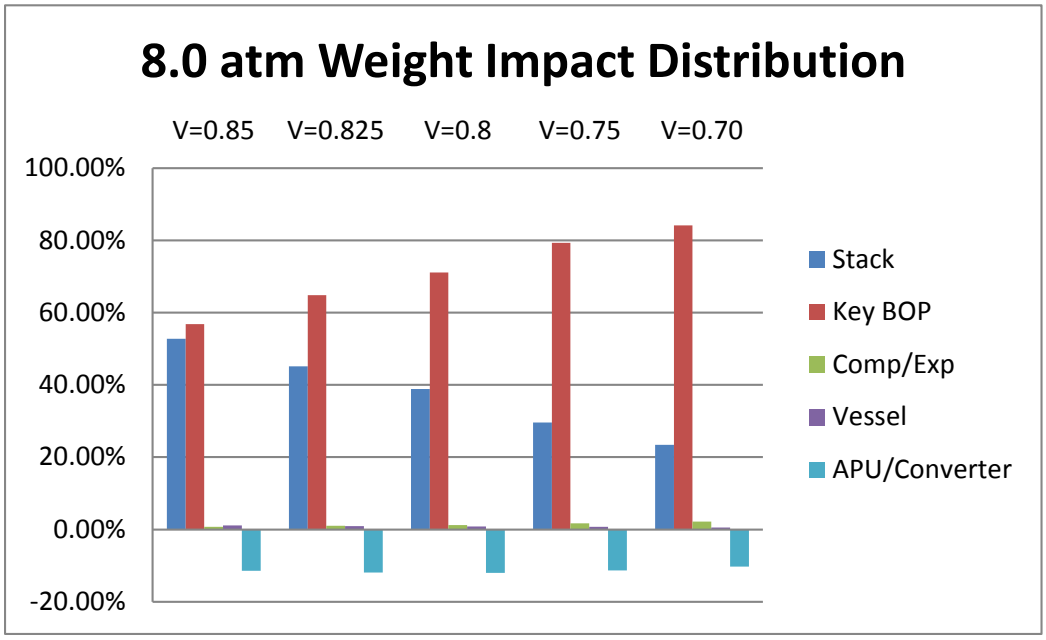

Figure 2.8. Weight Distribution as a Function of Cell Voltage and Pressure for 0.8 (top) and 8.0 atm (bottom)

Figure 2.8 shows that the weight distribution (normalized to 100% total) of the SOFC system shifts significantly between the stack and the key balance of plant items (heat exchangers, anode blower, reformer) as the cell voltage is lowered. This is primarily driven by a reduction in the size and weight of the stack with some increase in cathode recuperator needed to handle higher air circulation rates needed to cool the stack at lower voltages. At high pressure, the impact of the stack weight is significantly reduced due to the increase in stack performance at higher pressure. In the current methodology the weight of the compressor/expander and vessel are minor contributors to the overall system weight.

2.3.1 Fuel Savings Due to Efficiency

The existing engine generators increase fuel burn by 141.4 kg/h to produce 944 kW at 53% efficiency evaluated at the 230 VAC bus. The DC power system produces 972 kWe to the ±270 V bus. The mass rate of fuel savings depends on the SOFCPU efficiency. Table 2.4 provides the mass rate of fuel savings for electrical generation prior to taking into account increases in main engine fuel consumption resulting from increases in aircraft weight.

Table 2.4. Mass Rate of Fuel Savings for Electrical Generation. Does not include effect of SOFCPU mass.

Efficiency	Fuel Burn Rate in SOFCPU, kg/h	Fuel Savings for Electrical Generation over Engine Generators, kg/h
80%	99	42
75%	106	36
70%	113	28
65%	122	19
60%	132	9

2.3.2 Impact of SOFCPU Weight on Aircraft Fuel Consumption

The Piano-X model[1] of the Boeing 787-8 was used to assess the fuel consumption impact of adding weight to the aircraft. Flight distances of 1000, 3000, 5000 and 7000 nautical miles[2] were simulated. For each flight distance the weight sensitivity was assessed by calculating the fuel consumption for a light, medium and heavy payload range.

The light payload was determined as 242 passengers x 95.3 kg = ~23,000kg. This represents an aircraft carrying a load of passengers but negligible additional cargo. The payload was then increased in 1000kg increments to determine fuel consumption for payloads between 23,000 and 28,000 kg. For a medium payload range, payloads ~50% higher were assessed. Fuel consumption rates for payloads between 34,000 and 38,000 kg were calculated.

To define a heavy payload range, the operating empty weight is subtracted from the maximum landing weight of 16,7829 kg to determine a maximum payload of 53297 kg with zero weight of fuel. This defines the highest payload with which the aircraft can safely land. Steps are taken over a range of 47,000 to 53,000 kg payload.

For each simulation, the aircraft climbs to cruising altitude and cruises at Mach 0.85. However, the Piano-X model was allowed to select the numerous flight parameters that affect the overall fuel consumption, including factors such as the aircraft speed and rate of climb to cruising altitude, the initial cruise altitude, the aircraft speed and rate of descent at the end of flight, and the appropriate weight of fuel including reserve fuel. For example, the altitude for most efficient steady state cruise varies with aircraft weight. Figure 2.9 shows Piano-X predictions for fuel consumption at cruise as a function altitude for a range of aircraft weights. This indicates that a lightly loaded 787 cruises most efficiently at ~43,000 ft while a heavily loaded aircraft cruises more efficiently at ~37,000 ft.

[1] Piano-X Copyright 2008, Lissys Ltd. / D Simos (www.piano.aero), 787 data version December 2008
[2] 1 nautical mile = 1.15 miles, abbreviated nm

The Piano-X model calculates the fuel consumed and time required for the climb, cruise and descent portions of the flight. The Piano-X model includes a time and fuel consumption allowance to account for taxi-out, takeoff, approach, and taxi-in, with about 20 min time being allotted to these phases of the flight.

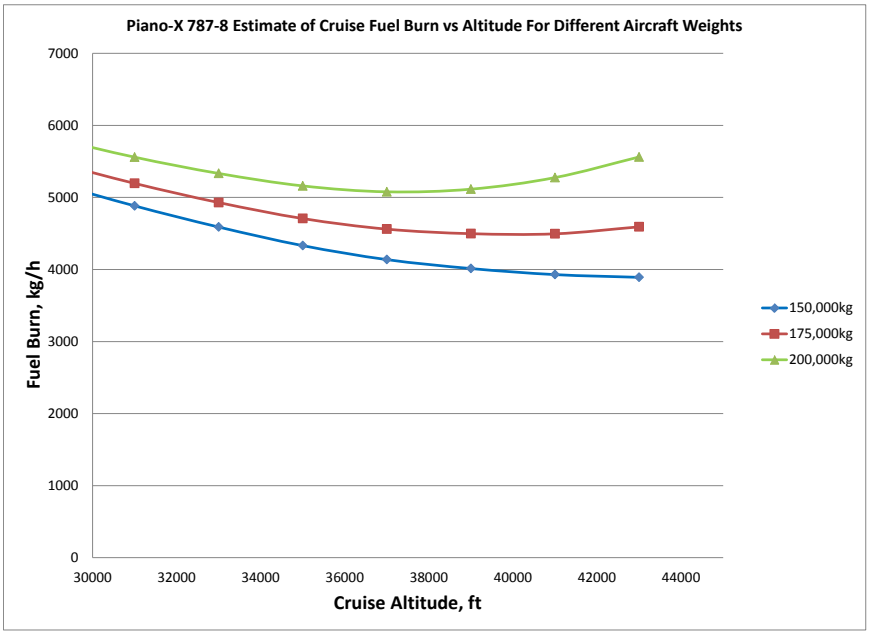

Figure 2.9. Piano-X Predictions of 787-8 Fuel Consumption as a Function of Aircraft Weight and Cruise Altitude

For each specified flight distance and payload the Piano-X model selects the flight parameters and calculates the fuel consumption. As the model responds to different flight distances and payloads it makes discrete step changes in the flight profile to remain within the capability of the aircraft and preserve efficiency. For example, for a 1000 nm flight the model changes the selection of initial cruise altitude from 43,000 ft to 39, 000 ft at a payload of 38,000 kg. This creates a corresponding non-continuous shift in fuel consumption rate as payload is varied. The impact of these discrete steps is minimized by examining the payload to fuel relationship over a broad range of payloads.

Figure 2.10 shows the relationship between fuel consumption and payload. Fuel consumption is expressed as kg per 1000 nm in order to compare different trip lengths. At flight distances of 1000 nm and 3000 nm, the impact of an added kg of weight is to burn an additional 0.053 kg of fuel per 1000 nm of trip. Overall fuel efficiency for the 3000 nm trip is higher because a greater proportion of the trip is at cruise altitude where the aircraft is more efficient. At 5000 nm and 7000 nm the overall fuel efficiency declines relative to 3000 nm and the impact of an added kg of weight increases. The reduced efficiency is the result of the requirement to carry a heavier fuel load during early portions of the flight. Similarly, the increased impact for changes in aircraft weight is due to the fact that if fuel consumption goes up due to an increase in aircraft weight the fuel consumption increases by an additional increment in order to accommodate the additional fuel weight being carried. This effect is less important for shorter flights but becomes more important for longer flights.

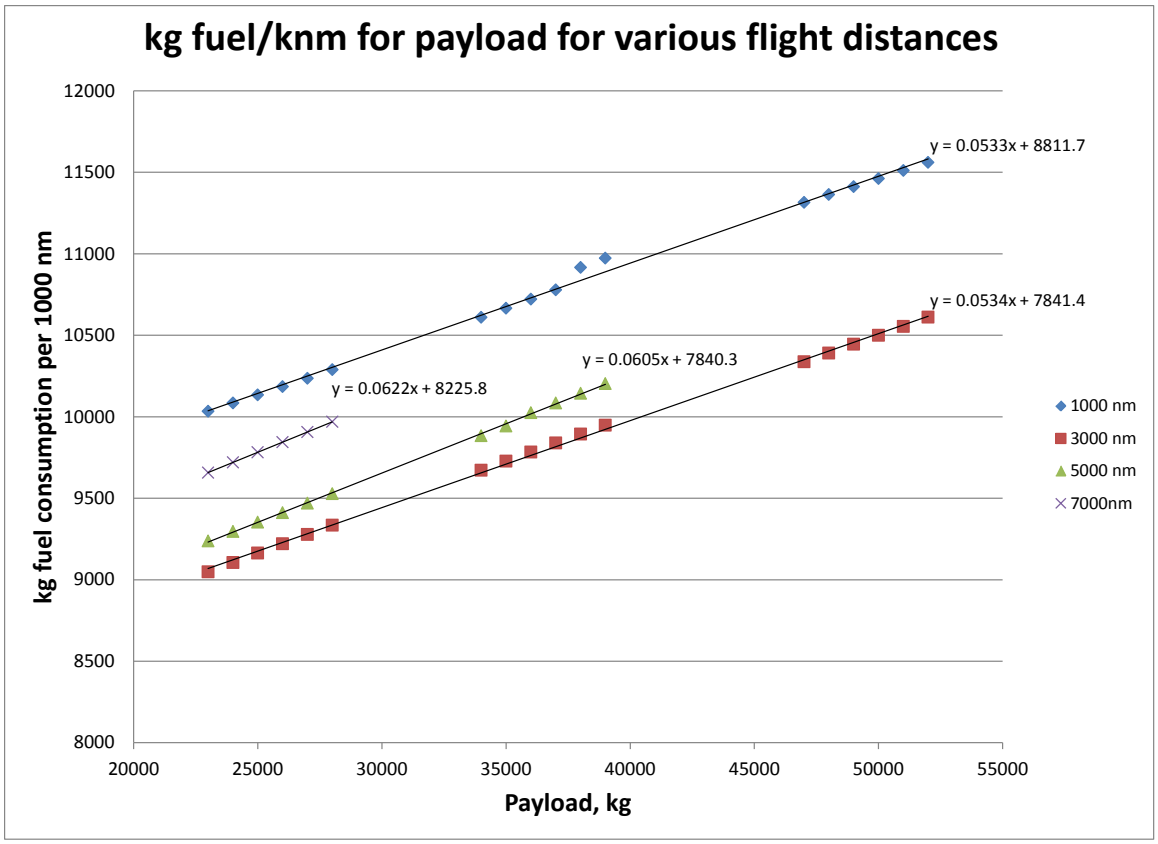

Figure 2.10. Piano-X Predictions of 787-8 Fuel Consumption vs. Payload for Various Trip Lengths

2.3.3 Breakeven Weights

Incorporating the SOFC power system will increase the aircraft weight by an amount equal to the weight of the hardware added minus any equipment (such as the turbine APU) which is eliminated. A breakeven weight is defined to be the weight impact at which the additional fuel consumed as a result of the weight addition is equal to the fuel saved due to the higher efficiency of the generating system.

With a constant rate of electrical generation the fuel saved per unit time is constant throughout the flight. However, the impact of added aircraft weight on fuel burn rate varies with the aircraft operating condition. During the climb and descent phases of a flight the average velocity is about approximately three-quarters the velocity during cruise. For flights up to 5000 nm, the average impact of an added kilogram of aircraft weight on fuel burn rate (i.e., kg/h increase in fuel burn per added kg of aircraft mass) is about 22% to 32% greater in cruise than the average of climb and descent[1]. Thus, for the climb and descent phases the aircraft weight at which fuel consumption will be equal is higher than the equivalent value at cruise. As a result, shorter flights which have a shorter duration cruise segment have higher overall breakeven weights.

[1] For the 7000 nm flight the impact is about 3% less in cruise than the average of climb and descent. It is suspected that this change in weight sensitivity is related to the high takeoff weight associated with the fuel load needed for the 7000nm flight.

A constant electrical generation rate results in more fuel being burned per mile to generate electricity during the climb and cruise segments of the flight while the aircraft velocity is lower. This relationship exists for the engine generators as well as the SOFC. For a given efficiency difference between the SOFC and engine generator, the fuel savings per mile will be greater for a shorter flight with a lower overall average velocity. Figure 2.11 shows the average fuel burn for electrical generation as a function of trip distance. The breakeven weight as a function of SOFCPU efficiency and flight distance is shown in Figure 2.12[1].

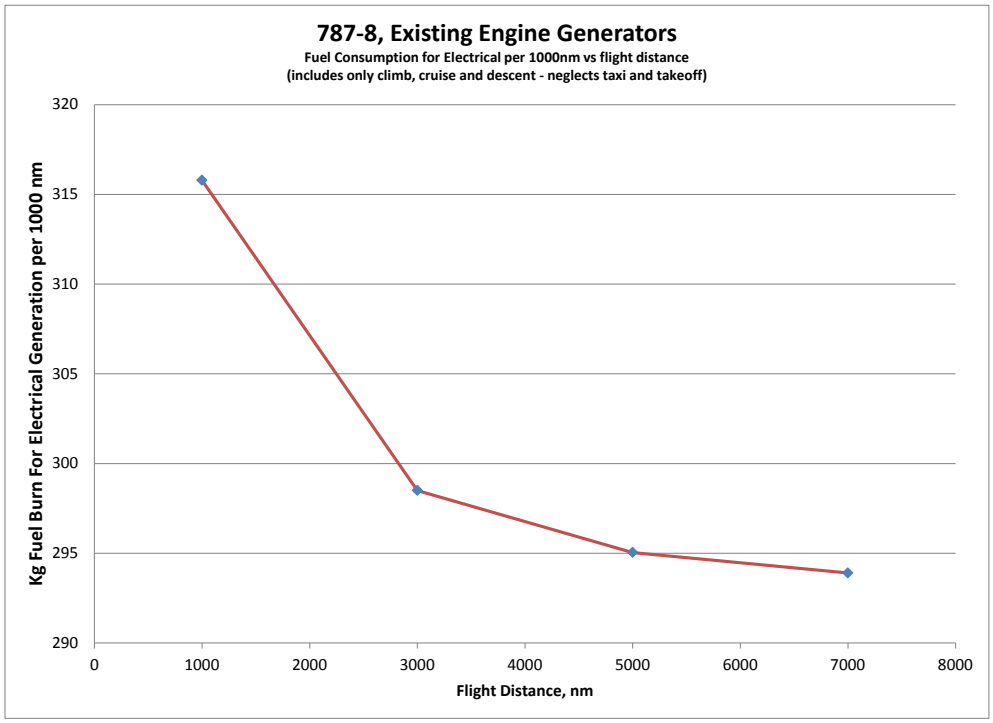

Figure 2.11. Fuel Consumption Per 1000 nm For Electrical Generation Using Existing Engine Generators as a Function of Flight Distance

[1] The plot is generated assuming a light payload in the 23,000 to 28,000 kg range. Similar plots for medium or heavy payloads could be prepared but a medium payload plot would exclude 7000 nm and a heavy payload would exclude 5000 nm and 7000 nm distances since these are beyond the capability of the aircraft.

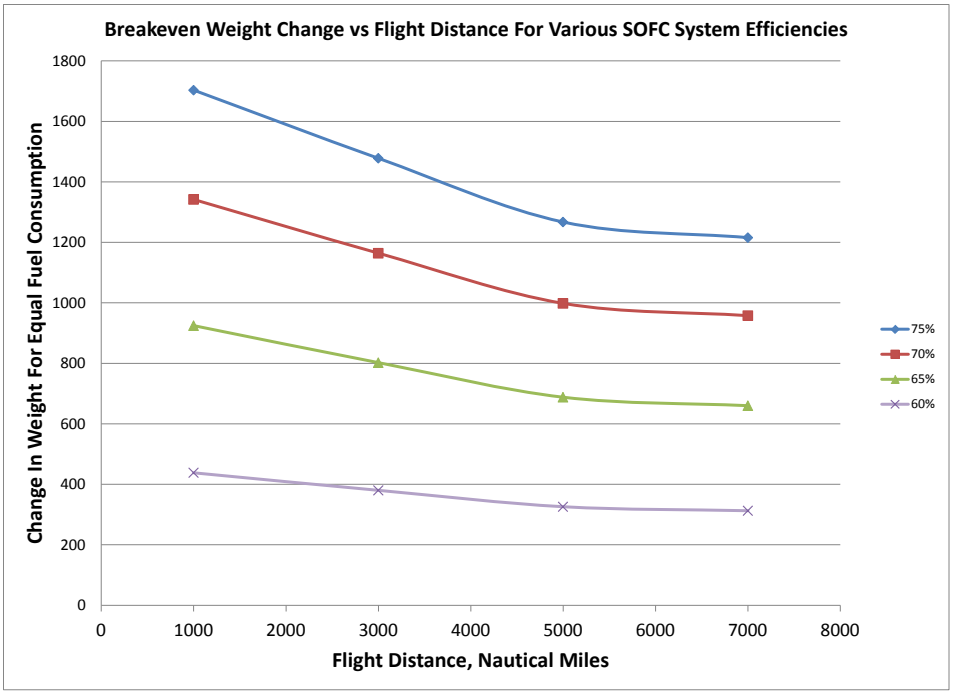

Figure 2.12. Breakeven Weights (kg) for Different System Efficiencies and Flight Distances

Also, the total time over which electrical power is generated includes taxi time during which fuel is burned for electrical generation but distance is not achieved. This effect has not been taken into account in Figure 2.12. Fuel savings during taxi-in and taxi-out would be equal for all flight distances but the effect per 1000 nm is greatest for shorter flights. About 13% of the total time is on the ground for a 1000 nm flight while for a 7000 nm flight the portion of the time is only ~2%. Additional discussion of the impact of ground operations fuel savings is provided in Appendix B.

It should be noted that the discussion to this point assumes constant operating efficiency for both the engine generators and SOFC electrical generation systems. In reality the performance of actual systems will vary based on conditions. The efficiency of the engine based generators while the engines are at very low power while taxiing on the ground is not known. Also, the SOFC compressor expander performance will vary with aircraft speed and altitude due to the impact on the compressor expander power.

2.3.4 Comparing Breakeven Weight to Estimated Weight Impacts

The break even weight for a given SOFC system efficiency can be compared to the estimated weight impact for that system to determine how much over, or under, the breakeven weight various system configurations may be for various trip lengths. This comparison is made for a cell voltage of 0.825 V/cell and 8 atm operating pressure in Figure 2.13.

Figure 2.13. Plot Comparing the Estimated System Weight in Scoping Calculation to the Breakeven Weight for 8 atm, 0.825 V/cell

The difference illustrated in Figure 2.13 indicates the reduction in the estimated system weight that would be required before the SOFC system would save fuel consumption for a given length of trip. The extent of weight reduction needed is less for shorter flights.

Initial weight estimates do not yet include insulation, connecting ducting and tubing and support structure. The weight of these items will increase the weight savings required to achieve the breakeven weight. However, the full benefit of elevated pressures is not reflected in balance of plant hardware which will tend to reduce weights at higher pressures. The difference between the breakeven weight and the estimated system weight can be calculated for a variety of system pressures and cell voltages to determine an optimum range that provides the smallest difference between the estimated weight and breakeven weight over a range of trip lengths. These plots are produced below in Figure 2.14 and Figure 2.15.

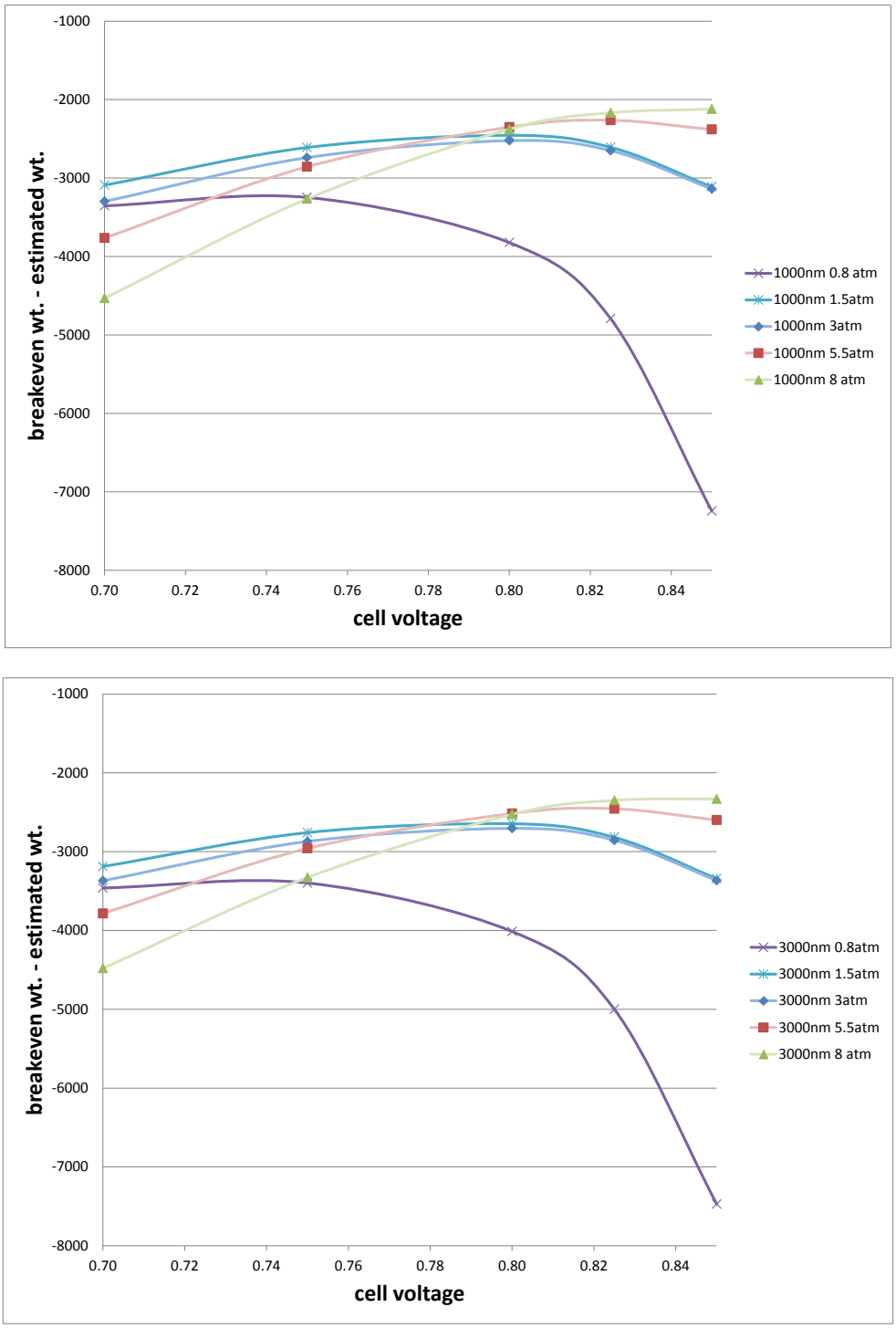

Figure 2.14. Breakeven Weight (kg) Minus Estimated SOFC System Weight as a Function of Operating Pressure and Cell Voltage. Top, 1000 nm trip length, bottom 3000 nm trip length.

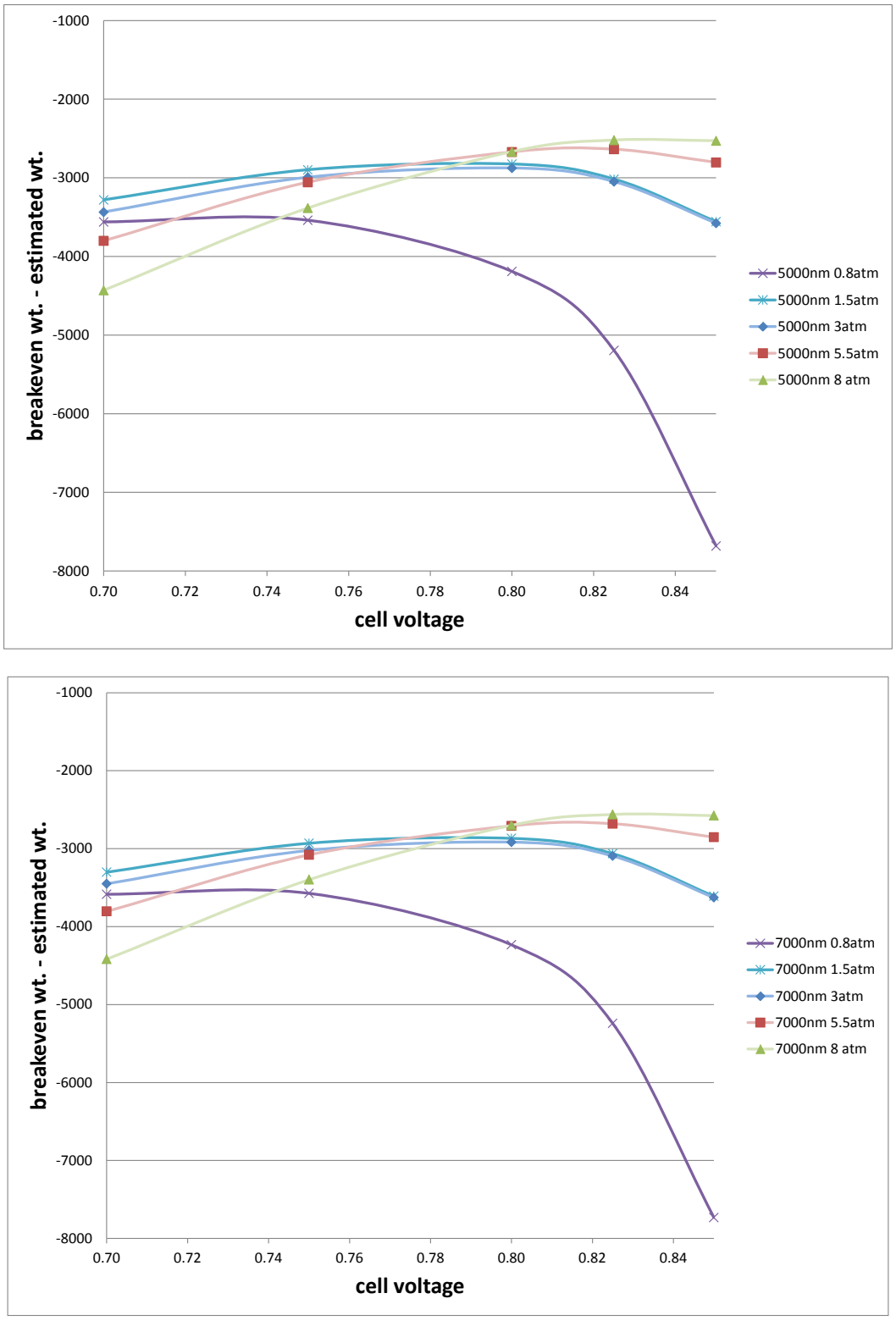

Figure 2.15. Breakeven Weight Minus Estimated SOFC System Weight as a Function of Operating Pressure and Cell Voltage. Top, 5000 nm trip length, bottom 7000 nm trip length.

The first observation from the plots is that the spread between the estimated weight and the breakeven weight is significantly smaller when operating with the fuel cell pressurized to at least 1.5-atm pressure. This advantage is related to a reduction in the size and weight of the stack required. As higher pressures are used further reductions in the stack weight are achieved but at the cost of system efficiency. As pressure increases the minimum difference between system weight impact and breakeven weight occurs at higher cell voltages.

The overall optimum performance condition occurs at 8 atm and 0.825 V. However, the 5 atm and 0.80 V/cell is nearly as good.

3.0 Conceptual Design for 8 atm, 0.825 V/cell

The preliminary calculations suggest that the conditions that will come closest to achieving the breakeven weight are about 8 atm and 0.825 V per cell. This section will develop a preliminary design in greater detail to improve the estimate of the overall weight impact and system performance. In order to take credit for elimination of the Turbine APU the SOFC power generation is separated into three independent systems, each contained in its own pressure vessel with its own compressor/expander. This provides redundancy, making it unlikely that a single failure could result in a critical loss of electrical generation capacity. The high level conceptual layout for the system is shown in Figure 3.1.

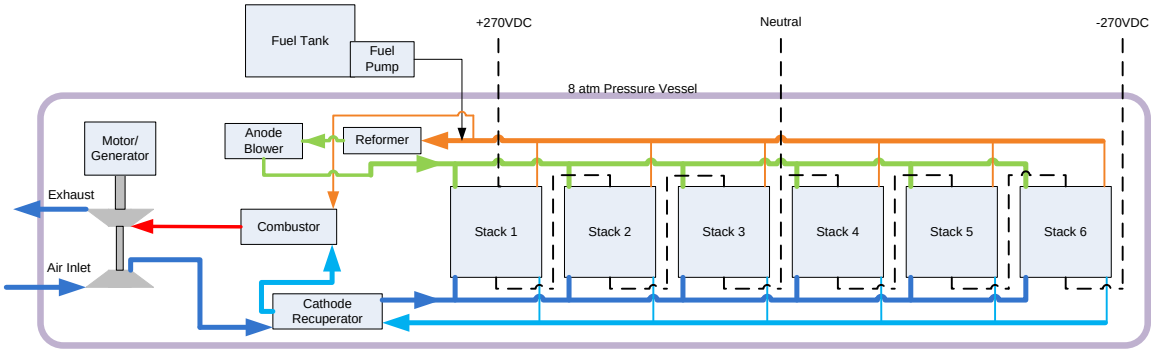

Figure 3.1. Conceptual Layout of SOFC Power System. Three independent systems are envisioned to provide redundancy.

The design of the system was completed based on a gross DC output of 821 kW. Based on corrections to the 787 electrical system efficiency inputs it is expected that the actual power output would need to be approximately 972 kW. Rather than redesign the system to accommodate the higher power level, the power density of the 821 kW system will be assumed to be representative and linearly scaled to estimate the weight of the 972 kW system (i.e. multiplied by 972/821 = 1.18). The details of the system are broken down into categories similar to the breakdown used for the scoping calculations, as follows:

3.1 SOFC Stacks

The fuel cell design is based on the Delphi Gen4 stack, although several modifications are assumed to be made to tailor the stack to the current design. Power density in the active area of the cell is estimated to be 0.76 W/cm^2 at 0.825 V/cell. This represents a significant increase compared to power density in the Delphi APU which is believed to operate with about 0.27 W/cm^2 at 0.8 V/cell. Several changes contribute to this 2.8X increase in power density:

- A recently developed material set which shows power densities 1.75X higher than the previous material set is assumed to be used for the SOFCPU. (see Appendix C)
- The fuel cell is operated at 8 atm absolute pressure. Compared to operation at 1 atm, this provides a 2.32X increase power density. (see Appendix C)
- The operating voltage is selected to be 0.825 V/cell which improves efficiency but reduces power density by a factor of 0.84X compared to what would be obtained at 0.8 V/cell.

- The remaining factor, a ~0.82X[1] reduction, is attributed to the reforming approach and flowsheet configuration. The aircraft system uses anode recycle steam reforming compared to the Delphi APU which uses POX with limited anode recycle. While this choice results in a reduction in power density due to dilution with steam and CO_2, the impact is modest since dilution with nitrogen is avoided. Anode recycle steam reforming provides a critical boost to overall system efficiency due to the conversion of waste heat to chemical energy. In addition, the fact that 85% of the anode exit gas is recycled improves the overall fuel utilization.

The stacks containing the new material set and operating at 8 atm are modified and arranged as follows:

- The stacks are organized in stacks of 109 cells in order to provide 109*0.825 = 89.9V or ~90 V/stack. This is taller than the nominal 30-cell Delphi Gen4 APU configuration although Delphi has modeled up to 100 cells to assure adequate flow distribution.
- In each of 3 independent systems, six stacks connected electrically in series with a ground connection in the center of the series to provide ±270 VDC. This results in a total of 6 * 109 = 654 cells in each of the three systems.
- The active area flow length is increased by a factor of 1.36 in order to bring the total power for 3 systems to 821 kW. This adds 2.13 in. (5.4 cm) to the flow length, increasing the cell footprint to 12.613 in. x 11.58 in.[2]
- Connections to the stack are made anode on one end and cathode on the other rather than using a manifold plate connecting both flows from one end. This is done to reduce the weight.
- Pressure drop across the active area portion of the cell is intentionally increased to 24 in. H_2O and the sizes of the anode and cathode header holes adjusted to improve flow distribution as described below.

3.1.1 Stack Flow Distribution

Detailed calculations were performed to assure adequate flow distribution could be obtained within the SOFC stacks[3]. The higher power density, the increase in active area, and the increase to 109 cells all act to increase the molar flow of gas in the stack headers. However, operating at 8 atm reduces the velocity of gases in the headers which reduces the pressure variations that lead to flow mal-distribution. The higher pressure also lowers the velocity in the active area of the stack which reduces the pressure drop across the cells, and it is the pressure drop across the cells that acts to even out the flow distribution.

In order to get an acceptable flow distribution the pressure drop across the cell was increased significantly for both the anode and cathode flow channels to provide a total static pressure drop across the cell of 24 in. water. The sizes of the anode and cathode headers within the cassettes were then adjusted within the space available to optimize the flow distribution. The final flow distribution was well

[1] i.e. 2.8X increase in power density= (1.75X material set)(2.32 pressure)(0.84 cell voltage)(0.82 reforming)

[2] If the cell length were not increased the power output would be (3 systems)(654 cells/system) (403 cm2/cell)(.7643 W/cm2) = 604.3 kW. In order to match the target power output of 821kW the flow length of the active area is stretched by a factor of 821kW/604.3kW=1.36. This matches gross stack power to the net power requirement which is conservative since the expander provides slightly more power than the compressor consumes which adds about 1.3% to the net power.

[3] Calculations were performed in a manner described in: "Flow distribution in piping manifolds" R. L. Pigford, M. Ashraf, YD Miron, Ind. Eng. Chem. Fundamen., 1983, 22 (4), pp 463–471

within Delphi criteria for adequate flow distribution. Leveling the flow through an increase in stack pressure drop was judged to be preferable to expanding the stack frame to accommodate larger headers which would have increased the weight. Additional detailed information on the stack flow distribution is provided in Appendix D.

3.1.2 Stack Weight

The stack frame is similar to the Delphi Gen4 stack. The major difference in weight is related to stretching the dimension in the flow dimension in order to accommodate an increase in the flow distance over active area by 36%. This increases the cassette dimension in the flow direction from 9.451 in. to 11.578 in. The weight per cell increase due to the stretch is 620g to 759.5 g. The weight of a bare stack is then 759.5 * 109 = 82.8 kg.

In addition to the cells, a load frame was added to the stack as shown in Figure 3.2 below. The purpose of the load frame is to maintain the stack under compression at all times to protect the seals within the stack. The load frame serves a dual purpose of holding the header connections onto the top and bottom of the stack. Both the header boxes and load frame are electrically isolated from the stack itself through non-conductive gaskets. The load frame and header connection boxes are expected to add 13 kg to the stack weight resulting in an overall stack weight of 95.8 kg.

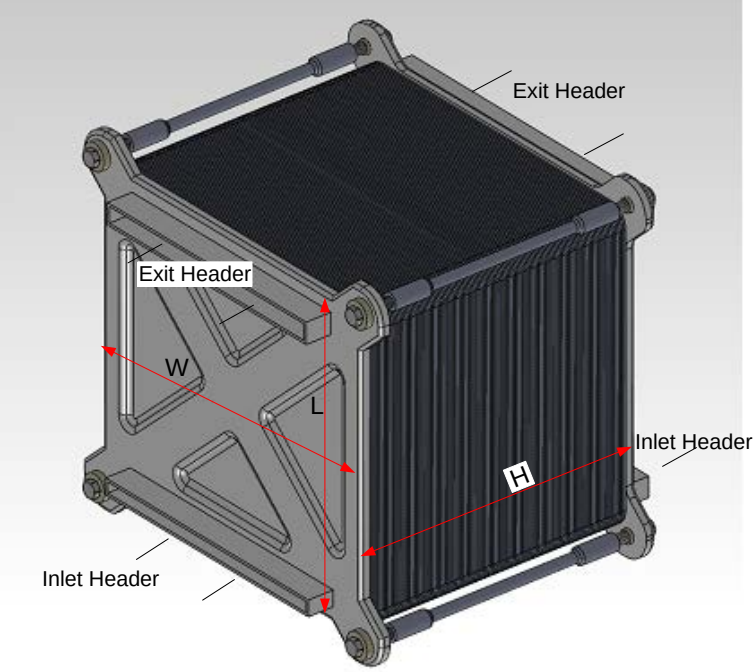

Figure 3.2. An Assembled 109 Cell Stack. Dimensions are 12.613 in. W x 11.578 in. L x 11.049 in. H. Header connections connect anode to one end of stack and cathode to other end with headers distributing flow in a “U” configuration for both sides.

3.2 Compressor/Expander

Due to the need to separate the generating system into three independent systems, each with a dedicated compressor/expander, the desired compressor must be scaled down by a factor of 3 in air flow relative to the Williams WR2. At the same time, the compression ratio must be increased from 4.2 to about 28.6 meaning several stages of compression would be required. Increasing the compression ratio is achieved by adding successive stages of compression to the shaft. In order to address the question of whether efficiency can be maintained as the scale is reduced, the thrust specific fuel consumption of smaller jet engines was examined.

3.2.1 Extrapolation Based on Jet Engines

At sea level, the Willams WR2 generates 125 lbf of thrust at a fuel consumption rate of 1.25 lb/h per lbf of thrust.[1] An engine generating 45 lbf of thrust at thrust specific fuel consumption of 1.50 lb/h per lbf has been developed by Ewald Schuster.[2] This engine moves 0.372 kg/s air at a pressure ratio of 3.5 while turning 100,000 rpm and weighs 6.5 lb. JetCat USA makes a number of smaller jet engines intended for large scale model aircraft with thrust capability between 13 and 45 lbf[3]. The model P120SX engine, shown in Figure 3.3, generates 30 lbf thrust or about one-quarter the thrust of the Williams WR2 with a thrust specific fuel consumption of 1.50 lb/h per lbf similar to the Schuster engine. Hence, fuel consumption per unit thrust for these two engines increases by 20% (1.50/1.25=1.20) when scale is reduced by a factor of 3 to 4. It is difficult to determine the degree to which this reduction in efficiency is the result of scale and the degree to which other design factors may affect the engine efficiency. Factors other than scale are likely since Williams produces engines for military applications while the smaller engines are targeted at hobbyist projects. However, it does appear it is possible to maintain reasonable efficiency when scaling down to the degree needed to split the air compression into three independent systems.

[1] Turbofan and Turbojet Engines: database handbook, by Elodie Roux. Available via Google books at: http://books.google.com/books?id=_5vA_5XK33sC&lpg=PA569&ots=oNXsP8u2r1&dq=GE%2090%20Elodie%20roux&pg=PA194#v=onepage&q&f=false

[2] http://cpl.usc.edu/eschuste/

[3] http://www.jetcatusa.com/p200.html

Figure 3.3. JetCat USA P120-SX Engine. The engine is 4.4 in. in diameter, weighs 3.1 lb, and generates up to 30 lbf thrust at 125,000 rpm. Fuel consumption at maximum power is 45 lb/h.

For purposes of the scaled design the JetCatP-200 engine was used as the basis for size and mass. This engine is 5.2 in. in diameter, weighs 5 lbs, and generates 52 lb thrust at 112,000 rpm. The length was stretched and the mass tripled to account for the need for three compression stages. This provides a total weight of 6.8 kg.

In addition to scaling to the desired airflow, the compressor/expander faces a challenge in that it is desired to maintain a constant SOFC pressure regardless of the static pressure, relative velocity and temperature of air outside the aircraft.

The main aircraft engines face a similar challenge in that they must operate over a range of altitudes and velocities which varies the inlet temperature and inlet/outlet pressures. The challenge differs in that the SOFC compressor will need to operate at nearly constant compressor outlet pressure over a smaller range of air flows while the engine may not need constant compressor outlet pressure but needs to operate over a wide range of air flows ranging from high rates for takeoff and climbing to low rates while idling. Axial compressors on aircraft engines use some combination of bleed valves and variable stator vanes to allow operation over a wide range air flowrates as well as over a range of air intake and exhaust pressure conditions. Bleed valves allow air from the compressor stages to be released. Variable stators pivot to alter the amount of air being compressed. These measures are necessary to prevent a surge condition in which flow reversal in the compressor causes unstable operation. Similar measures may be required for the compressor/expander designed for the SOFCPU in order to provide the desired flowrate of air at a constant controlled pressure while the aircraft operates at different altitudes.

The speed control of the SOFCPU compressor expander will be accomplished using a motor-generator that will convert excess power to electrical energy, or under conditions where more shaft power is needed, convert electrical energy into shaft power. If needed, pressure control could be improved by placing compression and expansion turbines on separate spools with each tied to a motor generator. The compressor would then be linked to the expander via an electrical link between the motor generators allowing the compressor and expander shafts to operate at different velocities. Alternatively, this might be done only with one compressor and one expander stage in order to minimize efficiency losses associated with the electronic link. Electronically linking the compressor and expander is similar to an

approach being investigated for automotive turbo-chargers.[1] In the case of the turbo-charger the objective is to allow the boost pressure to rise before the energy is available in the exhaust, eliminating the lag in turbo power.

In the event the compressor cannot maintain 8 atm in the SOFC there would be an option to reduce the voltage in the SOFC in order to increase power when pressure is low. However, this is undesirable as it would reduce the SOFC efficiency and introduce additional losses due to the need to provide DC/DC conversion to restore the ±270VDC bus voltage.

Finally, it may be necessary to either coat chrome containing metal alloy surfaces in the compressor, or make the parts from an alloy that either forms a non-chromia surface or does not contain chrome in order to prevent chrome volatility and resulting poisoning of the fuel cell cathode. If the compressor itself is fabricated in titanium this would eliminate concern over chrome volatility. Chrome volatility is a greater concern in the cathode recuperator and the issue is discussed further in that section.

3.2.2 Comparison to Extrapolation using Turbochargers

The operation of the SOFC compressor/expander is conceptually similar to a turbo charger on an internal combustion engine. In each case, air is compressed, used for combustion and hot exhaust gases are expanded to recover mechanical energy to drive the compressor. In the turbocharger a cooled charge is delivered to the engine (using a charge cooler) while in the SOFC and jet engine application it is desired to maintain the temperature of the compressed gas to improve efficiency. Most automotive turbocharger compressors are made in aluminum alloy due to the moderate level of compression (and corresponding temperatures) being achieved. Higher performance turbo chargers use titanium compressors to improve strength at high temperature. For the SOFC compressor-expander, the compressed air is expected to be on the order of 500°C meaning aluminum compressor materials would not be compatible. While materials issues could be avoided by cooling between multiple compression stages this would also cool the exhaust gases via a reduction in the temperature at the cold end of the recuperator and would adversely affect the power obtained from the expander.

Despite these differences, the comparison to a turbo charger may be useful from the standpoint of confirming the approximate size of equipment required. In addition to requiring a higher compression ratio than achievable in a single stage turbocharger, the design of the SOFC system compressor-expander is complicated by the fact that it must operate both under conditions at sea level and at cruise altitude. This implies it must have a different compression ratio at cruise altitude than it does on the ground. Prior to takeoff, the air inlet is at the ambient ground temperature and both inlet and outlet are at ~1 atm. Cruising at Mach 0.85 at 40,000 ft the inlet pressure is estimated to be at about[2] 0.28 atm and -30°C while the exhaust exits to a pressure of 0.185 atm. The desired compression ratio at 40,000 ft is 8/0.28 = 28.6 while at ground level a compression ratio of 8/1 = 8 is desired.

Single stage turbocharger pressure ratios top out in the 4 to 5 range with some turbochargers designed for very large diesel engines being capable of pressure ratios up to 5.25. To achieve a pressure ratio of 28.6 multiple stages of compression would be required. About three stages of turbo charging operating at

[1] http://www.aeristech.co.uk/

[2] This is estimated as the stagnation condition for air at Mach 0.85 with free stream conditions of 0.185 atm and -56.7C corresponding to 40,000 ft altitude.

a pressure ratio of 3.057 would provide approximately the appropriate compression at cruise altitude (i.e., 0.28 atm x (3.057)^3 = 8 atm). At atmospheric pressure, a compression ratio per stage of about 2.0 would be desired (1 atm x 2.0^3 = 8 atm). The system has an air flow of about 50 lb/min.

Variation in compression ratio can be achieved by varying the turbo speed. A sample performance map for a turbocharger that is approximately the right scale for the air flow is shown in the Figure 3.4.[1] At the left side of the diagram the performance map is limited by the surge line. At this condition too much air compression is occurring resulting in unstable operation. Operation at this condition can damage the compressor. The right hand side of the diagram is bounded by the choke line. This is a qualitative limit defining a region in which there is insufficient air compression and efficiency is dropping rapidly with increasing air flow. Speed lines run between the surge and choke limits. Contours of constant efficiency are plotted which show how efficiency varies with mass flow and speed. The red circle indicates where the turbos would operate at cruise altitude (~103,000 rpm, PR=3). The green circle indicates the operating point for sea level (~84000 rpm, PR=2). At intermediate pressures the speed would be selected to provide the desired operating point along the green line to achieve the pressure of 8 atm at the SOFC. It is envisioned that each compressor expander stage would be installed on a shaft with an electric motor generator which would be used to control the shaft speed.

The approach to speed control is similar to a new turbocharging technology being developed for automotive applications in which each the expander and compressor are electronically rather than mechanically linked[2]. Applying this approach to an axial compressor such as the miniature jet engine would provide the added flexibility in that the speed of the compressor and expander would not need to match, making precise control of the SOFC pressure more straight forward under transient conditions.

[1] Explanatory Labels added to figure obtained from:
http://www.turbobygarrett.com/turbobygarrett/catelog/Turbochargers/GT40/GT4088R_751470_4.htm
[2] http://www.aeristech.co.uk/

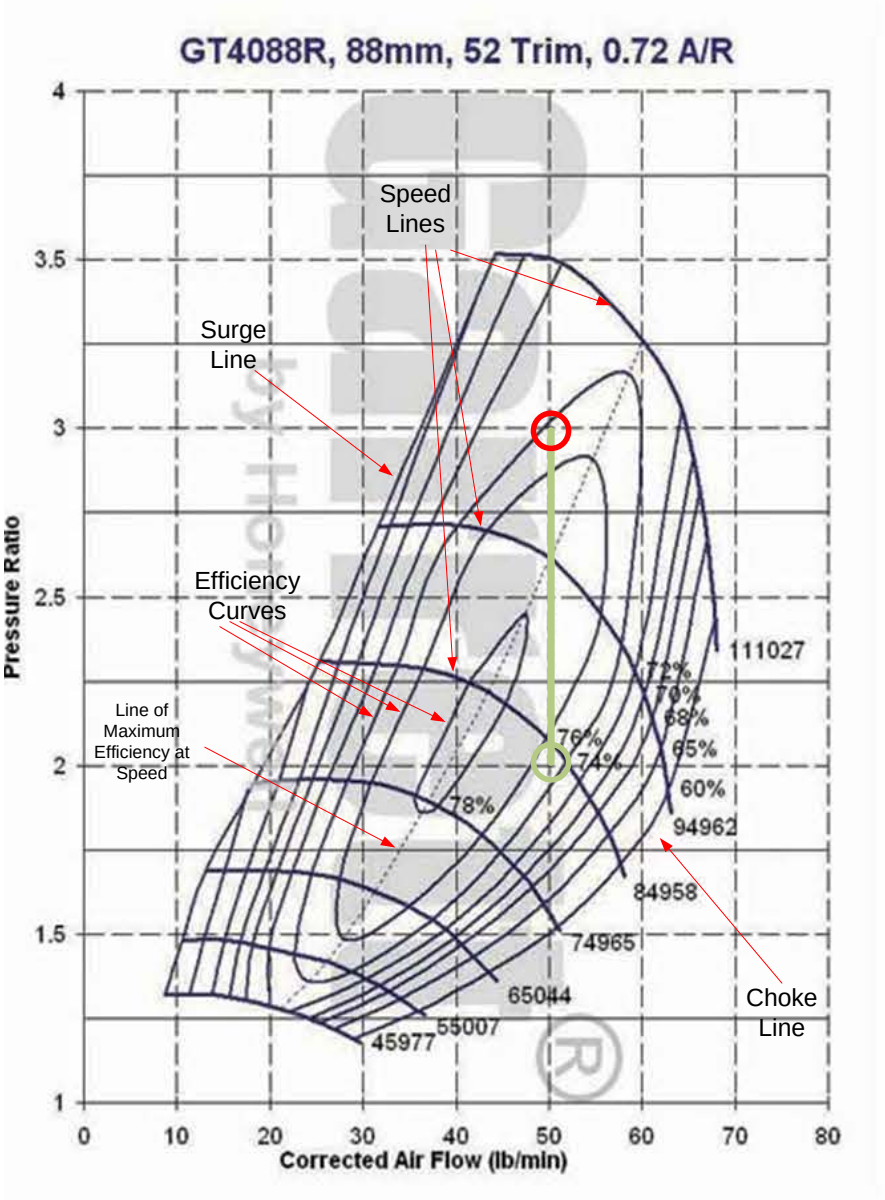

Figure 3.4. Compressor Map for Turbo Capable of 50 lb/min at a Pressure Ratio of 3.[1] Circle added to show operating point for that condition.

[1] Map and subsequent dimensions from
http://www.turbobygarrett.com/turbobygarrett/catelog/Turbochargers/GT40/GT4088R_751470_4.htm

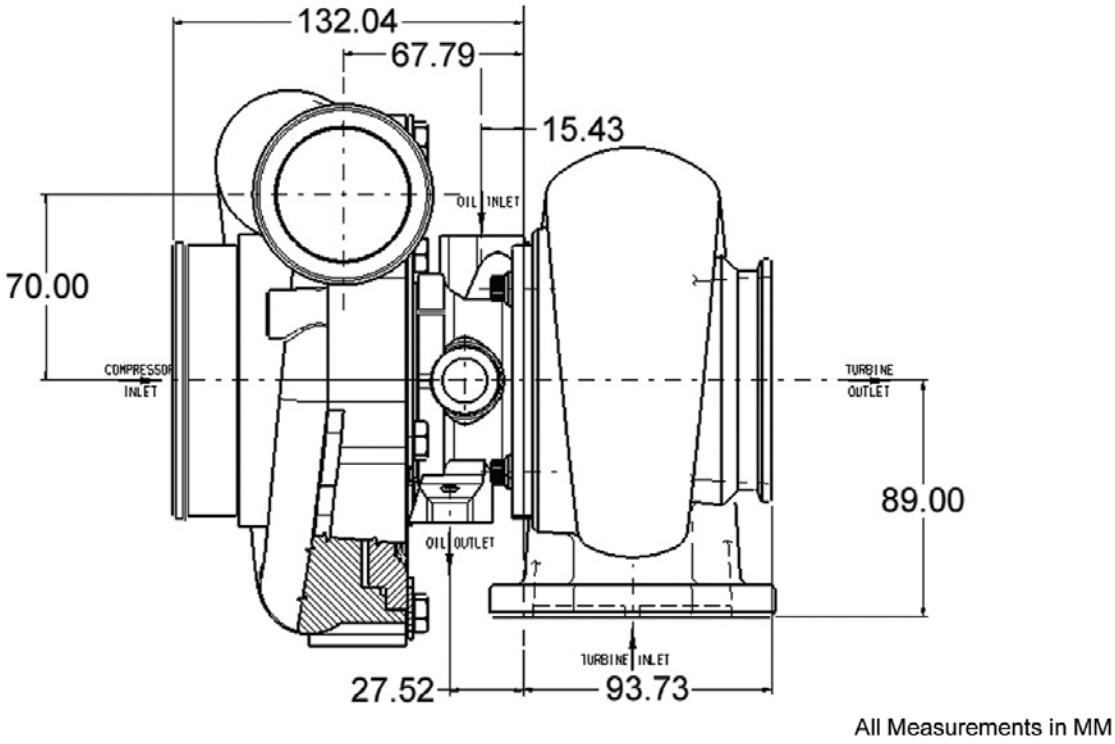

Figure 3.5. Dimensions on Turbo for Map Shown in Figure 3.4

Figure 3.5 shows the size of the selected turbocharger. The design would require 3 such units and in the actual design the size would vary with the air pressure making the each successive stage of compression smaller than the previous due to the relative volumetric air flow in each stage.

The overall size of the turbocharger tends to confirm the conclusion based on the Williams WR2 jet engine that the size and weight of the compressor-expander is unlikely to be a critical factor in determining the feasibility of the SOFC power system.

At an operating pressure of 8 atm, efficiency of the axial compressor will be a key to achieving efficient operation of the SOFC power system. Modeling of the system assumed 80% efficiency in the compressor based on the Williams WR2 jet engine compressor which achieved a pressure ratio of 4.1. Typical aviation axial compressors have pressure ratios per stage of 1.15 to 1.6 and exhibit efficiencies of 80 to 85%.[1] There do not appear to be examples of multi-stage axial compressors in the desired size range. The Williams WR2 compressor as well as typical turbochargers have a radial or centrifugal blade exit which compared to an axial flow arrangement may introduce a larger increment in size per additional stage as well as a greater flow loss between stages making it harder to maintain efficiency. Similar concerns apply to the expansion section. Designing for more than one operating point presents an additional challenge. The efficiency of the turbocharger shown above approaches the assumed 80% value used in modeling at maximum efficiency but is only about 75% at the selected operating points. Presumably, a compressor would be designed for maximum efficiency at cruise condition and would then need to accept a slightly lower efficiency when operating at other compression ratio conditions.

[1] See table 1 in chapter 2 of www.netl.doe.gov/technologies/coalpower/turbines/refshelf/.../2.0.pdf

3.2.3 Option for Compressor/Expander Outside the Pressure Shell

The compressor/expander is located primarily inside the pressure shell with the inlet and exhaust lines penetrating the pressure shell. This allows the gas temperatures at the point where the penetration of the pressure shell occurs to be compatible with the titanium pressure shell. The exhaust gases are reduced to ~250°C during the expansion.

However, the turbo-compressor/expander is expected to operate at high rpm (in the neighborhood of 100,000 rpm), and while the service interval is not determined, it is likely to be the most demanding component in terms of maintenance. Other mechanical components include the fuel pump located outside the pressure shell and the anode recycle pump which is inside the pressure shell but operates at a lower speed and lower pressure ratio compared to the compressor expander. Because it is inconvenient to open the entire pressure vessel cross section to perform maintenance, it may be desired to move the turbine outside the pressure shell. Moving the turbine outside the pressure shell will require careful consideration of the high temperature (740°C) combustion exhaust line as it passes through the pressure vessel. The compressed gas from the turbine at ~500°C is also a concern.

The assumed alloy of the vessel Ti-6Al-4V is typically applied only up to ~350°C. The highest temperature Ti alloys offer useful maximum temperatures up to about 600°C (Gogia 2005). Hence the vessel wall in the region of the penetrations will need to be protected from high temperatures or the alloy changed to a high temperature alloy such as Inconel. Titanium can safely be connected to metals with higher temperature capability such as Inconel 625,[1] so it is also possible to transition between Inconel and titanium. Options for the vessel contruction are discussed in greater detail in section 3.7.

3.3 Cathode Recuperator

The cathode recuperator takes air from the outlet of the compressor and preheats it to 700°C using the 800°C exhaust gases. The heat exchanger is produced from a stack of sheet metal pieces which have been photo-chemically etched and then diffusion bonded to form laminar flow heat transfer channels. This design approach allows a highly compact heat exchanger with low pressure drop to be produced. The design benefits from the 8 atm operating pressure which reduces pressure drop and allows smaller channel heights to be used resulting in a more compact device with higher heat transfer coefficients. Since the heat exchanger is maintained within a pressurized shell at ~8 atm and the two sides of the heat exchanger are at similar pressures the heat exchanger does not have to withstand high differential pressures.

3.3.1 Chrome Volatility

Use of stainless steels or nickel-based alloys containing chrome in the high temperature portions of the air inlet to the cathode presents an issue related to cathode poisoning due to volatility of chrome (Yang et al. 2005, Simner et al. 2001). The volatility of chrome in the presence of moisture and oxidizing conditions has been examined as a function of temperature by Gindorf et al.(2005). In order to avoid fuel cell degradation due to chrome volatility, the cathode recuperator and ducting leading from the cathode recuperator to the fuel cell are proposed to be fabricated in Haynes 214 alloy. When heated, the Haynes

[1] http://www.stainless-steel-world.net/titanium/ShowPage.aspx?pageID=173

214 alloy forms an alumina scale which limits the volatility of chrome into the gas stream. This approach is believed to be more straightforward than the alternative approach of coating all exposed surfaces due to the large amount of exposed area within the cathode recuperator.

3.3.2 Recuperator Design

The recuperator is constructed from 0.041-inch thick Haynes 214 sheet metal. The metal is etched from each side to a depth of 0.0155" in regions where flow channels are desired. The sheets are then stacked so that etched areas line up to create 0.031" high flow channels separated by 0.010-inch thick walls. A total of 124 sheets are required to provide the target performance. Endplates are placed on the top and bottom to facilitate diffusion bonding of the sheets to form the exchanger as well as to allow welding to the top and bottom without risk of damage to the diffusion bonded stack. Flow in the heat transfer zone of the exchanger is laminar and counter-current. Of the total length, 8 inches is dedicated to counter-current heat transfer while 3 inches on either end is dedicated to headers to allow incoming gases to distribute evenly between the various channels. The exhaust gases enter and exit the ends of the heat exchanger while the incoming air enters and leaves the exchanger from the top and bottom. Excluding the external header attachments the heat exchanger block measures 14.2 in. L x 5.2 in. H x 10 in. W. Prior to installation the heat exchanger is oxidized to grow an alumina scale on the surface. As discussed above, the alumina scale is required to prevent volatility of chrome from the exchanger surfaces which would poison the fuel cell cathode and result in degraded performance.

3.3.3 Recuperator Performance

The cathode recuperator is designed to provide the preheated air stream at a temperature of 700°C while the cathode exhaust is at 800°C. The effectiveness of the exchanger is 70.2%. This is somewhat different than the similar recuperator for atmospheric systems which must be on the order of 90% effectiveness because the recuperator receives air preheated by the compression operation. The total of pressure drop through the hot and cold sides of the exchanger is estimated to be 16 inches of water. Some additional pressure drop may be seen in header transitions. Overall pressure drop including header transitions is estimated to be on the order of 20 in. of water.

3.4 Combustor

The burner size is estimated based on an axial flow of 20 m/s and a length to diameter ratio of 2:1 which results in a combustion chamber measuring 9 inches long x 4.5 inches inside diameter. The axial velocity was selected by analogy to other combustors. The reduction in flame speed expected due to the relatively low quality of the fuel roughly offset the increase associated with the high inlet temperature. The walls of the burner are assumed to be constructed using Inconel 625.

3.5 Fuel Supply

The fuel for the SOFCPU is assumed to be either a synthetic Fischer-Tropsch liquid fuel with properties similar to jet fuel or a deeply desulfurized jet fuel. The fuel is assumed to be loaded into a dedicated tank that is maintained separate from the jet fuel used for the main engines. Avoiding sulfur contamination in the fuel fed to the SOFC power system is critical because the sulfur is a poison for both

the reformer catalyst and the fuel cell anode (Rasmussen et al. 2009, Kishimoto et al. 2010). Attempting to operate the SOFC power system with conventional jet fuel would result in a rapid reduction in both the ability to reform the fuel (possibly leading to hydrocarbon breakthrough and initiation of coking of the unreformed fuel within the SOFC) as well as the ability to produce power from the stacks.

In the current estimate, weight is included for the fuel pump but changes in weight related to the fuel tanks is not included. Ultimately, if the SOFC power system results in a reduction in fuel consumption, the main fuel tanks may become slightly smaller but require a partition to handle a separate fuel. The overall weight impact on the tanks is not clear. It is assumed the existing system used to produce reduced O_2 air for the head space in the fuel tanks would be adequate for the new two fuel tank system.

3.5.1 Fuel Pump

The fuel pump is located outside the pressure vessel. As a result, the fuel pump must be able to pressurize the fuel to the pressure vessel pressure of 8 atm absolute (~118 psia) plus provide the back pressure created by flow. A fuel flow rate of 70 lb/h (~662 ml/min) is required. The fuel pump is assumed to consist of three MZR-7205 micro-annular gear pumps, seen in Figure 3.6, operating in parallel. Each pump is capable of 288 ml/min meaning three pumps in parallel have more than enough volume capacity. The pressure capacity is 40 bar or about 4 times what is necessary. The maximum power is 44W per pump for a total parasitic draw of 132W per system. This amounts to about 0.05% of the net power making it negligible. Each pump including an integral controller weighs 1.08 kg for a total weight of 3.24 kg per system. The three pumps per system approach would provide a degree of redundancy on fuel delivery, preventing a single pump failure from shutting down the power system.

Figure 3.6. MZR-7205 Fuel Pump. Pump dimensions are 1.4 in. diameter on head with overall length of 6 in. Three pumps in parallel are proposed as the fuel pump system for each of the three independent power systems.

3.6 Steam Reformer

After gases exit the SOFC anode ~15% of the gas is routed to the combustor. The remainder of the gas is mixed with fuel before entering the reformer. In the reformer, the mixture of anode waste gas and fuel reacts over a catalyst to generate fresh reformate which is then recycled back to the anode inlet via the anode recycle pump. The reformer uses a catalyst consisting of a small amount of rhodium metal dispersed onto a magnesia-alumina spinel support. The catalyst material is then coated onto a FeCrAlY metal foam. As the mixture of hot anode exhaust and fuel passes through the foam, the fuel reacts with

steam to form CO and H_2. The reaction is endothermic which results in a decrease in the reaction temperature as the reaction proceeds. Some of the CO formed shifts to CO_2 via the exothermic WGS reaction. In addition, as the CO and H_2 concentration increases, the exothermic methanation reaction becomes important. These reactions help to prevent the reforming reaction from quenching due to the drop in temperature, allowing an adiabatic steam reforming reaction to be performed. The assumed operation does not include the addition of air to the reforming mix (as in an ATR or POX reformer) nor does it require a heat input from a separate combustion stream (as in a conventional steam reformer). This type of steam reformer operation is important to achieving the high efficiency of the overall SOFC power system.

The operation of this type of reformer has been demonstrated experimentally both in reforming experiments as well as with actual anode gas recycle from an SOFC. The fuel used in these experiments included both a Syntroleum S8 and Shell GTL. Both fuels are Fischer-Tropsch liquids with properties similar to jet fuel but with near zero sulfur. Fitting of data to the temperature vs. conversion profile obtained within the reformer suggested an activation energy of approximately 200 kJ/mol. The activation energy is roughly consistent with a value for 180 kJ/mol for carbon-oxygen bond formation on the planer surface of rhodium crystallites during methane steam reforming determined by van Grootel et al. (2010).

The reforming catalyst assumed for the design would be expected to show a small increase in activity with increasing pressure at a fixed temperature. However, this effect is minor compared to the effect that pressure has on the reaction temperature. Operation at 8 atm has a major impact on reformer size through the influence it has on the finish temperature due to the higher methane formation occurring at pressure. At 1 atm, and 800°C anode outlet, the final temperature is ~570°C with 1.8% methane while at 8 atm a temperature of ~ 643°C is expected with 3.5% methane. Based on this temperature difference and an activation energy of 180 kJ/mol, the low temperature zone of the reformer (which dominates overall size) shrinks by a factor of about 7.75. The catalyzed foam for the reformer is expected to require a volume of 15 liters (913 $in.^3$) with a weight of 11.3 kg. The foam is placed within a duct running down one side of the stacks as will be shown in the assembly.

3.7 Insulated Pressure Vessel

A pressure vessel capable of holding 8 atm is needed to contain the stack and hot heat exchangers. The heat loss from the vessel must be limited in order to maintain system efficiency and also to protect adjacent structures or systems within the aircraft. Heat loss may impact the process efficiency through a reduction in the temperature entering the expander which would reduce the power produced by the expander.

Several options for the insulated pressure vessel were considered including:

Insulate Inside the Pressure Shell – By insulating inside the pressure shell the material of construction of the pressure vessel does not need to be compatible with the interior temperatures. This allows an aluminum or titanium alloy to be considered for the pressure vessel. However, this increases the diameter of the pressure shell which offsets some of the weight savings. Also this requires a non-vacuum insulation which results in a greater insulation thickness.

Vacuum Insulation Outside the Pressure Shell − In this case the diameter of the pressure vessel is reduced but the pressure shell must be compatible with the high temperature of the interior of the vessel. In this case the alloy is assumed Inconel 625 which is a nickel based alloy with good creep resistance. Using vacuum insulation outside the pressure shell requires a barrier on the outside of the insulation to maintain vacuum. However, the insulation layer is thinner and lighter due to the lower thermal conductivity.

MLI Insulation Outside the pressure shell − MLI insulation consists of multiple low-emittance films with thin separating layers to prevent physical contact between layers to minimize heat conduction. Unlike the more conventional vacuum insulation it cannot support the outside vacuum barrier against atmospheric pressure. As a result it must have a self-supporting outside pressure barrier.

3.7.1 Insulation Properties

Nano-Porous Vacuum Insulation – This insulation uses a vacuum to enhance the insulation performance. NanoPore 150 is selected as a representative of this approach. The insulation has a density ~0.24 g/cc when sealed with a low temperature polymeric vacuum barrier and has the ability to support itself against 1 atm pressure. This vacuum microporous insulation approach provides a barrier with conductivity of ~0.01 W/mK. The conductivity compared to other potential insulation choices is shown in Figure 3.7 below. The insulation shows good performance at a moderate vacuum of 100 mbar making problems related to degradation of vacuum less likely.

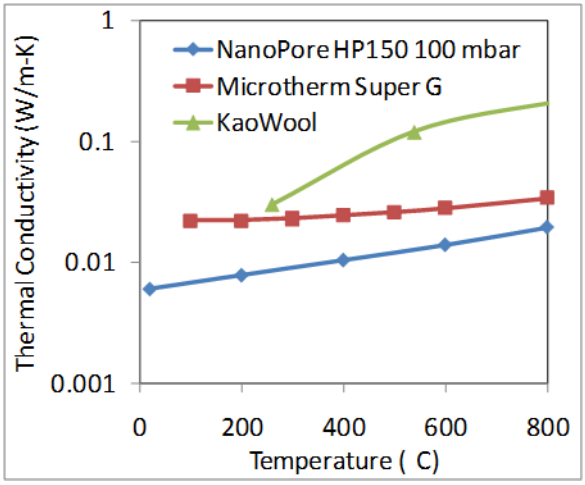

Figure 3.7. Nanopore HP150 Vacuum Insulation Conductivity Compared to Other Insulations

Microtherm Super-G − This insulation does not require a vacuum jacket. Microtherm super G insulation is based on pyrogenic silica with a mineral oxide opacifier and E-glass filament reinforcement. The insulation can be provided premolded to a curved cross section such as a pipe making application of the insulation to the body of the vessel straight forward. If mounted on the vessel interior, the vessel wall would not need to be capable of handling the high temperature of the vessel interior and could be made in titanium or aluminum as long as sufficient attention is paid to the potentially high temperatures where process gases leave the vessel. A more detailed graph of the conductivity is shown in Figure 3.8.

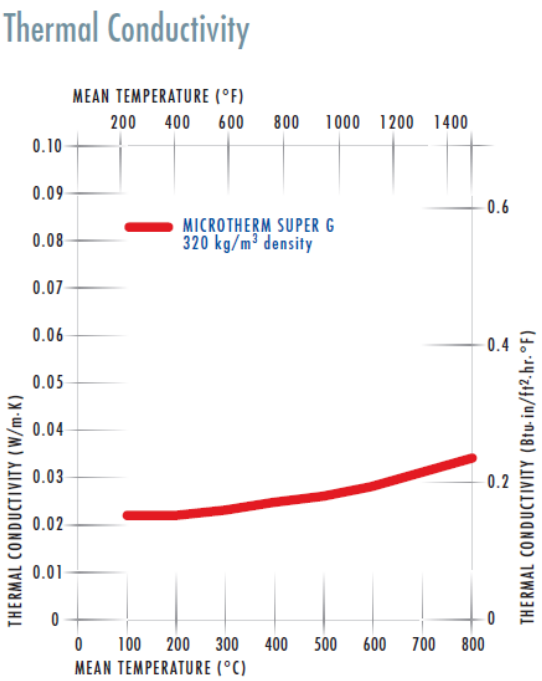

Figure 3.8. Thermal Conductivity of Microtherm Super G

MLI Insulation − MLI insulation would incorporate multiple low-emittance films in place of the continuous nanoporous insulation fill. The films would need to be prevented from contacting each other and a vacuum pulled to minimize the importance of thermal conduction in the insulation layer. This insulation could not support a vacuum barrier against 1 atm of pressure and so the exterior barrier must be self-supporting.

MLI insulations are common in cryogenic applications and in spacecraft where the requirement for a vacuum does not require a shell. The MLI typically consists of very thin aluminized polymeric film with low emittance that is separated by crinkling or use of a scrim layer to prevent direct contact between film layers. At sub-ambient temperatures the effective thermal conductivity can be <.0001 W/mK (for example see Bapat et al. 1990), while values as low as 10 μW/mK are achievable (Scurlock and Saull 1976). MLI insulation can readily be found for application at low temperatures. High temperature MLI films consist of aluminized Kapton or polyimide layer plus a spacer scrim such as glass cloth and are suitable for temperatures as high as 200°C to 400°C depending on construction. MLI for higher temperatures is less common due to the incompatibility of polymeric materials with the temperature. However, there has been some work examining higher temperature MLI insulations.

The performance of MLI insulations at temperatures up to 1000°C was examined by Daryabeigi and coworkers[1]. The insulations consisted of a proprietary film coated with gold that was separated by layers of fibrous insulation (primarily to prevent contact of films). A 4 film layer measured 13.3 mm thick,

[1] See http://www.google.com/url?sa=t&rct=j&q=high%20temperature%20mli%20insulation%20miller&source=web&cd=1&ved=0CCsQFjAA&url=http%3A%2F%2Fntrs.nasa.gov%2Farchive%2Fnasa%2Fcasi.ntrs.nasa.gov%2F20080013560_2008013513.pdf&ei=SZKDToXNEerkiALw1vDwBw&usg=AFQjCNG8uwL9n_XLWL_ZrKbRb9yAPFv9gQ

provided a density of 47.3 kg/m^3 and provided an effective thermal conductivity for a 1000°C temperature difference of 0.02 W/mK with a vacuum pressure of ~10Pa. The performance degrades if vacuum is degraded or lost, reaching about 0.06 W/mK at 1000 Pa and about 0.09 W/mK at atmospheric pressure.

Li et al. (2009) report results for a new high temperature MLI consisting of alumina silicate papers and a silica fiber net with silica aerogel granules as a filling. They report 0.08 W/mK at 1000°C and a density of 0.25 g/cm^3.

Some work has been done toward the development of "integrated MLI" which would provide a frame to support and separate layers and support the exterior pressure shell.[1] This approach could potentially decrease the weight to 1/3 the weight required to provide a pressure shell. Weight savings would be less for the current application since the inner shell is designed to contain the vessel pressure and only the outer shell would be impacted.

3.7.2 Approach to Design of Vessel and Vessel Structure

For purposes of comparing the potential design approaches, the straight side of the cylinder was set at 94.624 in., which allows space sufficient for 8 stacks with 0.25 in. space between each stack.[2] The actual vessel will contain six stacks with the extra two stacks worth of space provided to allow room for the hot balance of plant equipment. The required clear inside diameter was set at 20.75 in. This allows the stacks to be positioned in the center of the cross section with adequate room for anode and cathode ducting and an ~2-in. clearance from the corner of the stack to the inside wall (or insulation surface) of the vessel.

Acceptable heat loss from the vessel was taken to be 0.5% of the gross electrical output from the stacks. Heat loss at this level will have a very small impact on performance. This assumption results in a heat loss value of 1353 watts for each of the three vessels. The insulation thickness in each case was adjusted to limit the heat loss to this value.

The vessel was designed assuming an internal pressure with a differential relative to the outside pressure of 8 atm. This is slightly conservative since the stack pressure is expected to be 8 atm and the pressure outside the vessel will never actually be zero.

When the pressure shell is placed inside the insulation, failure is determined by creep rupture phenomenon. In this case, the rupture stress corresponding to the temperature and creep duration was estimated by correlation to creep data for the alloy using the Larson-Miller parameter. The allowable stress was taken as one third of the predicted creep rupture stress.

For the low temperature titanium shell pressurized from the interior, the failure of the vessel is determined by the yield stress. An allowable stress was obtained by dividing the yield stress by 1.5. When considering aluminum for the same application, the allowable stress was determined by dividing the yield stress by 2. The greater margin relative to yield was applied in recognition that vessel strength may need to be increased to account for fatigue phenomenon which is a greater concern for aluminum alloys. However, no detailed analysis of fatigue was attempted.

---

[1] http://www.techbriefs.com/component/content/article/5050, also http://www.quest-corp.com/image/integrated-multilayer-insulation-advanced-thermal-insulation

[2] 0.25 inches between cell cassettes. The stack frame was not considered in this calculation.

For self-supporting shells required to create a vacuum space suitable for use of the MLI insulation, the exterior shell must resist a 1 atm external pressure against a near zero internal pressure, without relying on interior support. In this case the failure of the shell is dominated by elastic buckling. The buckling pressure was estimated using a theoretical expression for a thin wall perfectly cylindrical cross section. Application of this expression is non-conservative since defects in the cross section reduce the buckling pressure. In an attempt to compensate for this a safety factor of 3 was applied to the expected 1 atm pressure loading and the wall thickness adjusted to show buckling failure at 3 atm. The wall thickness determined was applied to both the straight side of the cylinder as well as the hemispherical ends without performing any additional buckling analysis for the vessel ends.

3.7.3 Properties for Vessel Materials of Construction

For the case where insulation is placed on the exterior of the pressure shell, Inconel 625 was selected for its high temperature compatibility and creep resistance. For the case where insulation is placed on the inside of the pressure shell the shell is not exposed to the high temperature interior of the vessel and lower temperature alloys can be considered. Two alloys were considered, Ti-Al6-4V and Aluminum 7075-T6. The key material properties used when assessing the design with these materials are summarized below.

- *Inconel 625* – The thickness of the vessel is designed based on a safety factor of 3 relative to creep rupture. Design conditions assumed operation at 700°C with 8 atm differential pressure, and a creep lifetime requirement of 10,000 hrs. This results in an allowable stress of 7119 psi. The density is 8.44 g/cc.
- *Titanium Ti-6Al-4V* – The yield stress is taken as 128,000 psi and a safety factor relative to yield of 1.5 is applied to arrive at an allowable stress of 85333 psi. The density is 4.43 g/cc. Young's modulus is 16500 ksi. Poisson's ratio is 0.342.
- *Aluminum 7075-T6* − The yield stress is taken as 63,000 psi and a safety factor relative to yield of 2 is applied to arrive at an allowable stress of 31,500 psi. The density is 2.81 g/cc. Young's modulus is 10,400 ksi. Poisson's ratio is 0.33.

3.7.4 Vessel Structure and Insulation Results

Table 3.1 shows the estimated masses for each of the analyzed configurations. The lower density of the MLI insulation was overwhelmed by the mass required to provide an outer vacuum shell that was stable against elastic buckling. The nanopore vacuum insulation was somewhat better that than MLI, primarily due to the fact that a thin 0.005-in. skin could be used to provide the outer vacuum barrier while relying on the insulation to support the barrier against the inside pressure shell. The lightest weight solution was the Microtherm Super-G Insulation installed on the inside of the pressure shell. Using this approach an aluminum or titanium pressure shell could be used, minimizing the weight of the pressure shell. The titanium shell was slightly lower weight but the aluminum shell could be used if cost is a driver between the two approaches.

Table 3.1. Estimated Weights for Analyzed Pressure Shell and Insulation Combinations

Vessel and Insulation Combination	Weight of One Vessel, kg	Weight of 3 Vessels, kg
Inconel Inner+Nanopore Vacuum+5mil skin	194.3	582.8
Inconel Inner + MLI Vaccum + Ti outer	361.3	1084.0
Inconel Inner + MLI Vacuum + Al Outer	314.3	942.8
Microtherm Inside + Aluminum Outside	122.0	366.1
Microtherm Inside + Titanium Outside	115.7	347.2

Based on this analysis the design approach of a titanium shell with Microtherm Super G insulation installed on the interior is assumed for the remainder of the analysis.

3.8 Anode Recycle Pump

The anode recycle pump receives hot (~643°C) reformate from the adiabatic reformer and pumps reformate to the fuel cell anode. The overall pressure rise across the blower is assumed to be 33 in. of water. Of this rise, 24 in. is due to the pressure drop across the stack which is intentionally increased by a factor of ~4 in order to improve flow distribution. The remaining 9 in. is to allow for a small pressure drop in the steam reformer plus a pressure drop allowance to account for pressure drops for flow through ducts were not determined. Pressure across the blower is assumed to be 7.985 atm at the inlet and 8.056 atm at the outlet. Due to the elevated pressure, the pressure ratio across the blower is a very low value of ~1.01.

The estimate of the size and mass of the blower was based on scaling an R&D Dynamics Centair S1244. The S1244 is an anode gas recycle blower with a maximum inlet temperature of 750°C. It is powered by a permanent magnet BLDC motor and uses high speed foil gas bearings. The blower design provides for thermal isolation between the motor and the process stream which results in the blower being heavier than an equivalent low temperature blower.

Because the inlet pressure is about 8 atm, the pressure ratio for the blower is very low (~1.01). Based on the gas inlet temperature, pressure, composition and pressure ratio, it is estimated that about 4 of the S1244 blowers would be required to meet the required flow of one SOFC power system. Rather than design with 4 separate blowers in parallel, the mass was estimated to be a factor of 4 higher than a single blower for a mass of 20.88 kg.

The dimensions of the blower were increased in constant proportion of 1.587X to arrive at a blower volume which is 4X that of a single blower[1]. The S1244 is equipped with fins that enable air-cooling of the motor. It is assumed that these fins are removed and a liquid cooling jacket is provided with 2 inches of microtherm super-G insulation surrounding the motor to limit heat leak into the motor. The fins and the liquid jacket and tubes are assumed to offset in terms of weight impact and the weight of the insulation is estimated to add approximately 2.22 kg while the thickness of the insulation adds to the dimensions.

The blower requires a controller and on the aircraft it would be preferable to operate on DC power. The controller offered with the original S1244 is designed to operate on 110 V AC so the controller

[1] i.e. if height, length and width are increased by a factor of 1.587 volume increases by 1.587^3 = 4.00

weight was based on other DC supplied BLDC motor controllers. The power capacity for the controller was set to 50% greater than the steady state blower power required. This resulted in a controller weight of 1.81 kg. The controller is assumed to be located outside the pressure vessel.

The masses associated with the anode recycle blower are summarized below for one system:

- Blower 20.88 kg
- Insulation 2.22 kg
- Controller 1.81 kg
- Total 25.3 kg.

The total weight for three independent systems is then 75.9 kg.

3.9 SolidWorks Model, Structure, Ducting and Spatial Layout

The components were modeled in three dimensions and fit into a pressure vessel in order to improve the fidelity of the weight estimates. A structure inside the insulation was added and brackets to support the stacks were added. Ducting to convey gases between components were included. One-quarter in. of insulation was added to primary cathode and anode inlet/outlet ducts. Other ducts and surfaces are currently not insulated. The physical layout of the system is illustrated in Figure 3.9 through Figure 3.12. The exterior dimensions on the vessel are a diameter of 25.5 in. with a straight wall length on the cylinder of 104 in. The overall length including hemispherical ends is 129.5 in.

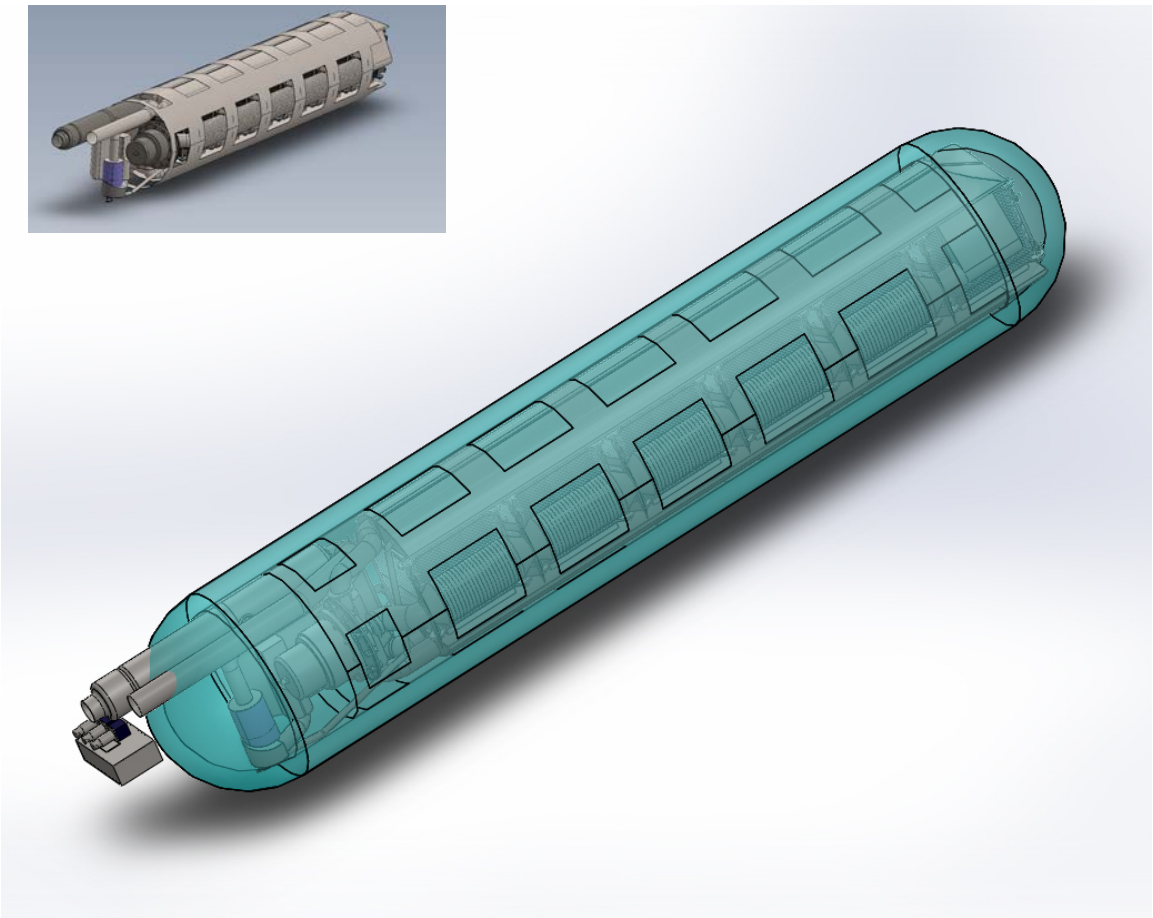

Figure 3.9. External View of System with Outer shell, Insulation and Inner Shell Made Transparent. The edge of the interior support shows as black lines. Top left shows the interior structure fame without insulation or exterior vessel wall.

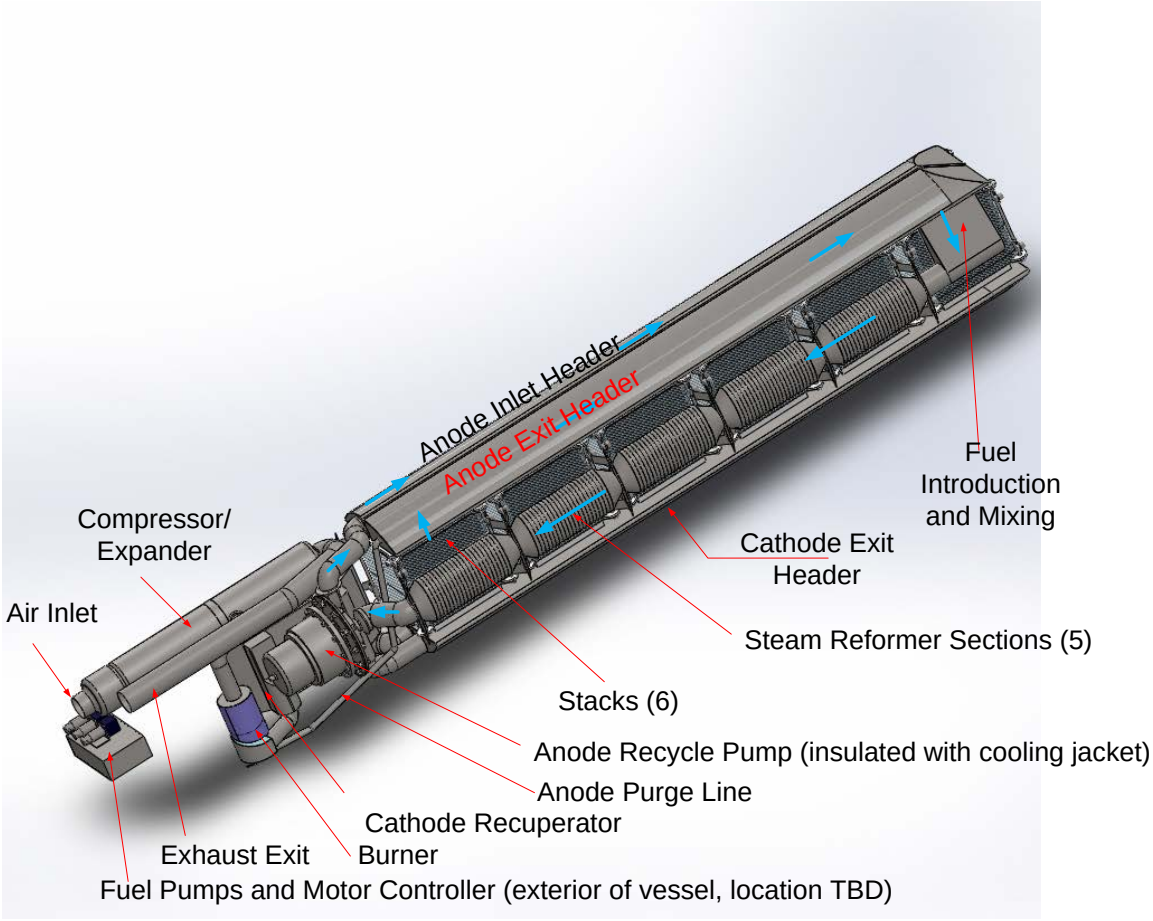

Figure 3.10. View With Vessel, Insulation and Inner Structure Removed. Blue Lines Illustrate Anode Recirculation Loop.

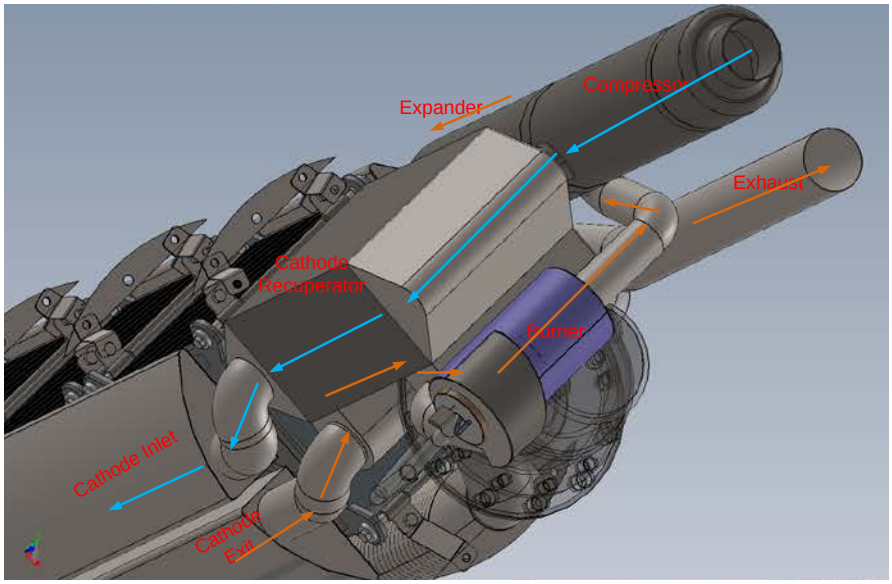

Figure 3.11. Opposite Side View Showing Air Pathway. Blue lines show the air path into the fuel cell while orange lines show the path after leaving the fuel cell.

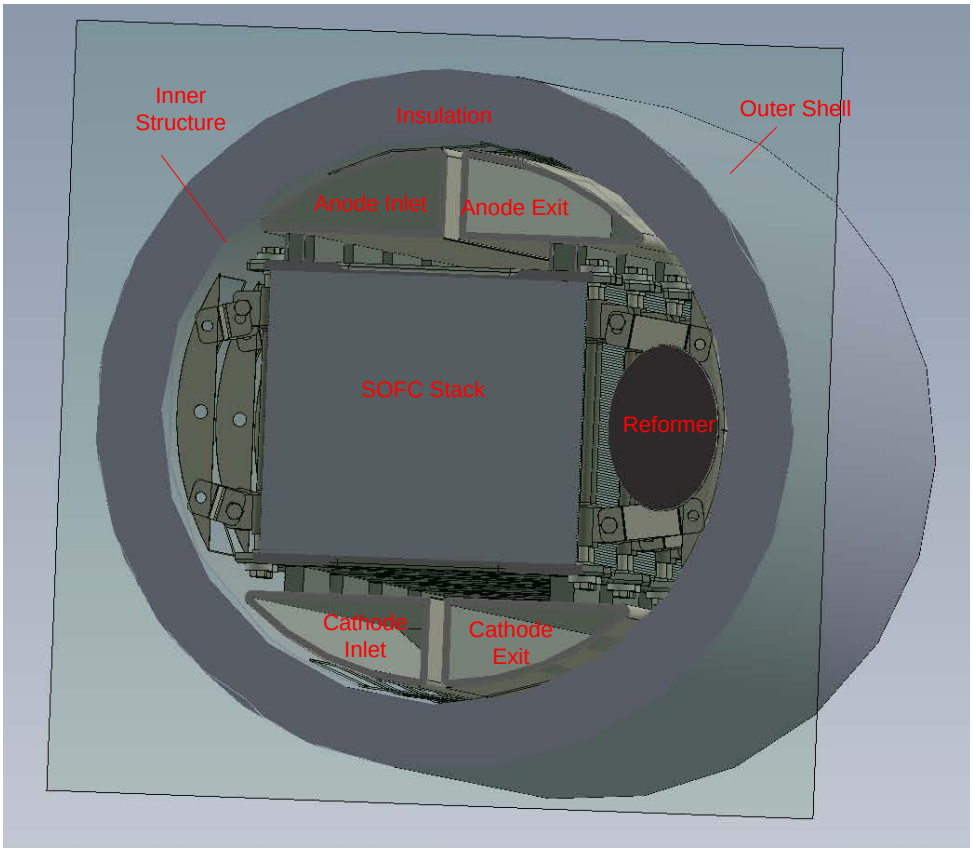

Figure 3.12. Cross Section View Showing the Arrangement In the Portion Containing SOFCs

The weight distribution from the Solidworks model of the system is summarized in Table 3.2. It is notable that the overall weight is dominated by the stacks, insulated pressure shell, and main stack header ducts. These components account for 85% of the mass of the overall system.

Table 3.2. Single Power System Weight Distribution (three systems required for aircraft)

Component in Assembly	Mass, kg	wt%
Stack and Frame	581.6	62.0%
Shell and Insulation	135.9	14.5%
Main Fuel Cell Headers and Insulation	80.3	8.6%
Cathode Recuperator	43.9	4.7%
Support Frame and Brackets	34.1	3.6%
Anode Blower	23.5	2.5%
Steam Reformer	18.7	2.0%
Compressor/Expander	6.8	0.7%
Combustor	1.3	0.1%
Other Ducts and Misc.	12.4	1.3%
Total	938.5	100%

The weight impact to the aircraft would need to include three independent systems and need to account for the mass removed from the aircraft. The weight impact to the aircraft is:

- SOFCPU (821kW) 2815
- SOFCPU (972kW proportionally scaled) 3333
- Removal of Turbine APU - 245
- Reduction in Converter weight - 266
- Net Impact to aircraft weight (972kW) 2822 kg.

The system mass estimate based on the Solidworks model is significantly less than the initial scoping estimate of 4287 kg for the 8 atm, 0.825V/cell case (see section 2.3). There are several key factors that contribute to the reduction in weight, primarily having to do with the balance of plant component weights, including

- It was decided to use a high temperature anode blower capable of operating on the reformer outlet gas directly. This eliminated the anode recuperator which was included in the system used to make initial weight estimates.

- The operation at 8 atm has two impacts on the cathode recuperator. First, the pressure drop for flow is much less for the pressurized gas, allowing smaller channels with higher heat transfer coefficients to be used in the design. In addition, the incoming air is preheated to ~500°C by the compression operation reducing the duty and effectiveness required of the exchanger to preheat the cathode air to 700°C.

- The elevated pressure increases methane formation in the steam reformer which keeps the temperature higher and kinetics faster. Also, as the reformer is scaled up, the relative mass of catalyst foam relative to the reformer shell increases.

- The weight per unit output on the anode blower scales favorably and the fact that the anode gas is pressurized greatly reduces the mass of the blower required to circulate the anode gas through the system.

Table 3.3 provides details of the reductions in the mass estimates for balance of plant components in the final 8 atm design. The savings obtained in these BOP components more than offset the increase due to ducting, structure and other items being added. The comparison of the aircraft weight impact to the breakeven weight for the estimated 70.4% efficiency of the system is shown in Figure 3.13.

Table 3.3. Comparison of Several BOP Component Weights: Preliminary Estimate vs. Conceptual Design (conceptual design weights at 821kW scaled linearly to 972kW)

BOP Component	Preliminary Calculation, kg	3 times the single system component weights, Conceptual Design, kg
Cathode Recuperator	771.1	155.9
Anode Recuperator	435.3	0
Steam Reformer	566.8	65.4
Anode Blower	844.4	83.5

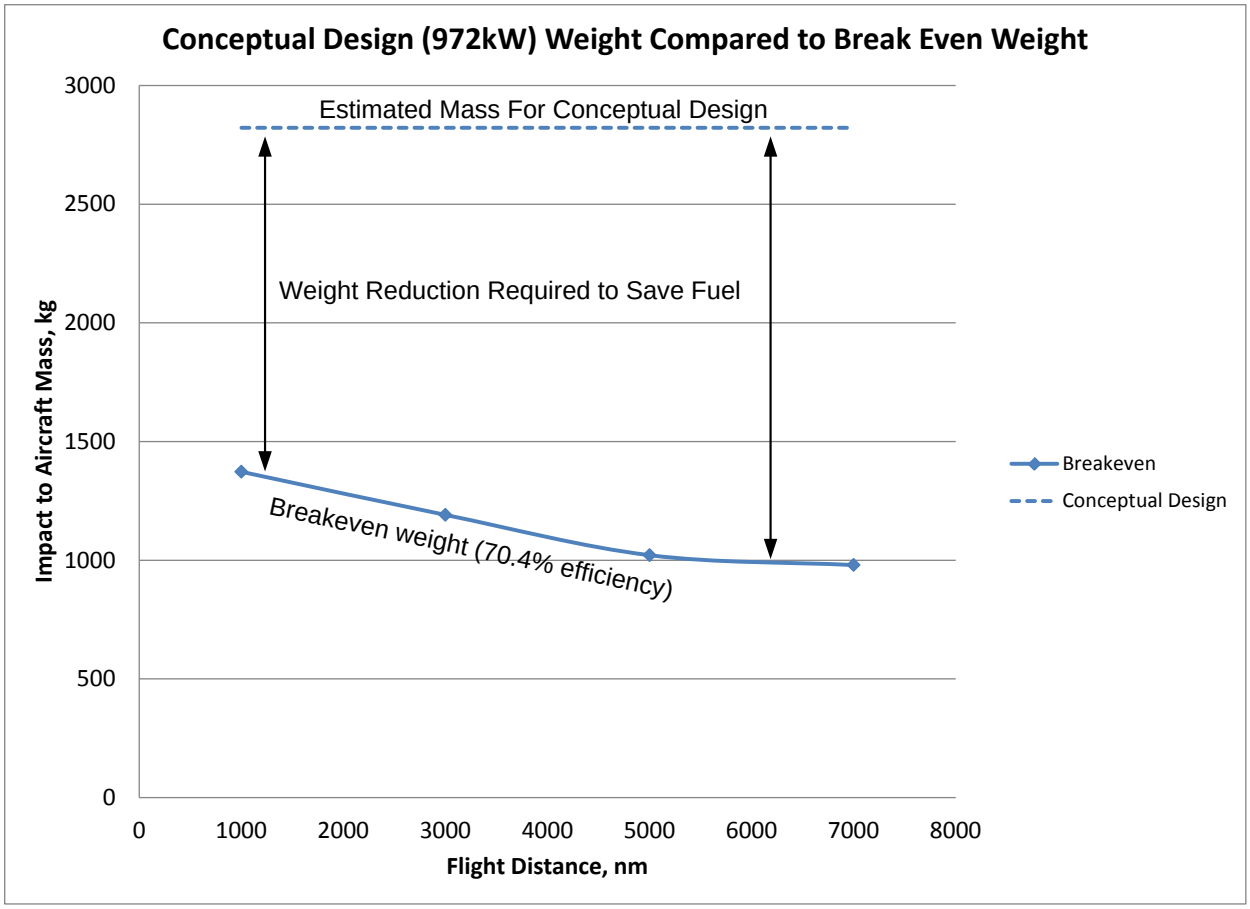

Figure 3.13. Comparison of the Impact to Aircraft Weight in Conceptual Design (scaled to 972 kW) to Calculated Breakeven Weight for Achieving Overall Fuel Savings

3.10 Potential Mass Increases and Performance Reductions Relative to Conceptual Design

Although the conceptual design represents a significant improvement relative to initial scoping estimates there are still several areas where increases in weight or reductions in efficiency could occur as the design becomes more complete.

3.10.1 Exterior Shell

The final pressure shell will likely be heavier than currently estimated. The exterior shell is currently designed only for pressure stresses and does not include a flange or other closure to allow access to the vessel interior for maintenance. Weight will need to be added to the vessel to handle stresses occurring as the system weight is transferred to the aircraft structure. Also, as currently drawn there is no firm connection between the interior frame and the external shell and some firm structure may be needed.

3.10.2 Compressor/Expander

The scaling for the compressor/expander and the ability to maintain efficiency and reliability when going to higher compression ratios needs to be confirmed. Also, the ability to construct a compressor expander that will maintain efficiency over the range of inlet and outlet pressures that will be encountered will need to be confirmed. Reliability and maintenance interval for a small diameter compressor/expander is also a potential concern due to the very high rotational speed required in the device.

3.10.3 Electrical Components and Penetration

The current design does not show the electrical connections and the penetration of the pressure shell to bring the power cables out of the vessel. This will have a minor impact on the weight although cooling at the penetration point may be required to prevent local shell overheating due to thermal conduction along the electrical conductor. In addition the current system does not include electrical startup heaters that are expected to be needed to bring the stacks to operating temperature. Space is currently reserved on the side of the stacks opposite the reformer to allow routing of power cables.

3.10.4 Interior Insulation

The interior of the vessel is envisioned to run at high temperature so insulation is not required inside the primary shell insulation to reduce heat loss. However, some additional insulation to avoid thermal transfer between components might ultimately be required in some areas. Most likely this would take the form of relatively low density batting or lightweight radiation shields between components to reduce the thermal transfer.

3.10.5 Cathode Recuperator Header Configuration

The cathode recuperator header connection arrangement used in the assembly differs from the original header design. The modified header arrangement needs to be evaluated for flow distribution. If an acceptable distribution cannot be obtained for the arrangement shown it may be necessary to expand the headers or rearrange the piping to use the initially intended header arrangement. The primary impact would be if the overall vessel needed to stretch in order to accommodate an arrangement that was not as tightly integrated.

4.0 References

Bapat, S.L., KG Narayankhedkar, TP Lukose, Experimental investigations of multilayer insulation, Cryogenics, volume 30 issue 8, August 1990, pages 711-719.

Braun, R., M. Gummalla and J. Yamanis, J. of Fuel Cell Sci. and Tech., Vol. 6 (2009) 031015.

Daggett, D., S. Eelman and G. Kristiansson, Proceedings of AIAA/ICAS International Air and Space Symposium and Exposition, July 2003, Dayton, OH, AIAA 2003-2660.

Daggett, D., "Fuel Cells & Hydrogen Airplanes", Presented to Canada and US Fuel Cell & Hydrogen Partner Meeting, Seattle, WA, (2004).

Daggett, D., N. Lowery and J. Wittmann, ''Fuel cell APU for Commercial Aircraft,'' presented at the H2Expo, Hamburg, Germany, Sept. 2005.

Eelman, S., D. Daggett, M. Zimmermann and G. Seidel, High Temperature Fuel Cells as Substitution of the Conventional APU in Commercial Aircraft, DGLR Jahrestagung, München, 2003, DGLR-JT2003-183

Eelman, S., I. del Pozo y de Poza and T. Krieg, "Fuel Cell APU's In Commercial Aircraft – An Assessment Of SOFC And PEMFC Concepts", 24th International Congress Of The Aeronautical Sciences, 2004

Gindorf C., et al., 2005. "Vaporization of Chromia in Humid Air", Journal of Physics and Chemistry of Solids, Volume 66, Issues 2-4, February-April 2005, Pages 384-387. See also: Erratum to "Vaporization of Chromia in Humid Air", Journal of Physics and Chemistry of Solids, Volume 66, Issue 10, October 2005, Page 1851.

Gogia, A. K., 2005. "High Temperature Titanium Alloys", Defence Science Journal, Vol.55, No.2, April 2005, pp149-173

Gummalla, M., A. Pandy, R. Braun, T. Carriere, J. Yamanis, T. Vanderspurt, L. Hardin and R. Welch, "Fuel Cell Airframe Integration Study for Short-Range Aircraft", NASA/CR – 2006-214457/VOL1 (2006).

Kishimoto, H., T. Horita, K. Yamaji, M. Brito, Y. Xiong and H. Yokokawa, J. Electrochem Soc. 157 No. 6 (2010) B802-B813.

Li, J.F., F He, XD He., New-type high-temperature multilayer insulation material. Cailiao Kexue yu Gongyi/Material Science and Technology, v 17, n 4, p 531-534, August 2009; Language: Chinese; ISSN: 10050299; Publisher: Harbin Institute of Technology

Rajashekara, K., J. Grieve and D. Daggett, IEEE Industry Applications Magazine, July-August, 2008, 54-60.

Rasmussen, J. and A. Hagen, J. Power Sources 191 No. 2 (2009) 534-541.

Scurlock, RG, B. Saull. 1976. Development of multilayer insulations with thermal conductivities below 0.1 μW/cm K, Cryogenics, May 1976

Simner. S.P., J. W. Stevenson, K. D. Meinhardt, and N. L. Canfield, in Proceedings of the 7th International Symposium on Solid Oxide Fuel Cells, H. Yokokawa and M. Dokiya, Editors, PV 2001-16, p. 1051, The Electrochemical Proceedings Series, Pennington, NJ 2001.

Srinivasan, H., J. Yamanis, R. Welch, S. Tulyani and L. Hardin, "Solid Oxide Fuel Cell Feasibility Study for a Long Range Commercial Aircraft Using UTC ITAPS Approach", NASA/CR – 2006-214458/VOL 1 (2006).

Van Grootel, P.W., EJM Henson, RA van Santen, 2005. "The CO Formation Reaction Pathway in Steam Methane Reforming by Rhodium". *Langmuir* 2010, *26(21)*, 16339-16348

Yang, Z., G. Xia, S. Simner and J. Stevenson, J. Electrochemical Soc. 152 No. 9 (2005) A1896-A1901.

Appendix A

Other Topics

Appendix A

Other Topics

A.1 Water Recovery From Exhaust

The 787 has two 135 gal potable water tanks for a total potable water capacity of 270 gal[1] (1022 liters). The water is UV treated during the loading onto the aircraft. If completely filled the potable water represents a weight of 1019 kg. If water could be recovered from the SOFCPU exhaust at a rate exceeding 100 kg/h and used as potable water it might significantly reduce the weight of water that needs to be loaded at the start of a flight.

In the selected condition (8 atm, 0.825 V/cell), the exhaust stream containing the water vapor is at 742°C, 7.86 atm entering the expander and 251°C, 0.185 atm exiting the expander. Water can be recovered either before or after the expander. The configuration for water recovery after the expander is shown in Figure A.1.

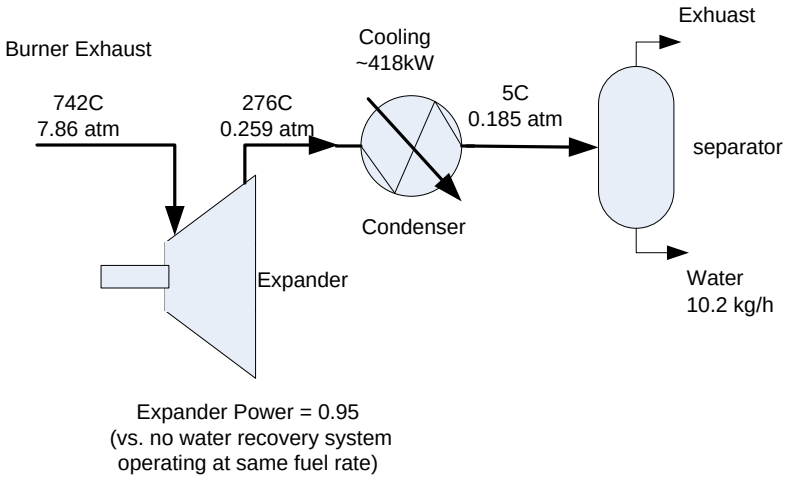

Figure A.1. Recovery of Water From Exhaust After Expansion (duty and mass are for 927 kW)

Placement of the condenser downstream from the expansion increases the pressure at the expander outlet, reducing the power from the expander. In this case a 1 psi pressure drop was assumed. The condenser must cool the gas from 276°C to a temperature near the ice point without plugging the exchanger with ice. Recovery of water at 5°C is only 10.2 kg/h due to the low pressure downstream of the expander. At 3°C the recovery can be increased to 29.9 kg/h which is still well short of the desired water recovery of >100kg/h. However, it would be very difficult to operate this exchanger at 3°C without forming ice and plugging the exchanger. As a result, the approach of condensing water downstream from the expander is considered impractical.

More complicated water recovery approaches might still be practical downstream of the condenser. For example, the water could be intentionally frozen to a surface and then thawed to recover water or a

[1] www.Boeing.com/commercial/aeromagazine Q3 2008 pg 5, *Preparing Ramp Operations for the 787-8*

desiccant could be used to recover the water from exhaust and then water recovered by heating the desiccant. However, these approaches were not evaluated.

Recovery of water by condensation upstream of the expander is shown in Figure A.2. In this case the gas is cooled in a recuperator before the condenser and after water is separated the gas is reheated in the recuperator to reduce the amount of expander power lost. There would be a pressure drop associated with the recuperator and condenser that would reduce expander power but since the stream is at high pressure the pressure drop will be ignored for the initial analysis. The expander power is reduced by the loss of moles of gas due to water condensation as well as due to a reduction in temperature associated with the assumed recuperator effectiveness of 85%.

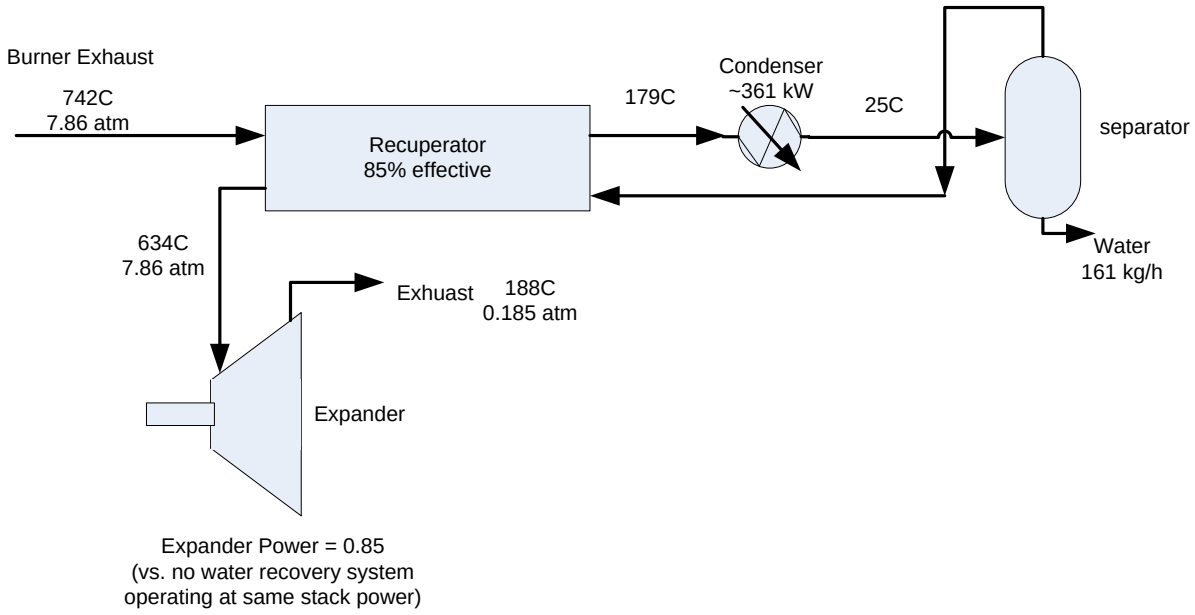

Figure A.2. Recovery of Water Upstream from the Expander (duty and mass are for 927kW)

The expander power obtained is reduced to only 85% of the power obtained at the same fuel rate and stack power without water recovery while the compressor power is unaffected. In order to maintain an output of 972 kW the overall system must be scaled up by 12.7% to provide the additional power to the compressor, increasing the system mass. Neglecting the additional mass of the recuperator and condenser the increased size of the power unit increases the mass by 422 kg. At the same time, the efficiency is reduced from 70.4% to 62.4%, resulting in a decrease in the system weight that must be achieved in order to break even on fuel consumption. The overall impacts to the system weight and breakeven weight are as follows for a 3000 nm flight.

Water Loading Savings –919 kg reduction in initial water weight with no reduction in final water weight. This assumes 100 kg is initially loaded and the remaining 919 kg is recovered from SOFCPU exhaust. As water is used, it ends up in the greywater storage tank regardless of source so at the end of flight the water amounts will be the same. This might be averaged to about 919/2 = 460 kg average weight reduction. This may overstate the savings since the tank may only be filled about half full for a 3000 nm flight since the maximum range of the aircraft is over 7500 nm.

Increase in SOFCPU Mass – After renormalizing the system to 972 kWe net power the weight increases by 422kg. This is driven primarily by an increase in the stack weight and supporting components required to make up for the loss in expander power.

Decrease in Breakeven Weight – The overall system efficiency is estimated to drop from 70.4% to 62.4% which reduces the extent of fuel savings and reduces the mass of the system for which overall fuel savings approach zero. The breakeven weight is reduced from 1191 kg to 591 kg due to the reduction in efficiency which represents a reduction of 600 kg. Stated another way, the allowable weight at which the system would save fuel is cut in half.

Hence, at this point, the overall benefit analysis for a long distance flight is

- Benefit: 460 kg reduction in average potable water tank content weight
- Cost: 422kg increase in SOFCPU mass, 600kg reduction in breakeven weight.

This indicates the costs are likely to outweigh the benefits of water recovery for this flowsheet. Two factors that will detract further from the benefit have not been analyzed. These include:

Drag associated with drawing in cooling air for the condenser. Assuming ram air is drawn in at -29.6°C and 0.279 atm and exits the condenser at +5°C, the flow of compressed ram air required is 52,603 acfm (16488 scfm (ref 0°C)). This is about a factor of 9 greater flow than is being drawn in to supply the SOFCPU. Assuming the ram compression is the only driving force for air movement (no forced air fans) the power involved in the adiabatic ram air compression is 272 kW. The power to move the cooling air ultimately will be reflected as an increase in drag or as parasitic power if compressed with fans.

Weight of the condenser, cooling air ducting, recuperator and separator. The weight of these components was not estimated since the water condensation concept did not appear feasible prior to including their weight.

It should be noted that the rate of water recovery calculated for the flowsheet of 161 kg/h is more than is required to meet the average aircraft water needs which are estimated to be ~70 kg/h.[1] It may be possible to provide a bypass such that burner gases would go directly to the expander once adequate water had been collected. Incorporating this might increase the breakeven weight since efficiency would be higher when not collecting water and an average of the two efficiencies would apply. This would not affect the system weight since it would need to be sized to provide the required power while water was being collected.

Assuring Water Quality - Water supplies on aircraft are regulated by the EPA. Some effort may be required to obtain regulatory approval to use combustion condensate as drinking water. For example, EPA regulations require "all water sources must be from a watering point water system selected in accordance with Food and Drug Administration regulations [21 CFR Part O&M plan 1240 subpart E][2]. While a thorough examination of regulation is beyond the scope of this examination it is likely that

[1] Estimate assumes the water tanks are fully utilized for a 7000-nm, 14.5-h flight. Tank capacity of 1019 kg/14.5 hrs = 70kg/h.

[2] http://water.epa.gov/lawsregs/rulesregs/sdwa/airlinewater/index.cfm Aircraft Drinking Water Rule: A Quick Reference Guide

portions of the system that are not at temperatures sufficient to sterilize would need to be configured to be flushed with disinfectant to prevent bacterial growth.

In addition, some sort of water treatment would probably need to be applied after withdrawing water from the tank. Currently, water loaded into the potable water tanks is UV treated as it is loaded. If running a condenser directly to the potable water tank, treatment after withdrawal from the tank may be needed. UV water treatment systems designed to treat water after being withdrawn from the aircraft potable water tank are currently available and appear to have relatively low weight and power consumption. For example, International Water Guard offers a model IWG-A4 which is capable of treating 1 gpm and weighs in at 2.8 kg while drawing 11.2 watts power from 28V DC[1]. In addition to bacterial concerns, measures to prevent contamination from particles related to corrosion or attrition within the SOFCPU may be needed. An examination of whether fine particulate associated with semi-volatile compounds within the power system might affect water quality would be required. If strictly particulate, filters suitable for aircraft use are available. For example, Pall corporation has qualified a point of use filter for use on the Airbus A380.[2] More elaborate measures may be needed if contaminants are found that dissolve in the condensate.

A.2 On-Board Desulfurization of Fuel

The design of the current system assumes that sulfur free fuel is loaded onto the aircraft into a dedicated SOFCPU fuel tank. The fuel loaded may be a synthetic fuel produced through a Fischer-Tropsch reaction which results in an essentially zero sulfur fuel or may be an extremely low sulfur fuel produced by desulfurization of jet fuel. Fischer-Tropsh fuels are likely to become more available in the future. Shell recently began operating a 140,000 barrel/day production facility in Qatar[3] producing a variety of products including aviation jet fuel. Petroleum based jet fuel could be desulfurized either at the airport or at a refinery and then provided to the airport as a separate fuel stream. In any case, all these options require that a separate fuel stream be handled and loaded onto the aircraft. The operation of the aircraft would be simpler if the SOFCPU could utilize the same fuel as the jet engines. To do this, the desulfurization would need to be handled on-board.

Sulfur contamination in the fuel impacts two areas of the system. In the reformer, the activity for reforming is reduced and the potential for carbon formation is increased. For the steam reforming catalyst selected[4], maintaining sulfur in the fuel feed below ~0.1 ppm by weight should avoid adverse effects. As poisoning occurs it may be detected by the temperature profile within the reformer. If insufficient activity remains in the reformer, unreformed jet fuel will be passed to the fuel cell resulting in hydrocarbon cracking and carbon formation in the fuel cell anode.

In the SOFC, if the anode is poisoned by sulfur the power density of the stack at a given voltage is reduced. The magnitude of the impact of sulfur contamination on power density is illustrated in Figure A.3.

[1] http://www.water.aero/product_iwg-a4.html
[2] http://www.pall.com/main/Aerospace-Defense-Marine/Product.page?id=54593
[3] http://www.shell.com/home/content/aboutshell/our_strategy/major_projects_2/pearl/ships_first_products/
[4] catalyst consists of rhodium dispersed on a magnesia alumina spinel support

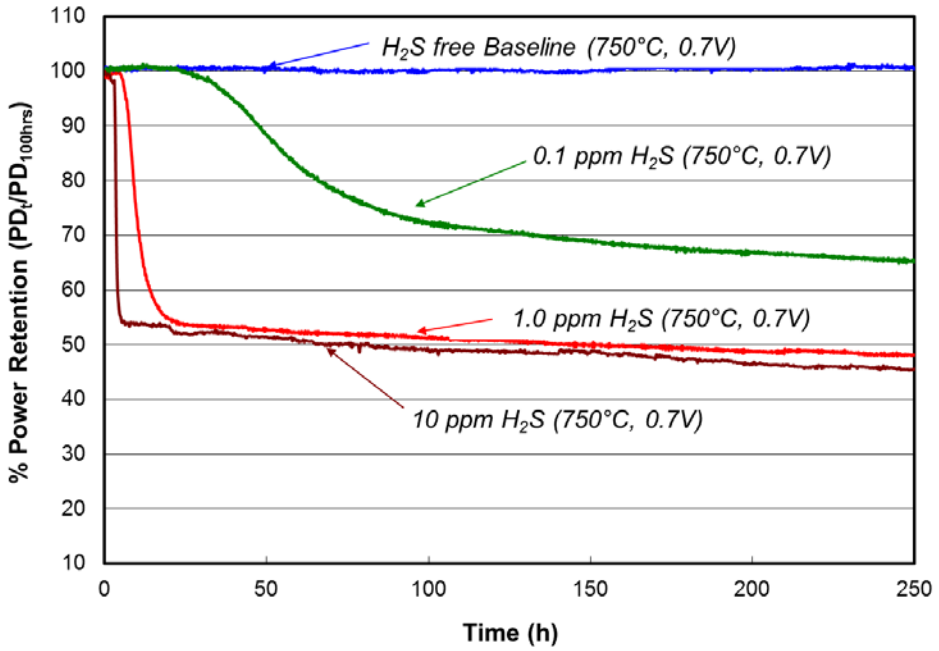

Figure A.3. Effect of H_2S Concentration in Anode inlet Gas on Power Density at 0.7V. (1 atm, button cell, concentrations are ppm volume, anode feed is dry basis 50% N_2, 50%H_2, humidified to 3% water).

As Figure A.3 illustrates, sulfur present in the anode feed significantly impacts the output from the SOFC. To prevent this drop in power density, an adsorbent such as ZnO would be used to scavenge sulfur in the form of H_2S at the reformer outlet even if desulfurized fuel enters the reformer in order to protect the anode from any residual sulfur contamination.

A very rough estimate of the system mass to perform desulfurization on board can be made based on comparison to a system developed at PNNL to desulfurize military JP8 fuel to ~0.1 ppmw to allow steam reforming of the fuel. The sulfur specifications for JP-8, Jet A and Jet A-1 are all 3000 ppmw. However, most jet fuels are much lower than the limit, typically in the range of 500 to 1000 ppmw.

The conceptual layout of the desulfurization system is assumed to be as shown in Figure A.4.

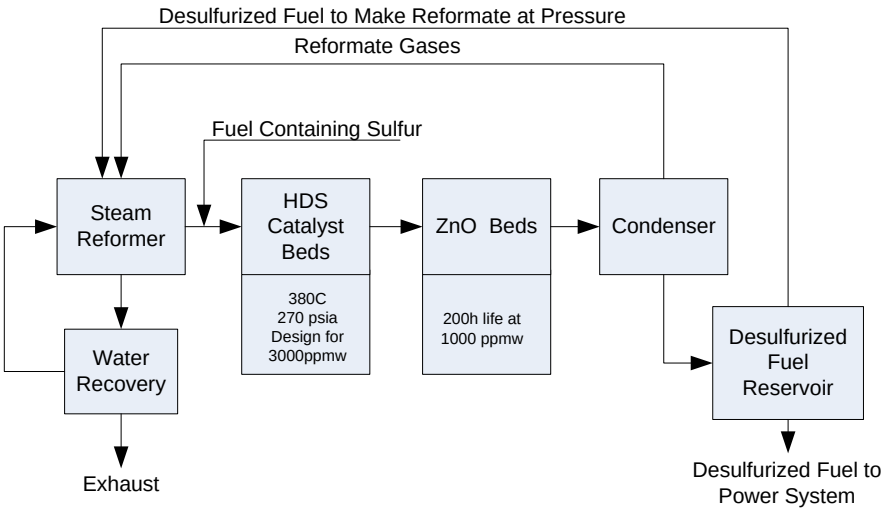

Figure A.4. Conceptual Layout of Desulfurization System

Water and desulfurized fuel is pumped up to pressure, vaporized and reacted in the steam reformer to produce a reformate stream. Sulfur containing fuel is vaporized and added to the reformate stream and introduced to the HDS catalyst bed where the organic sulfur is converted to H_2S. The gaseous fuel and reformate then pass through a ZnO bed where H_2S is adsorbed. The fuel is then condensed and the liquid fuel stored in a clean fuel reservoir until it is needed. The reformate gases which do not condense are then used as combustion fuel to supply the reformer.

The major weight impact of the system is associated with the HDS catalyst and ZnO beds. To arrive at an estimate, scaling of a 10 kWe system was applied[1]. The HDS catalyst is sized to provide desulfurization of 3000 ppmw fuel while the ZnO bed is sized to provide 200 hours when operating on 1000ppmw jet fuel. The weight of a 6-inch diameter schedule 10 shell is calculated to contain the beds and then 50% is added to account for the reformer, insulation and other items. The key mass items are shown in Table A.1.

Table A.1. Mass Contributions to Desulfurization System (972 kWe)

Component	Mass, kg
HDS Catalyst	169.0
ZnO adsorbent	149.7
Pressure Shells	339.9
Other Components	329.3
Total	987.9

[1] A system producing 60ccm of desulfurized JP-8 used a 4.7 liter bed of HDS catalyst with density 0.93g/cc. Testing with ZnO indicated a useable capacity of ~16.3wt% and a density prior to reaction of 72lb/ft^3. The ZnO bed mass increases during reaction. The bed mass after reaction was used to estimate the ZnO bed mass.

Including the desulfurization system would increase the system mass by about 35%. In addition to the added mass of the desulfurization system there would be some loss of efficiency associated with the use of fuel to make reformate to drive the desulfurization. This reduction in efficiency would reduce the breakeven weight by several hundred kg making it more difficult to save fuel on-board the aircraft.

On the other hand, a requirement to provide desulfurized fuel to the aircraft may result in the aircraft carrying desulfurized fuel for electrical generation sufficient to cover multiple legs of a trip if intermediate airports do not have a supply of desulfurized fuel.

Finally, performing desulfurization on-board the aircraft will make the overall system less reliable. When desulfurized fuel is produced on the ground, it is possible to analyze a large blended tank of fuel to confirm the desulfurization effectiveness prior to loading onto an aircraft. With desulfurization on-board, any problems with the desulfurization operation become a failure mode for the power generation system.

Appendix B

Ground Operation

Appendix B

Ground Operation

Breakeven weights are calculated based on the airborne portion of an aircraft trip. The potential for fuel savings will also involve ground operations. An SOFCPU would save fuel relative to the engine based generators during taxi-in and taxi-out segments of the trip. The amount of fuel savings is uncertain as the relative efficiency of the engine generators when the main engines are at very low power is not known.

However, offsetting this may be the impact of operating for a longer period of time due to the expected slow startup dynamics of the SOFCPU. It is expected that it may take a couple hours to startup the SOFC from a cold state. As a result it will likely be desired to maintain the SOFCPU operating during the time the aircraft is at the gate between flights. Typically aircraft power is provided from ground sources while the aircraft is at the gate. If ground electrical is not available the turbine APU would be operated. Hence, operating the SOFCPU at the gate will burn more fuel while saving ground electrical where the electrical is available or save fuel relative to the turbine APU where ground power is not available.

To enhance the reliability and state of readiness of the SOFCPU, it may be desired to maintain the SOFCPU operating at a low level during downtime overnight in order to prevent it from cooling. Depending on the relative prices of jet fuel and electricity, the keep warm function could be achieved using electrical ground power. In either case there will be a cost associated with keeping the SOFCPU warm overnight.

As a result, it is currently not clear whether the SOFCPU would save fuel compared to a conventional APU. While the turbine APU is much less efficient when operating, it is capable of starting up and shutting down rapidly and can be cooled to ambient with only a small penalty in terms of time required to restart.

Appendix C

Development of Algorithm for Predicting Stack Performance

Appendix C

Development of Algorithm for Predicting Stack Performance

C.1 Introduction

In assessing various design options for the SOFCAPU, ChemCAD software was used to simulate the mass and energy balance of the overall system for a specified cell voltage and single pass fuel utilization value. The size of the stack needed to satisfy the specified condition was then assessed using a relatively compact, empirically-based algorithm which predicts SOFC stack power density. The algorithm adequately represents the effects of multiple variables on stack power density including:

- Cell voltage
- Pressure
- Inlet and outlet temperatures
- Fuel inlet composition and single pass fuel utilization on the anode
- Level of inlet oxygen and utilization on the cathode.

This appendix discusses the development of the algorithm. The algorithm was developed in three stages. The first stage, which established performance as functions of temperature and fuel concentration, was performed on a previous project using a well-established, scaled up cell materials set. The second stage incorporated the performance boost of a new materials set, which has been tested at small scale (button cells), but which has not yet been scaled up to full cell size. The third stage added an estimation of the effect of pressure.

C.2 Performance as Functions of Temperature and Fuel Concentration

On a previous project, an empirical algorithm was developed that accounts for the effects of temperature and fuel concentration. The algorithm is based on experiments conducted with a full sized (105 cm^2 area) planar cell in flow-through configuration. It is important to conduct such experiments in flow-through configuration rather than with button cells, because the fuel composition that is adjacent to the anode in button cells cannot be accurately known.[C1] The anode was standard nickel metal-yttria stabilized zirconia (Ni-YSZ) cermet. The cathode was $La_{0.6}Sr_{0.4}Co_{0.2}Fe_{0.8}O_3$ (LSCF 6428). This is the materials set that was developed at PNNL and transferred to Delphi, which is using it in their current stack fabrication.

The test apparatus is shown in Figure C.1. The cell was mounted on a hearth plate in a furnace. A load was applied for the glass-sealing step. Incoming gasses passed through coils within the furnace so that they were pre-heated to the furnace temperature before entering the cell. The cell that was tested is referred to as a “strip cell”. Its active area is confined to a relatively narrow strip near the gas inlet. This is done by screen printing the cathode onto about one third of the normal active area. The cell tested had an active area of 38.4 cm^2. The gas flow rates were relatively high so that even at high current densities the fuel and air utilizations were very low. The maximum fuel utilization was ~2% at 820°C and the lowest voltage of relevance, 0.75 V. Under these conditions the fuel composition at the anode surface

was highly uniform. Temperature gradients were also minimized, due both to the high flow rates and the massive hearth plate. A range of fuel compositions was tested, representing reformate as it would enter a normal stack and as it would be progressively depleted as it passed through the cells. Data was collected at three temperatures, 660, 740, and 820°C and for five fuel concentrations. The current-voltage (I-V) curves are shown in Figures C.2 through C.4.

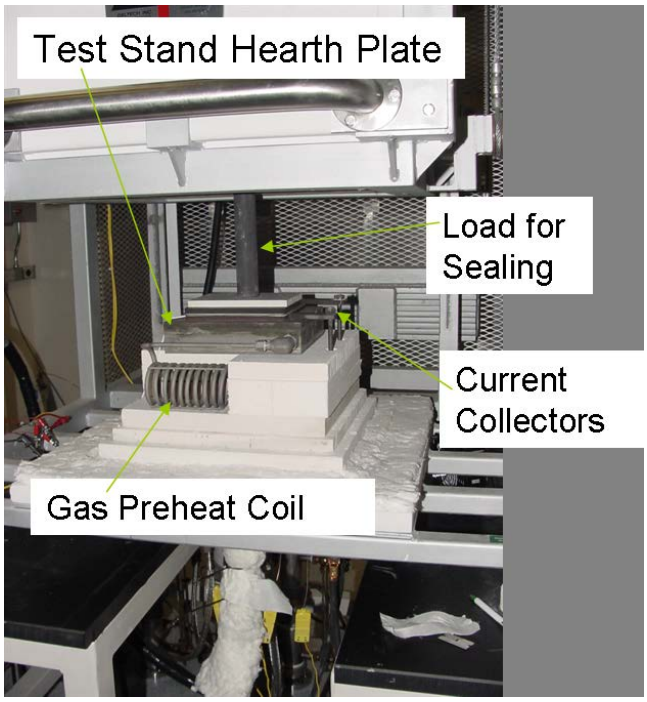

Figure C.1. Test Apparatus for Strip Cell Experiments

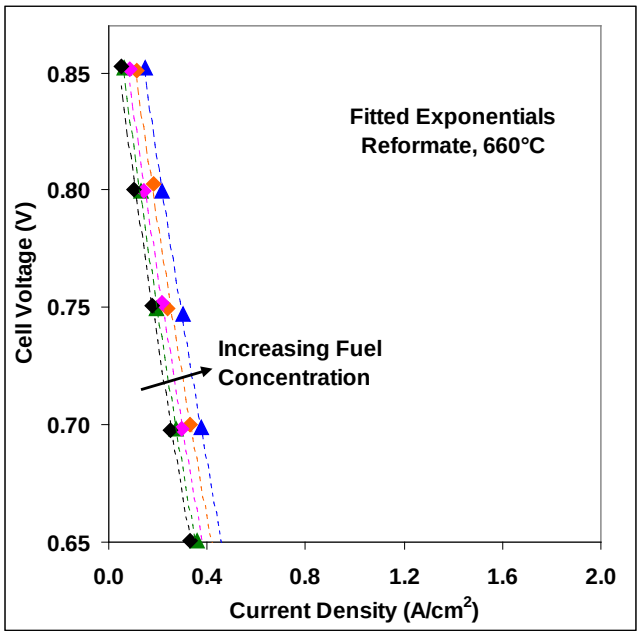

Figure C.2. I-V Curves for Strip Cell Data Taken Near 660°C.

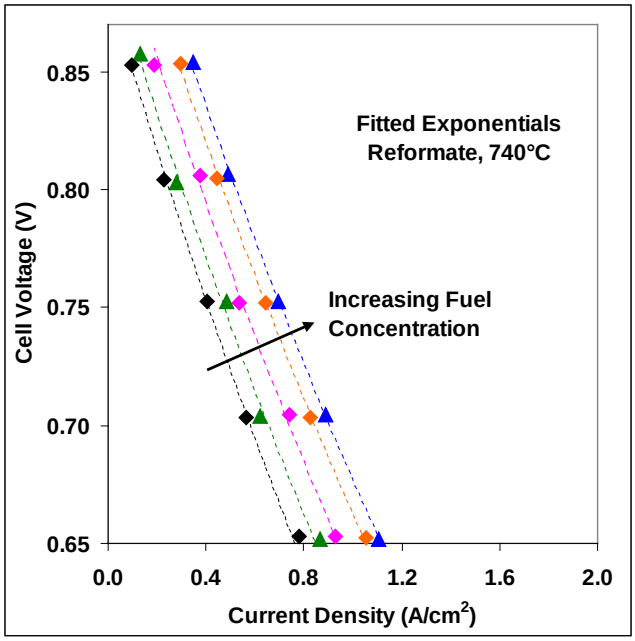

Figure C.3. I-V Curves for Strip Cell Data Taken Near 740°C

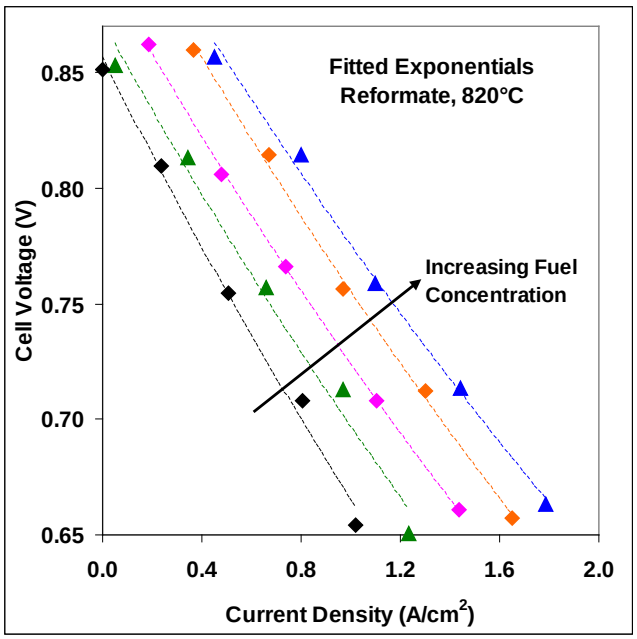

Figure C.4. I-V Curves for Strip Cell Data Taken Near 820°C

The scales in Figures C.2 through C.4 do not change, so that the substantial effect of temperature on increasing current is apparent. The broken lines are fitted exponentials of the form

$$V = PreX * \exp(X*I)$$

where V is the cell voltage, PreX is a pre-exponential multiplier, X is an exponential multiplier, and I is the current density (A/cm^2). The fitted parameters are listed in Table C.1 along with the fuel compositions, measured temperatures and calculated open circuit voltages (Voc).

Table C.1. Data From Strip Cell Tests and Parameters Fitted to I-V Curves

Temp	H_2	CO	H_2O	CO_2	CH_4	Pre X	Exponent	Fuel	V_{OC}@EQ
656	0.506	0.076	0.320	0.089	0.009	0.963	-0.856	0.616	1.006
655	0.215	0.027	0.615	0.143	0.000	0.898	-0.917	0.242	0.946
655	0.365	0.124	0.309	0.196	0.005	0.934	-0.867	0.511	0.995
654	0.258	0.080	0.419	0.242	0.001	0.912	-0.886	0.342	0.969
653	0.138	0.039	0.540	0.283	0.000	0.884	-0.924	0.177	0.935
738	0.509	0.093	0.320	0.076	0.001	0.962	-0.351	0.607	0.982
736	0.208	0.035	0.622	0.136	0.000	0.898	-0.381	0.242	0.915
738	0.356	0.148	0.321	0.174	0.001	0.945	-0.356	0.506	0.966
737	0.244	0.097	0.434	0.225	0.000	0.922	-0.372	0.341	0.937
735	0.128	0.049	0.550	0.274	0.000	0.886	-0.405	0.177	0.900
826	0.501	0.104	0.328	0.066	0.000	0.942	-0.195	0.606	0.953
819	0.200	0.042	0.629	0.128	0.000	0.872	-0.224	0.242	0.882
824	0.341	0.164	0.337	0.158	0.000	0.932	-0.210	0.506	0.935
823	0.230	0.111	0.448	0.211	0.000	0.895	-0.212	0.341	0.903
821	0.119	0.058	0.559	0.264	0.000	0.857	-0.252	0.177	0.862

The pre-exponentials are plotted versus the open circuit voltages in Figure C.5. The pre-exponentials are correlated to, but lower than the open circuit voltages (black dashed line) because the exponential functions do not fit the I-V curve precisely at the highest voltages near open circuit. The trends are linear for each temperature and the fitted linear coefficients, A and B, are shown in the figure.

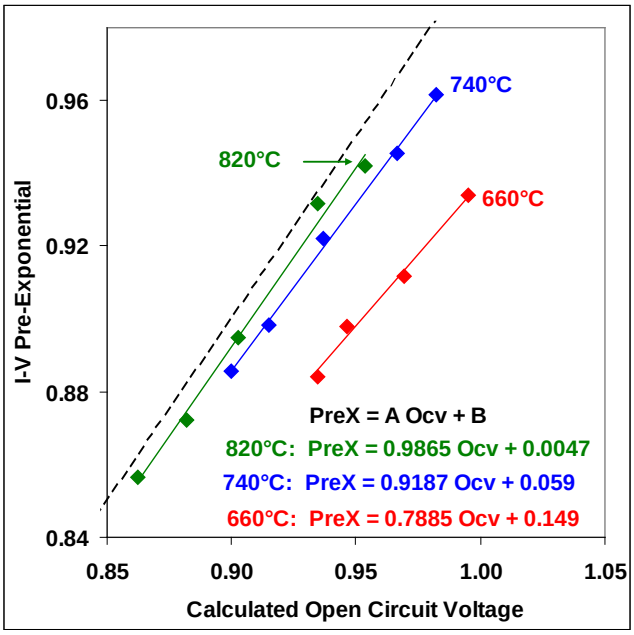

Figure C.5. Fitted Pre-Exponential Coefficients Plotted As Functions of Open Circuit Voltage

The exponential coefficients are plotted as functions of the inverse fuel concentration,1/F, in Figure C.6, where F = H_2 + CO + 4CH_4 (mole fractions). F is listed in the ninth column of Table C.1.

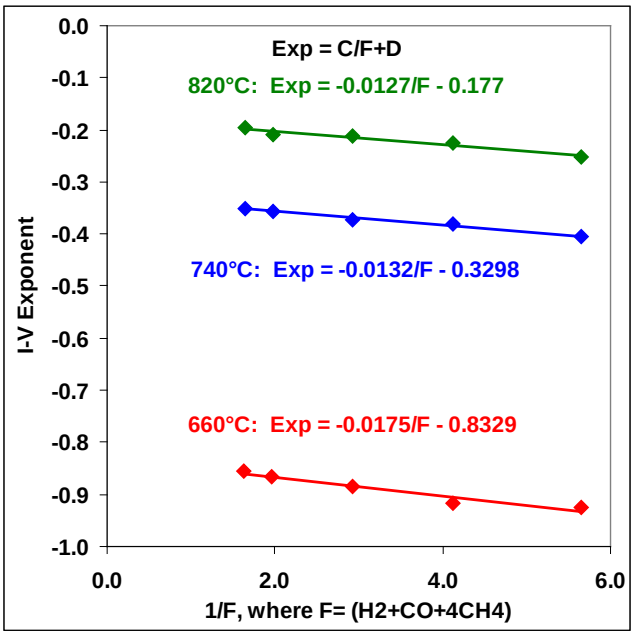

Figure C.6. Fitted Exponential Coefficients Plotted as Functions of Inverse Fuel Concentration

The trends are again linear and the fitted linear coefficients, C and D, are shown in the figure.

The linear coefficients, A and B, from Figure C.5 are plotted as functions of inverse temperature in Figure C.7. The trends are approximately linear and the fitted coefficients are shown in the figure.

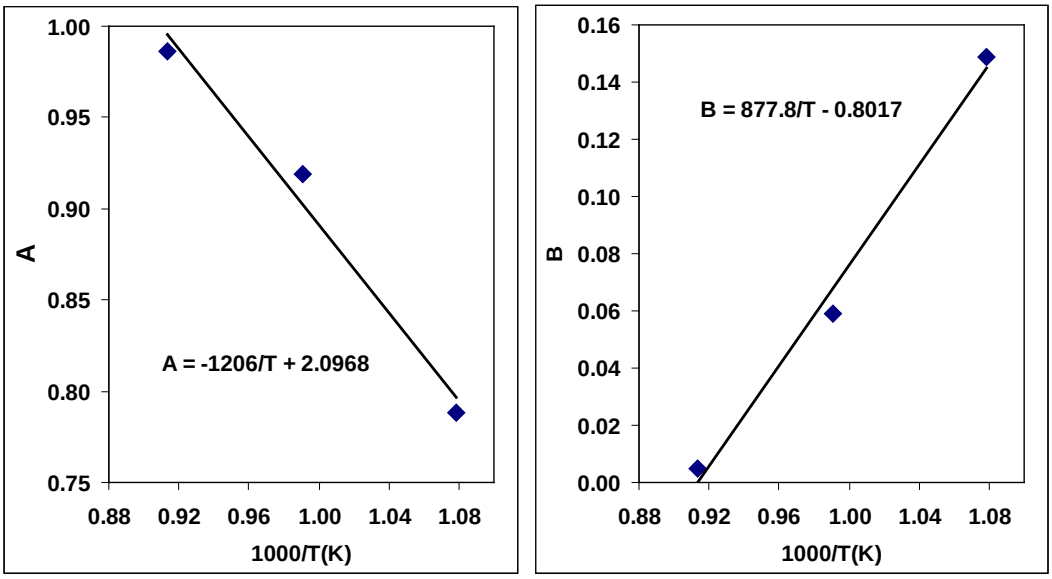

Figure C.7. Linear Coefficients A and B Plotted as Functions of Inverse Temperature

The linear coefficients, C and D, from Figure C.6 are plotted as functions of inverse temperature in Figure C.8. The trends had to be fitted with quadratics. It should be noted here that, because these polynomials were required at this stage of the algorithm development, the resulting algorithm should not be relied upon (extrapolated) outside of the temperature range tested (660 to 820°C).

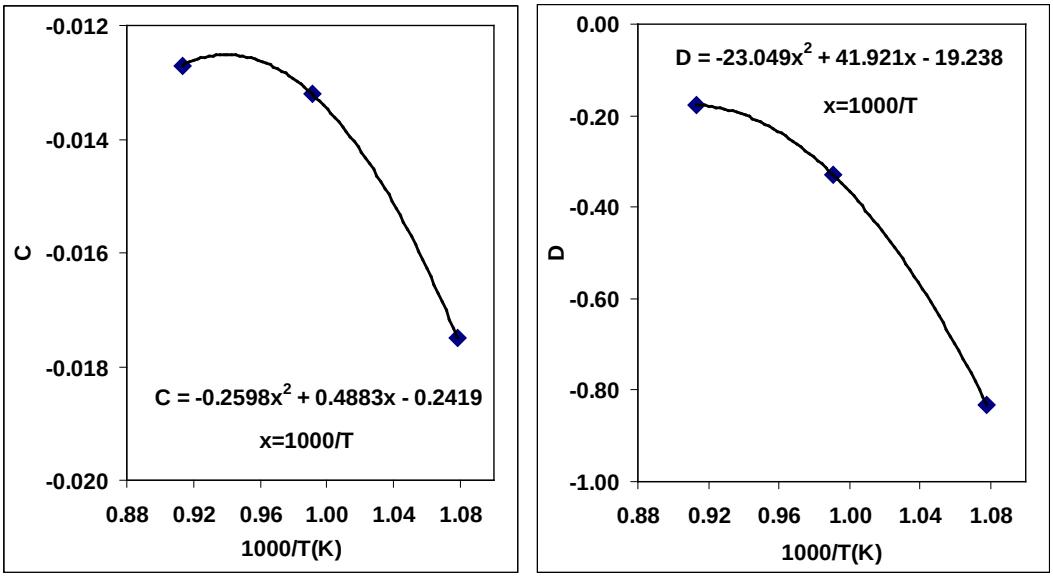

Figure C.8. Linear Coefficients C and D Plotted as Functions of Inverse Temperature

The algorithm to give voltage as a function of temperature, fuel concentration and current density is:

A= -1.206*(1000/T) + 2.0968
B= 0.8778*(1000/T) - 0.8017
PreX=A*Ocv+B

C= -0.2598*(1000/T)^2 + 0.4883*(1000/T) - 0.2419
D= -23.049*(1000/T)^2 + 41.921*(1000/T)- 19.238
X=C/F+D
V=Prex*exp(X*I)

Figures C.9 through C.11 show the I-V data and the I-V curves generated by the above algorithm.

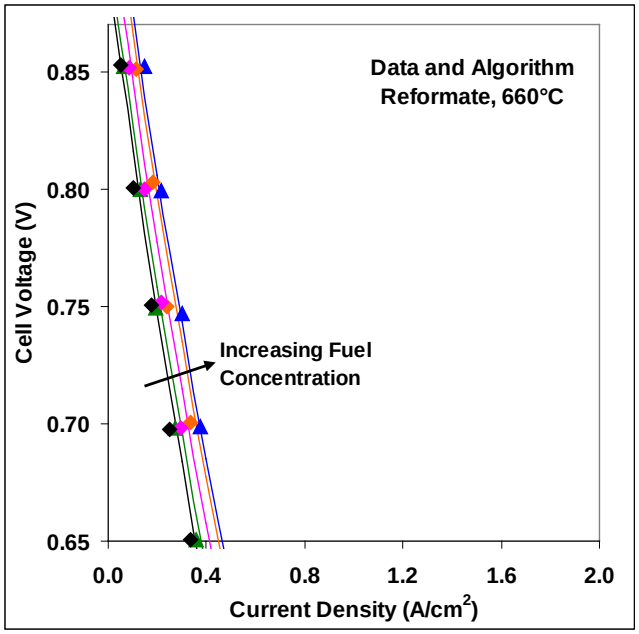

Figure C.9. Strip Cell I-V Data (points) taken near 660°C Plotted with I-V Curves Generated by the Algorithm

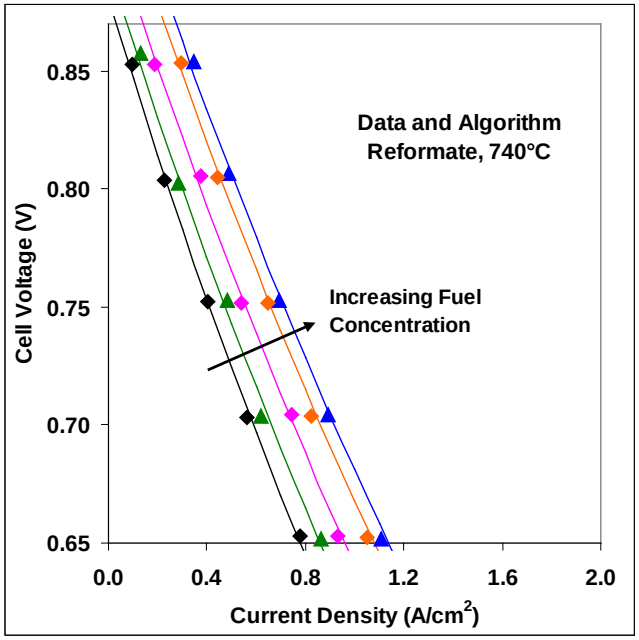

Figure C.10. Strip Cell I-V Data (points) taken near 740°C Plotted with I-V Curves Generated by the Algorithm

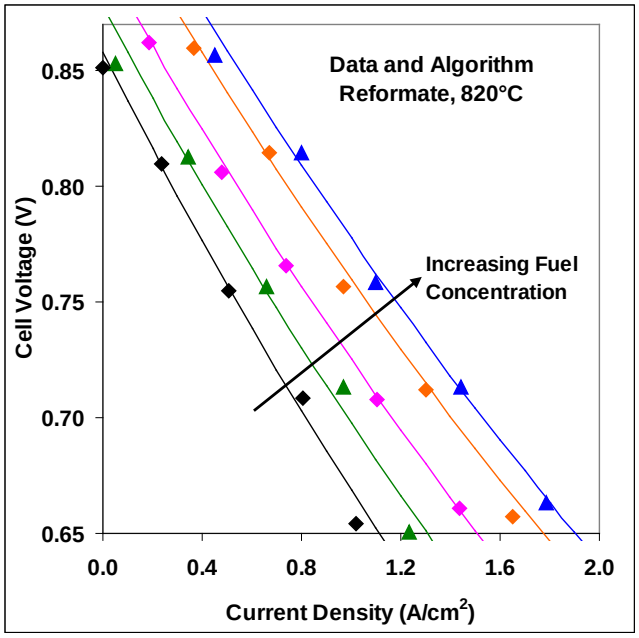

Figure C.11. Strip Cell I-V Data (points) taken near 820°C Plotted with I-V Curves Generated by the Algorithm

C.3 Performance Boost of New Materials Set

Recently, PNNL has developed a new materials set (anode and cathode) that produces substantially higher power density than the standard materials set. The proprietary compositions are discussed in Appendix D. The new set has not yet been scaled up or transferred to Delphi, but it has shown promising results in button cell testing. Figure C.12 compares the power density for the new cell materials to that for the standard materials. These tests were done at 750°C with 48.5% hydrogen, 3% steam, balance nitrogen. The power density is 75% higher within the range of relevant voltages (0.75-0.9V). This boost is accounted for in the algorithm by first calculating the current density for the standard materials set using the algorithm developed above and then multiplying by 1.75.

The new cathode shows good stability, as shown in Figure C.13. This test, spanning 4000 hours was also conducted at 750°C with 48.5% hydrogen, 3% steam, balance nitrogen. The cell was controlled to a constant current density of 0.65 A/cm^2. The cell had the anode from the standard materials set.

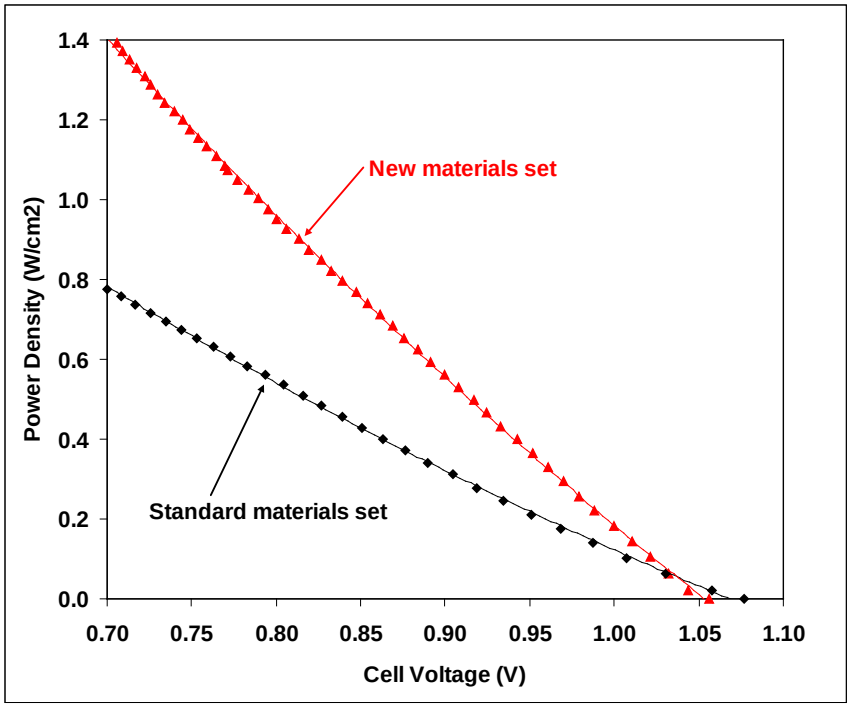

Figure C.12. Comparison of Power Density of New and Standard Cell Electrode Materials

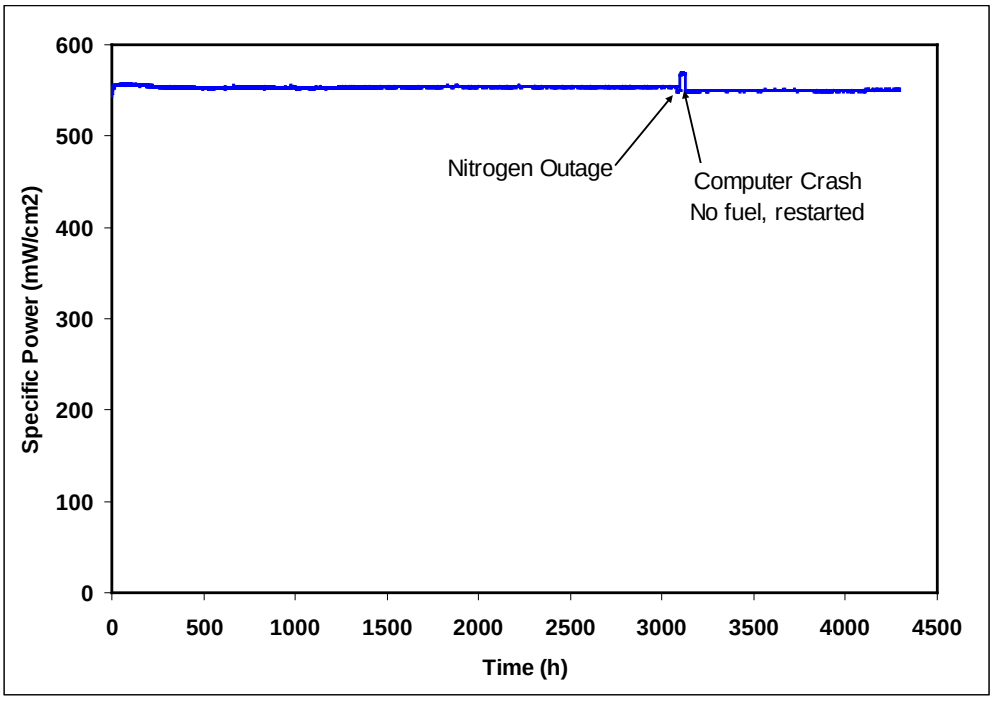

Figure C.13. Long-Term Test of Cell with New Cathode Material

C.4 Effect of Pressure on Cell Performance

There is scant data in the literature from experiments measuring the effect of pressure on SOFC performance. Singhal[C2] reported data taken on cathode-supported tubular cells at 1000°C from 1 to 15 atm with 89% hydrogen fuel. The cathode was doped lanthanum manganite, with YSZ electrolyte and Ni-YSZ anode. Minh[C3] reported data for 1, 2, and 3 atm taken at 800°C on a thin electrolyte anode-supported cell with YSZ electrolyte, Ni/YSZ anode and LSM cathode. The fuel composition was reported. The Fuel Cell Handbook[C4] reported that the effect of pressure follows the relation,

$$\Delta Vp(mV) = 59 \log (P_1/P_2)$$

although no description of how this relation was derived was given.

Minh[C3] tested to 3 atm, then developed an unspecified model and extrapolated the model results to 10 atm. Figure C14 shows the scanned data (points) with fitted exponentials.

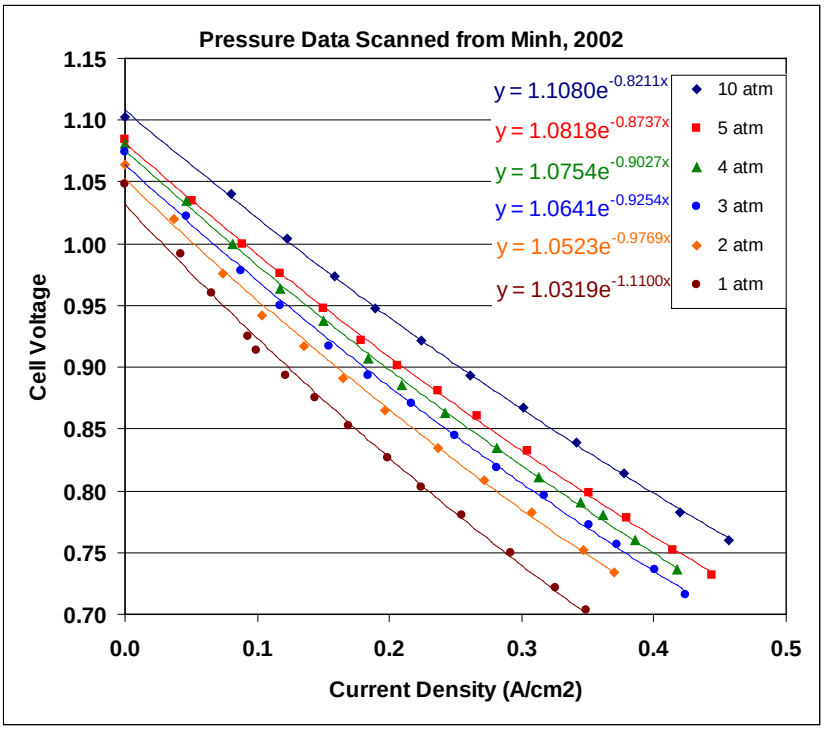

Figure C.14. I-V Curves for Range of Pressures. Data scanned from model of Minh[a2] with fitted exponentials.

The pre-exponential parameters, Q, for the higher pressures in Figure C.14 were normalized by the parameters for 1 atm and plotted as a function of ln(P) in Figure C.15. The data were fitted by a quadratic, forced through (0,1). The same was done with the exponential parameters, X, in Figure C.16.

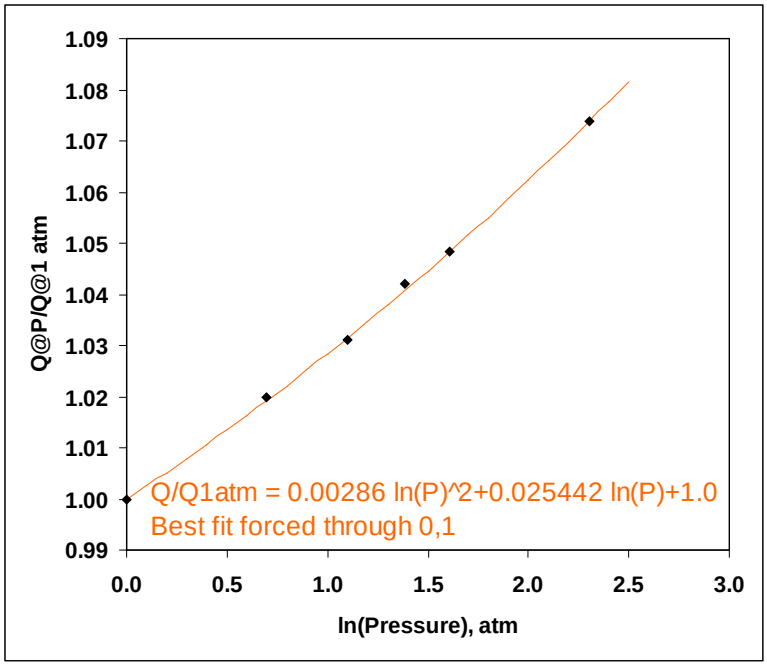

Figure C.15. Normalized Pre-Exponential Parameters from Figure C.14 Plotted as a Function of ln(P)

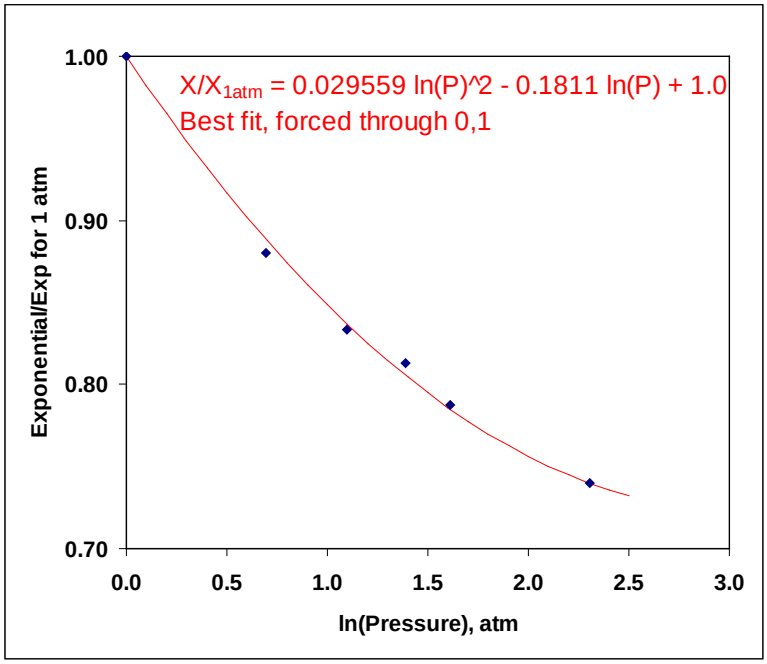

Figure C.16. Normalized Exponential Parameters from Figure C.14 Plotted as a Function of ln(P)

The algorithm to account for the effect of pressure is then:

X_P/X_{1atm}= 0.029559*ln(P)^2-0.1811*ln(P)+1.0
Q_P/Q_{1atm}=0.00286*ln(P)^2+0.025442*ln(P)+1.0

C.5 Comparison of Pressure Algorithm to Recent Data

Due to the scant data in the literature on the effects of pressure, a series of experiments were performed under this project to measure pressure effects on button cells (~2 cm^2 active area) over a range of temperatures and for both the standard and the new materials sets, using synthesized reformate (mix of bottled gasses) for the fuel. Since the system modeling, reported in the main body of this report had to be begun well before any measurements at pressure were available, the system modeling used the algorithm discussed above.

However, data at a range of pressures from about one to seven atmospheres is now available for the standard materials set. The data were taken at 650, 700, 750 and 800°C using a synthetic reformate to match that used in the system modeling for steam reforming of synthetic kerosene with 85% anode recycle. The exact reformate composition was adjusted for equilibration at each temperature and pressure. Equilibrium was calculated for both the water-gas shift and the methanation reactions. The compositions ranged from 22% H_2, 13% CO, 29% H_2O, 35% CO_2, 0.2% CH_4 at 650°C and 1 atm to 17% H_2, 9% CO, 33% H_2O, 38% CO_2, 3.0% CH_4 at 650°C and 7 atm.

The I-V data points are plotted in Figures C.17 through C.20. The lines are derived from the pressure algorithm applied to the data taken at one atm. The algorithm developed from Minh's data and model fits quite well at 800°C, the same temperature at which he performed his measurements. However, as the temperature decreases, the algorithm increasingly overestimates the voltage. It is clear that the effects of temperature and pressure interact. Increasing pressure at 800°C gives a larger percentage increase in power density than increasing pressure at lower temperatures.

Since the majority of the power is generated in the hotter end of the stack and the algorithm is reasonably accurate down to 700°C, we believe that the stack sizes calculated using the algorithm should be within a few percent of what they would have been had the recent data been available to calibrate the model. Certainly the changes would not have altered the conclusions of this report.

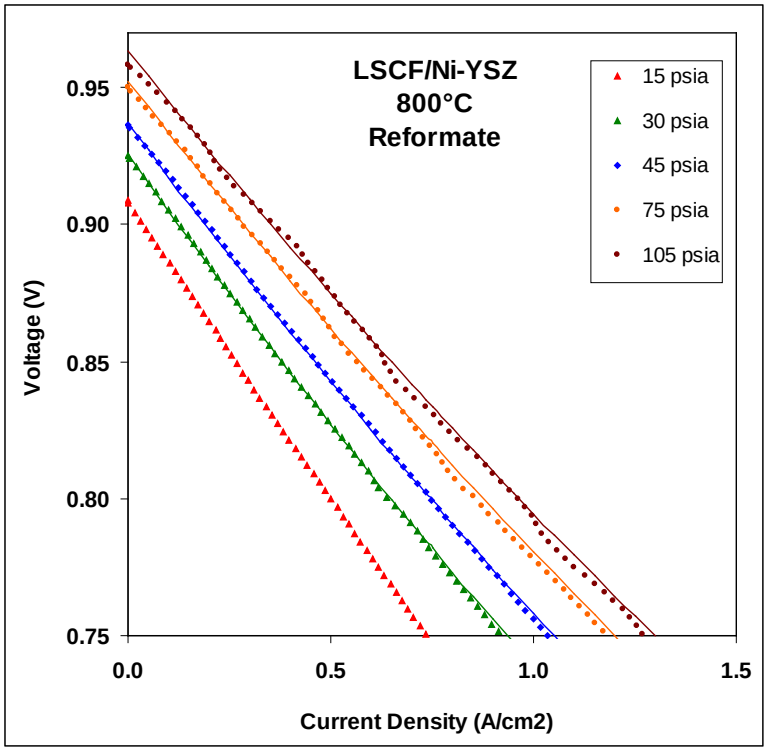

Figure C.17. Comparison of I-V Data Points taken over a Range of Pressures at 800°C to the Algorithm Developed from Minh's Model

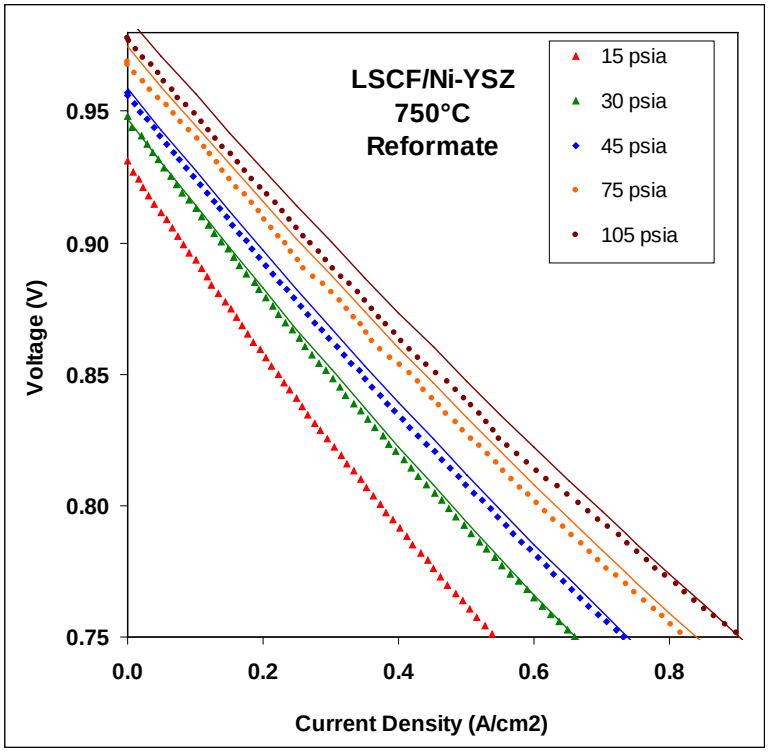

Figure C.18. Comparison of I-V Data Points taken over a Range of Pressures at 750°C to the Algorithm Developed from Minh's Model

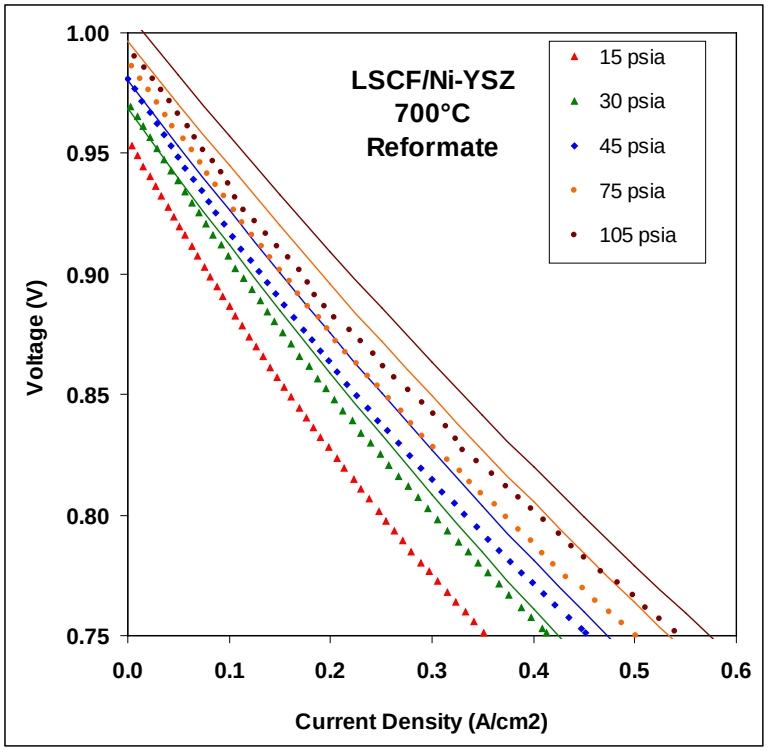

Figure C.19. Comparison of I-V Data Points taken over a Range of Pressures at 700°C to the Algorithm Developed from Minh's Model

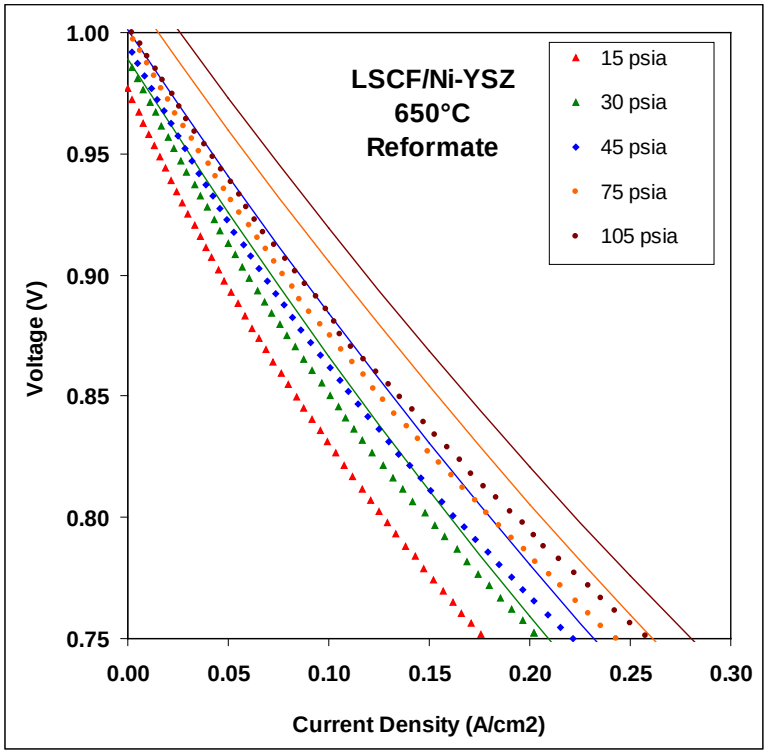

Figure C.20. Comparison of I-V Data Points taken over a Range of Pressures at 650°C to the Algorithm Developed from Minh's Model

C.6 References for Appendix C

C1. Chick, LA, et al. "Factors affecting limiting current in solid oxide fuel cells or debunking the myth of anode diffusion polarization" Journal of Power Sources 196 (2011) 4475-4482

C2. Singhal, S.C., "Recent Progress in Tubular Solid Oxide Fuel Cell Technology," Proceedings of the Fifth International Symposium on Solid Oxide Fuel Cells (SOFC – V), The Electrochemical Society, Inc., Pennington, NJ, 1997

C3. N. Minh, Solid Oxide Fuel Cell Hybrid System for Distributed Power Generation", presented at the Second DOE/UN International Conference and Workshop on Hybrid Power Systems, April 16-17, 2002 http://www.netl.doe.gov/publications/proceedings/02/Hybrid/hybrid02.html

C4. Fuel Cell Handbook, 6th ed. DOE/NETL-2002/1179 (2002).

Appendix D

Proprietary Information

Appendix D

Proprietary Information

In order to make this report more widely available the proprietary information in this appendix has been removed and issued as a separate document. The headings are included below to provide an outline of the type of information included in the appendix.

D.1 Proprietary Information on the New Cell Materials Set

D.2 Stack Flow Distribution

D.3 Boeing 787 Electrical System

Distribution

No. of Copies	
# 1, electronic	1 each, electronic
Pete Devlin Market Transformation Team Lead Fuel Cell Technologies Program DOE, EERE 1000 Independence Ave. SW Washington DC, 20585	Pacific Northwest National Laboratory Lawrence Chick Jamie Holladay Greg Whyatt

Pacific Northwest
NATIONAL LABORATORY

Proudly Operated by **Battelle** *Since 1965*

U.S. DEPARTMENT OF
ENERGY

902 Battelle Boulevard
P.O. Box 999
Richland, WA 99352
1-888-375-PNNL (7665)
www.pnnl.gov